MODELING EUTROPHICATION VULNERABILITY IN COASTAL LOUISIANA WETLANDS IMPACTED BY FRESHWATER DIVERSION: A REMOTE SENSING APPROACH

by

LYNN FERRARA BRIEN

M.A., University of New Orleans, 2009

AN ABSTRACT OF A DISSERTATION

submitted in partial fulfillment of the requirements for the degree

DOCTOR OF PHILOSOPHY

Department of Geography
College of Arts and Sciences

KANSAS STATE UNIVERSITY
Manhattan, Kansas

2015

Abstract

A major strategy in response to rapid degradation and loss of Louisiana's coastal wetlands has been the construction of siphon diversion projects. The diversions are designed to reintroduce nutrient enriched freshwater from the Mississippi River into wetland ecosystems to combat saltwater intrusion and stimulate marsh growth. The lack of consensus regarding the effects of river diversions on nutrient enrichment of wetland ecosystems is coupled with major concerns about eutrophication. Locating, assessing, and monitoring eutrophic marsh vegetation represent major challenges to understanding the impacts of freshwater diversions. As a result, this study was undertaken to investigate the feasibility of modeling eutrophication vulnerability of a coastal Louisiana marsh receiving turbid Mississippi River water. The major objective was to integrate remotely sensed data with field measurements of vegetation biophysical characteristics and historical ecosystem survey data to delineate landscape patterns suggestive of vulnerability to eutrophication. The initial step in accomplishing this goal was to model the spatial distribution of freshwater impacts using satellite image-based turbidity frequency data associated with siphon diversion operation. Secondly, satellite and spectroradiometer band combinations and vegetation indices optimal for modeling marsh biophysical characteristics related to nutrient enrichment were identified. Finally, satellite image data were successfully integrated with measures of historical and concurrent marsh biophysical characteristics to model the spatial distribution of eutrophication vulnerability and to elucidate the impacts of freshwater diversions.

MODELING EUTROPHICATION VULNERABILITY IN COASTAL LOUISIANA WETLANDS IMPACTED BY FRESHWATER DIVERSION: A REMOTE SENSING APPROACH

by

LYNN FERRARA BRIEN

M.A., University of New Orleans, 2009

A DISSERTATION

submitted in partial fulfillment of the requirements for the degree

DOCTOR OF PHILOSOPHY

Department of Geography
College of Arts and Sciences

KANSAS STATE UNIVERSITY
Manhattan, Kansas

2015

Approved by:

Major Professor
Kevin P. Price

Copyright

LYNN FERRARA BRIEN

2015

Abstract

A major strategy in response to rapid degradation and loss of Louisiana's coastal wetlands has been the construction of siphon diversion projects. The diversions are designed to reintroduce nutrient enriched freshwater from the Mississippi River into wetland ecosystems to combat saltwater intrusion and stimulate marsh growth. The lack of consensus regarding the effects of river diversions on nutrient enrichment of wetland ecosystems is coupled with major concerns about eutrophication. Locating, assessing, and monitoring eutrophic marsh vegetation represent major challenges to understanding the impacts of freshwater diversions. As a result, this study was undertaken to investigate the feasibility of modeling eutrophication vulnerability of a coastal Louisiana marsh receiving turbid Mississippi River water. The major objective was to integrate remotely sensed data with field measurements of vegetation biophysical characteristics and historical ecosystem survey data to delineate landscape patterns suggestive of vulnerability to eutrophication. The initial step in accomplishing this goal was to model the spatial distribution of freshwater impacts using satellite image-based turbidity frequency data associated with siphon diversion operation. Secondly, satellite and spectroradiometer band combinations and vegetation indices optimal for modeling marsh biophysical characteristics related to nutrient enrichment were identified. Finally, satellite image data were successfully integrated with measures of historical and concurrent marsh biophysical characteristics to model the spatial distribution of eutrophication vulnerability and to elucidate the impacts of freshwater diversions.

Table of Contents

List of Figures

List of Tables

Acknowledgements

This dissertation would have been impossible without the support of many wonderful people. I am especially thankful for the generosity, guidance, and encouragement of my doctoral advisor, Dr. Kevin Price and my friend and mentor, Dr. Matthew Bethel. Their positive outlook and unwavering faith in the project, and in my ability to complete the work, were invaluable. I am immensely grateful to Dr. Melinda Daniels for her crucial support early on and for her continued encouragement throughout my studies. Dr. Douglas Goodin deserves a special thanks for generously sharing his time and his unique and valuable insights, which led me to a greater understanding of my work.

I am also grateful for the opportunities provided by Dr. Matthew Bethel and the Pontchartrain Institute for Environmental Sciences at the University of New Orleans, as well as the assistance of Corey Miller, Rosina Phillippe, and Maurice Phillips in field data collection down the bayou. The invaluable assistance provided by William Boshart and Danielle Richardi of the Louisiana Department of Natural Resources is also greatly appreciated.

A special thanks is due the faculty and staff of the Department of Geography at Kansas State University, as well as my fellow graduate students, for their generous support and encouragement. I'll always be grateful for the incredible opportunities they provided me.

Finally, I want to thank my grade school Geography teacher, Ms. Ruth DiRosa, for being such an inspiring teacher and for broadening my view of the big wide fascinating world.

Dedication

This dissertation is dedicated to the people whose very existence fills me with joy: to my mother, my first and most beloved teacher and my fiercest ally; to the two remarkably loving and supportive young men I'm so proud to call my sons; and to the love of my life, my husband, whose patience, generosity, and unwavering support have known no bounds.

Chapter 1 - **Introduction**

Louisiana's coastal wetlands are rapidly deteriorating and disappearing due to natural and anthropogenic causes. Artificial flood control levees have effectively isolated the Mississippi River from its delta, exacerbating natural subsidence, erosion and storm effects (Lopez, 2009; Day *et al*., 2009a). The construction of extensive networks of canals for oil and gas exploration and the extraction of natural resources have also contributed to subsidence and erosion and promoted saltwater intrusion into freshwater marshes (Lopez, 2009; Day *et al*., 2009a). Over the last half century a major strategy for reducing or reversing wetland loss in Louisiana has been the construction of river diversions designed to reintroduce freshwater from the Mississippi River into wetland ecosystems to combat saltwater intrusion and stimulate marsh growth (Day *et al*., 2009a). During this same period, runoff of fertilizers, pesticides and other pollutants from agricultural and urban areas has increased, adversely affecting water quality in the rivers and streams of the 3 million km^2 Mississippi River Basin (Cloern, 2001; Mitsch, *et al.*, 2005; Siciliano, *et al.*, 2008). Excess nitrogen, in the form of nitrate-nitrogen, is transported in the Mississippi River to coastal areas in Louisiana, where the subtropical climate, associated warm water temperatures, and long growing season facilitate high nutrient uptake and denitrification rates (Mitsch, *et al.,* 2005). Since Louisiana's diversions introduce nutrient enriched Mississippi River water and sediment into wetland areas, eutrophication is a major concern (Sklar and Browder 1998; Lissner *et al.*, 2003; Lane and Day, 1999; Mitsch *et al.,* 2005; Day *et al*., 2009a).

Eutrophication generally refers to gradual nutrient enrichment in water bodies (Christropherson, 2009; Ferreira *et al*., 2011), but when loading rates are very high, nutrients also accumulate in soils and vegetation (Dettmann, 2001; Kamer *et al.*, 2001). In the presence of

excessive nutrient loadings, wetland ecosystem processes are altered, resulting in measurable changes in plant productivity, including increases in net primary productivity (U.S. EPA, 2002; Ferreira *et al*., 2011). Several studies have shown however, that despite increased above ground biomass, excess nutrient loading in salt marshes reduces below ground plant growth, root and rhizome biomass, and carbon accumulation, decreasing geomorphic stability and causing significant loss in marsh elevation (Darby and Turner, 2008a, 2008b; Turner *et al.*, 2009; Turner, 2010; Deegan *et al.*, 2012). In contrast, a study by Day *et al.* (2009b) reported finding high belowground biomass in marshes impacted by the river diversion at Caernarvon, Louisiana. Although high nutrient loading to coastal marshes remains a concern that should be monitored, studies of the effects of Louisiana's river diversions have been limited (Day *et al.*, 2009a; Boustany, 2010).

Research to develop effective methods for assessing and monitoring nutrient enrichment of Louisiana's coastal wetlands is needed. This study was undertaken to investigate the feasibility of modeling eutrophication vulnerability of a coastal Louisiana marsh receiving turbid Mississippi River water. The major objective was to integrate remotely sensed data with field measurements of vegetation biophysical characteristics and historical ecosystem survey data to delineate landscape patterns suggestive of vulnerability to eutrophication.

Chapter 2 describes the initial step in accomplishing the major objective of this study. It outlines a remote sensing-based method for differentiating marsh areas experiencing high and low freshwater impacts as a result of the operation of the West Pointe a la Hache (WPH) siphon diversion. Water turbidity frequency datasets representing pre- and post-siphon turbidity conditions are used to derive an estimate of turbidity due to siphon operation. Results are then classified based on level of turbidity, and adjacent vegetated areas are delineated and classified

by level of freshwater impact. The resulting model is assessed for accuracy using corresponding historical salinity data and analyzed with regard to the spatial distribution of freshwater impacts relative to the location of the siphon diversion.

Chapter 3 describes the development of a eutrophication vulnerability model based on the relationships between field measurements of vegetation parameters associated with wetland nutrient enrichment and data derived from field spectra and satellite imagery. Measurements of Leaf Area Index (LAI), plant height, and chlorophyll concentration are collected across vegetation productivity and freshwater impact gradients and correlated with spectral data to identify which spectral bands and vegetation indices are most predictive of the vegetation parameters. Based on the results, a model of predicted chlorophyll concentration is derived and assessed for accuracy and the spatial distribution of chlorophyll concentration relative to the location of the WPH siphon diversion is analyzed.

Chapter 4 builds on the previous chapters by integrating satellite image data with measures of historical ecosystem survey data and concurrent marsh biophysical characteristics to model the spatial distribution of eutrophication vulnerability and to elucidate the impacts of freshwater diversions. Vegetation parameters collected across vegetation productivity and freshwater impact gradients are integrated with corresponding historical ecosystem survey data and analyzed using an agglomerative hierarchical clustering method. The results are used to classify sample sites as exhibiting higher or lower vulnerability to eutrophication, after which spectral characteristics of the classified sites are used to develop the eutrophication vulnerability model. The model is assessed for accuracy and the results are analyzed relative to freshwater impacts.

Finally, Chapter 5 summarizes the findings of the previous chapters. The broader impacts of the study are discussed including its potential to inform the ongoing debate surrounding both the impacts of existing freshwater diversions and the planning and implementation of future restoration projects affecting coastal Louisiana wetlands.

References

Boustany, R.G., 2010. Estimating the benefits of freshwater introduction into coastal wetland ecosystems in Louisiana: Nutrient and sediment analyses. Ecological Restoration, 28(2), 160-174.

Christopherson, R.W., 2009. Geosystems, 7th Edition. Upper Saddle River, NJ: Pearson Prentice Hall, 639p.

Cloern, E.C., 2001. Our evolving conceptual model of the coastal eutrophication problem. Marine Ecology Progress Series, 210, 223-253.

Darby. F.A. and Turner, R.E., 2008(a). Below- and aboveground Spartina alterniflora production in a Louisiana salt marsh. Estuaries and Coasts, 31, 223-231.

Darby, F.A. and Turner, R.E., 2008 (b). Effects of eutrophication on salt marsh root and rhizome biomass accumulation. Marine Ecology Progress Series, 363, 63-70.

Day, J.W.; Cable, J.E.; Cowan, J.H., Jr.; DeLaune, R.; de Mutsert, K.; Fry, B.; Mashriqui, H.; Justic, D.; Kemp, P.; Lane, R.R.; Rick, J.; Rick, S.; Rozas, L. P.; Sneddens, G; Swenson, E.; Twilley, R.R., and Wissel, B., 2009 (a). The impacts of pulsed reintroduction of river water on a Mississippi delta coastal basin. The Journal of Coastal Research, 54, 225-243.

Day, J.; Lane, R.; Moerschbaecher, M.; DeLaune, R; Twilley, R.; Mendelssohn, I., and Baustian, J., 2009 (b). The impact of the Caernarvon diversion on above and belowground marsh biomass in the Breton Sound Estuary after Hurricane Katrina. Final Report submitted to the Louisiana Department of Natural Resources, Project 2512-07-01.

Deegan, L.A.; Johnson, D.S.; Warren, R.S.; Peterson, B.J.; Fleeger, J.W.; Fagherazzi, S., and W.M. Wollheim, 2012. Coastal eutrophication as a driver of salt marsh loss. Nature, 490(7420), 388-392.

Dettmann, E.H., 2001. Effect of water residence time on annual export and denitrification of nitrogen in estuaries: A model analysis. Estuaries, 24(4), 481-490.

Ferreira, J.G.; Andersen, J.H.; Borja, A.; Bricker, S.B.; Camp, J.; Cardoso da Silva, M.; Garces, E.; Heiskanen, A.; Humborg, C.; Ignatiades, L.; Lancelot, C.; Menesguen, A.; Tett, P.; Hoepffner, N., and Claussen, U., 2011. Overview of eutrophication indicators to assess environmental status within the European Marine Strategy Framework Directive. Estuarine, Coastal and Shelf Science, 93, 117-131.

Kamer, K.; Boyle, K.A., and Fong, P., 2001. Macroalgal bloom dynamics in a highly eutrophic southern California estuary. Estuaries, 24(4), 623-635.

Lane, R., and Day, J., 1999. Water quality analysis of a Freshwater Diversion at Caernarvon, Louisiana. Estuaries, 22(2A), 327-336.

Lissner, J.; Mendelssohn, I.; Lorenzen, B.; Brix, H.; McKee, K., and Miao, S., 2003. Interactive Effects of Redox Intensity and Phosphate Availability on Growth and Nutrient Relations of Cladium Jamaicense (Cyperaceae). American Journal of Botany, 90(5), 736-748.

Lopez, J. A., 2009. The Environmental History of Human-Induced Impacts to the Lake Pontchartrain Basin in Southeastern Louisiana since European Settlement – 1718 to 2002. Journal of Coastal Research, 54, 1-11.

Mitsch, W.; Day, J.; Zhang, L., and Lane, R., 2005. Nitrate-nitrogen retention in wetlands in the Mississippi River Basin. Ecological Engineering, 24, 267-278.

Siciliano, E.; Wasson, K.; Potts, D.C., and Olsen, R.C., 2008. Evaluating hyperspectral imaging of wetland vegetation as a tool for detecting estuarine nutrient enrichment. Remote Sensing of Environment, 112, 4020-4033.

Sklar, F., and Browder, J., 1998. Coastal Environmental Impacts Brought About by alterations to Freshwater Flow in the Gulf of Mexico. Environmental Management, 22(4), 547-562.

Turner, R.E.; Howes, B.L.; Teal, J.M.; Milan, C.S.; Swenson, E.M., and Tonerb, D.D., 2009. Salt marshes and eutrophication: An unsustainable outcome. Limnology and Oceanography, 54(5), 1634.

Turner, R.E., 2010. Beneath the Salt Marsh Canopy: Loss of Soil Strength with Increasing Nutrient Loads. Estuaries and Coasts, 34(5), 1084-1093.

US EPA, 2002. Methods for Evaluating Wetland Condition: Vegetation-Based Indicators of Wetland Nutrient Enrichment. Office of Water, U.S. Environmental Protection Agency, Washington, DC. EPA-822-R-02-024.

Chapter 2 - **A Remote Sensing-Based Method for Mapping Freshwater Diversion Impacts in Coastal Louisiana Wetlands**

Abstract

This study was conducted to investigate the feasibility of using turbidity frequency data to identify areas of Louisiana coastal wetlands most impacted by the introduction of turbid Mississippi River water. Siphon diversion projects operating in South Louisiana are designed to reintroduce freshwater into wetland ecosystems to combat saltwater intrusion and stimulate marsh growth. The primary goal of this research was to test whether an accurate remote sensing-based method could be developed for differentiating marsh areas experiencing high and low freshwater impacts associated with siphon operations. In conjunction with the US Army Corps of Engineers, water turbidity frequency datasets were derived from time series Landsat 5 Thematic Mapper (TM) satellite images to represent pre- and post-siphon turbidity conditions. Using turbidity frequency prior to commencement of siphon operation as a baseline, background turbidity was factored out to derive an estimate of water turbidity due to siphon operation. Turbidity estimates were then classified based on level of turbidity, and were assessed for accuracy using corresponding historical salinity data. Results indicate that areas classified as high freshwater impact areas (i.e., highest turbidity due to siphon operation) were associated with significantly lower levels of salinity. Areas classified as low freshwater impact areas (i.e., lowest turbidity during siphon operation) were associated with significantly higher levels of salinity. These results suggest that high and low freshwater impact areas were successfully delineated using this methodology.

Introduction

Like many wetland ecosystems throughout the world, Louisiana's coastal wetlands are deteriorating and disappearing at an alarming rate, due to both natural and anthropogenic causes. Natural subsidence and erosion have been exacerbated by isolation of the Mississippi River from its delta through the construction of artificial flood control levees (Lopez, 2009; Day *et al*., 2009a). Petroleum extraction and the construction of extensive networks of canals for oil and gas exploration have also exacerbated natural subsidence and erosion and promoted saltwater intrusion into Louisiana's freshwater marshes (Lopez, 2009; Day *et al.,* 2009a).

A number of restoration strategies have been devised in an attempt to reduce or reverse wetland losses. Major projects implemented in Louisiana during the past half century include river diversions designed to reintroduce freshwater into wetland ecosystems to combat saltwater intrusion and stimulate marsh growth (Day *et al*., 2009a). During this same period, runoff of fertilizers, pesticides, and other pollutants from agricultural and urban areas has increased, adversely affecting water quality in the rivers and streams of the 3 million km² Mississippi River Basin (Cloern, 2001; Mitsch, *et al*., 2005; Siciliano, *et al*., 2008). A major concern is that the diversions introduce nutrient enriched water and sediment from the Mississippi River into coastal ecosystems, potentially leading to wetland eutrophication (Sklar and Browder 1998; Lissner *et al.*, 2003; Lane and Day, 1999; Mitsch *et al.,* 2005; Day *et al*., 2009a). Studies by Darby and Turner (2008a; 2008b) found that excess nutrient loading in marsh ecosystems reduces below ground plant growth and, therefore, root and rhizome biomass and carbon accumulation. Similarly, a 30-year study of Massachusetts salt marshes, found that eutrophication may be accompanied by a decrease in the accumulation of organic matter belowground, causing significant loss in marsh elevation (Turner *et al*., 2009). The reduction in roots and rhizomes is likely to exacerbate the erosive effects of storms (Turner *et al.,* 2009). This is supported by

Howes, *et al*. (2010) who found that Louisiana marshes that received diverted freshwater for 18 years prior to Hurricanes Katrina and Rita were preferentially eroded as a consequence of the storms. In a synthesis of previous studies, however, Day *et al*. (2009a) reported that nitrogen loading rates in the outfall area of the river diversion at Caernarvon, Louisiana, as well as rates in the Atchafalaya River to marshes surrounding Fourleague Bay, were far less than loading rates used in the Darby and Turner (2008a; 2008b) studies. Furthermore, another study by Day *et al.* (2009b) reported finding high belowground biomass in marshes impacted by the Caernarvon diversion. Still, high nutrient loading to coastal marshes remains a concern and should be monitored (Day *et al*., 2009a). Further research is necessary to address this concern and the ongoing debate, yet studies of the effects of river diversions have been limited (Day *et al.*, 2009a; Boustany, 2010).

Satellite remote sensing offers an underutilized approach to monitoring possible eutrophication from freshwater diversions. Freshwater diverted from the Mississippi River contains high concentrations of suspended particulate matter (SPM) and appears cloudy as it enters the outfall area. In the presence of SPM the optical properties of water cause light to be scattered and absorbed by particles and molecules rather than transmitted through water in a straight line, thereby reducing water's transparency and increasing turbidity (ASTM-International, 2003; Guttler *et al.*, 2013). A clear water body is highly absorbent of light, acting as a dark object, especially in the near infrared wavelengths (700-800 nm). With increases in SPM, a water body will act more like a bright object, especially in the visible red wavelengths (600-700 nm) (Lillisand, 2004; Lodhi, 1997; Allen *et al*., 2008). Thus, clear and turbid waters differ in spectral response, with turbid water exhibiting significantly higher reflectance than clear water (Froidefond *et al*. 2002; Li, *et al*. 2003; Allen *et al*., 2008). Reflectance differences in the

near infrared and red wavelengths can be leveraged for mapping turbidity in river diversion outfall areas (Harrington and Schiebe, 1992; Miller and McKee, 2004; Allen *et al*., 2008). Furthermore, sediment laden river water transports pollutants to coastal zones and affects nutrient dynamics and phytoplankton productivity (Doxaran *et al*., 2009; Volpe *et al*., 2011; Guttler *et al.,* 2013). As a result, in addition to being a relative measure of the amount of SPM in water, turbidity is an important water quality parameter that can also be used as an indicator of eutrophication (Fraser, 1998; Guttler *et al*., 2013). Observation networks for monitoring water quality parameters, including turbidity, typically provide data that has high temporal but low spatial resolution, requiring interpolation of the data across large areas (Volpe *et al.,* 2011). Satellite imagery, although lower in temporal resolution, provides relatively high spatial resolution data useful for monitoring turbidity and freshwater diversion impacts.

The primary goal of this study was to test whether an accurate remote sensing-based method could be developed for differentiating marsh areas experiencing high and low freshwater impacts associated with siphon operations. Specific objectives were to use satellite imagery to identify wetland areas most frequently and least frequently exposed to turbid Mississippi River water as a result of the operation of the West Pointe a la Hache siphon diversion and to determine whether concurrent water salinity measurements within those areas support the resulting classification of high and low freshwater impacts. The ability to accurately model relatively high and low impact areas would allow for efficient sampling across a freshwater impact gradient, aiding in the monitoring of possible eutrophication due to freshwater introduction.

Study Area

The study area (Figure 2.1) is located within the Barataria Basin, an interdistributary estuarine wetland system of the Mississippi River Delta. Wetland vegetation in the estuary is characterized by a progression of fresh, intermediate, brackish, and salt marshes, moving to open water (Conner and Day, 1987). The study area is an approximately 138 km^2 portion of the estuary located in Plaquemines Parish, Louisiana. It has, like the larger Barataria Basin, been severely impacted by wetland degradation and loss, having experienced some of the highest rates of land loss in Louisiana's coastal zone (Conner and Day, 1987; Barras *et al*., 2003; Barras, 2009; Bethel *et al*., 2011).

The study area extent includes highly degraded and fragmented marsh areas north and northeast of Bayou Grand Chenier Ridge, as well as relatively intact core marsh west and southwest of the ridge, a juxtaposition of conditions allowing compelling comparisons. The West Pointe a la Hache (WPH) Siphon Diversion Project is located within the study area on the west bank of the Mississippi River at river kilometer 78.7 (mile 48.9) (Haywood and Boshart, 1998).

The diversion was designed to provide freshwater and sediment to the marshes for restoration and land building (OCPR, 2010; LaCoast, 2008). It is a relatively low-flow diversion consisting of eight 1.8 m diameter steel siphon pipes that cross over the levee, run underground, then discharge river water into an outfall pond. Four channels radiate southward from the pond to distribute freshwater to the surrounding marsh (Richardi, 2013). Although maximum discharge for the siphons is estimated as 2144 ft^3s^{-1} (61 m^3s^{-1}), based on high river stage and all siphons in full operation, freshwater flow at WPH typically ranges between 500-1000 ft^3s^{-1} (14-28 m^3s^{-1}) when the siphon is operational (Richardi, 2013). It is estimated that the siphon has operated approximately 60% of the time since flow began in January, 1993 (Richardi, 2013).

Although the siphons at WPH have had some effect in reducing salinity, land loss is still occurring in the project area (Boshart and Van Cook, 2007; Richardi, 2013).

Methods

Water Turbidity Frequency Datasets

Water turbidity frequency datasets were produced for this study by the U.S. Army Corps of Engineers (USACE) based on a technique developed by Allen *et al*. (2008) and outlined in Appendix A. The datasets are based on time series cloud-free Landsat images captured between 1984 and 2010 and corresponding to periods of pre- and post-siphon operation of the WPH diversion project. For the post-siphon operation time period, optimal Landsat image dates were chosen to coincide with siphon freshwater flow based on records obtained from Louisiana Coastal Protection and Restoration Authority (CPRA) Strategic Online Natural Resources Information System (SONRIS, 2011). Pre- and post-siphon operation satellite image dates and associated freshwater flows are provided in Table 2.1.

The USACE datasets consist of two turbidity frequency maps, adapted versions of which are provided in Figures 2.2 and 2.3. The pre-1993 turbidity map (Figure 2.2) depicts the frequency of classification of water pixels as turbid during the pre-siphon time period between 1984 and commencement of siphon operation in 1993. This turbidity frequency dataset was used to estimate baseline turbidity. The post-1993 turbidity map (Figure 2.3) depicts the frequency of classification of water pixels as turbid for image dates captured during periods of siphon operation between 1993 and 2010.

Estimating Highest and Lowest Turbidity Post-Siphon Operation

The USACE turbidity frequency datasets were used to derive an estimate of turbidity attributed to siphon operation. This was accomplished by comparing pre- and post-1993

turbidity. The USACE turbidity frequency datasets were reprojected to UTM, Zone 15, GRS 1980, NAD 83 and checked for consistent alignment. For each turbidity frequency map, five classes of water turbidity were identified using natural breaks in ArcGIS, a geographic information system (GIS) software. The highest turbidity classes in the pre- and post-siphon datasets were compared and areas of intersection were removed from the post-siphon turbidity data. The resulting subset provides a map layer representing areas of highest turbidity associated with freshwater flow during siphon operation, thus indicating locations that consistently received distributions of sediment-laden freshwater (Allen *et al*., 2008). This procedure was repeated for the lowest turbidity classes in the pre- and post-siphon datasets to create a map layer delineating areas of lowest turbidity associated with siphon freshwater flow.

Mapping High and Low Freshwater Impacted Marsh Areas

ArcGIS was used to identify marsh areas subject to relatively high and low freshwater impacts. Landsat 5 TM imagery captured April 17, 2011 was reprojected to UTM, Zone 15, GRS 1980, NAD 83 and checked for consistent alignment with the turbidity frequency maps. The imagery was subset to the study area and a land-water map was developed using a hybrid classification method described by Bethel *et al*. (2011) and outlined in Appendix B. A vegetation-only layer was created from the land-water map by masking pixels representing water and developed land. Restricting subsequent remote sensing and geographic information system processing to vegetation-only pixels minimized the influence of non-vegetation pixels and insured that final results were based solely on analysis of pixels classified as marsh vegetation. The vegetation layer was then included in a GIS with the map layers produced from the turbidity frequency data delineating highest and lowest turbidity associated with freshwater flow during siphon operation.

In the GIS environment 15 m buffers were created around areas of highest and lowest turbidity associated with siphon operation. Those areas within the highest turbidity buffers were classified as high freshwater impact areas and those within the lowest turbidity buffers were classified as low freshwater impact areas. Vegetated areas within the highest turbidity buffers were identified as marsh areas most consistently exposed to freshwater introduction, while vegetated areas within the lowest turbidity buffers were identified as marsh areas least impacted by freshwater introduction. Figure 2.4 shows the resulting freshwater impacts map delineating vegetated marsh areas subject to high and low freshwater impacts.

Accuracy Assessment

Hydrographic salinity data obtained from SONRIS were used to assess the accuracy of the freshwater impact map (SONRIS, 2012). Figure 2.5 shows the locations of salinity data collection sites within areas of high and low freshwater impacts. For salinity estimates during siphon operation, 12 salinity data dates were identified as dates of siphon operation nearest the Landsat image capture dates (Table 2.2). For no flow salinity estimates, 71 salinity data dates were identified for periods in which the siphon had not operated for a minimum of 7 days (Table 2.3). Estimates of mean salinity (ppt) during siphon freshwater flow and no flow periods were calculated for the 9 salinity data collection sites in high freshwater impact areas and for the 6 salinity data collection sites in low freshwater impact areas (Table 2.4). All salinity estimates were based on hourly bottom and surface salinity readings. The Mann-Whitney statistical method was used to test for differences in mean salinity in high and low freshwater impact areas during both freshwater flow and no flow periods (VassarStats, 2014).

Results

The spatial distribution of high and low freshwater impact areas depicted on the freshwater impacts map (Figure 2.4) suggests a general reduction in impact with increasing distance from the siphon diversion along a north to south gradient. The location of the Texas Company Canal coincides with a relatively abrupt change from high freshwater impacts north of the canal to low freshwater impacts to the south. In contrast to this general trend, relatively discontinuous and isolated areas of high turbidity were found distant from the siphon to the south and southwest between Bayou Grand Chenier Ridge and Bays Chene Fleur, Batiste, and Sansbois.

Greater fluctuation in mean salinity was observed among high freshwater impact sites compared to low impact sites (Figure 2.6). With the exception of site BA04-12, both high and low freshwater impact sites exhibited greater variation in mean salinity during periods of siphon operation compared to siphon dormancy (Figure 2.7). During siphon flow periods both high and low freshwater impact sites had significantly lower mean salinity ($Z = -3.09$, $P = 0.001$ and $Z = -2.8$, $P = 0.003$, respectively) compared to no-flow periods (Figure 2.8). Although no significant difference was found between high and low freshwater impact sites during periods of siphon dormancy, mean salinity during siphon operation was significantly lower at high freshwater impact sites compared to low impact sites ($Z = -2.65$, $P = 0.004$). The results suggest that siphon operation freshens water throughout the study area, but that water is freshened to a greater extent in areas classified as high freshwater impact areas as compared to areas classified as low impact areas. Furthermore, when salinity data for all dates (freshwater flow and no flow periods) were tested, this finding was replicated. That is, high impact sites were found to be statistically significantly lower in mean salinity than low freshwater impact sites ($Z= -2.42$, $P = 0.008$), suggesting that the overall effect of the siphon is to freshen the high impact areas significantly

more than the low impact areas and also suggesting that this effect may extend beyond siphon operation periods.

Discussion

Level of turbidity derived from satellite image-based turbidity frequency data was effectively used as a proxy for freshwater impacts to delineate areas most and least impacted by operation of the WPH siphon diversion project. The resulting freshwater impacts map accurately identified high and low impact areas based on corresponding time series salinity data. Analysis of salinity data showed that high impact areas were significantly fresher than low impact areas during siphon operation. Although there was no significant difference in mean salinity during siphon dormancy, high impact areas continued to show significantly lower mean salinity when all dates (during siphon flow and no flow periods) were tested, further supporting the results of the freshwater impacts classification. The spatial distribution of high and low freshwater impact areas agrees with previous findings showing increases in mean salinity along a north to south gradient in the WPH outfall area during siphon operation (Richardi, 2013; Boshart and Van Cook, 2004). The spatial distribution also suggests that siphon impacts generally decrease as distance to the siphon increases, in agreement with Day *et al*. (2009a), who found that suspended sediments in pulsed freshwater introduced by the Caernarvon diversion decreased with increasing distance from the diversion structure.

Discontinuous and isolated areas of high turbidity south and southwest of Bayou Grand Chenier Ridge are exceptions to the general trend of decreasing impact with increasing distance from the siphon (Figure 3). One possible explanation is that those areas may be undergoing increasing vegetation loss and soil erosion since commencement of siphon operation, thereby contributing to greater turbidity in adjacent waterways. Marsh fragmentation, degradation, and

loss in those areas are likely associated with marsh ponding, the perforation of once unbroken marsh with small ponds (Bethel *et al*., 2011). Water in shallow marsh ponds may exhibit higher turbidity due to bank erosion as well as wind induced bottom sediment mixing.

It should also be noted that during seasonal high river stage, freshening of the Barataria Basin by WPH siphon operation is augmented by Mississippi River waters that flow into the basin from the mouth of the river. This introduction of freshwater from the south may also help to explain areas classified as high impact on the freshwater impacts map that are exceptions to the general trend. Although the effects of seasonal freshening from the south are not quantified here, siphon flow and no flow dates used in this study are representative of all seasons. Based on the current results showing a north to south gradient of freshening effects, confirmed by Richardi (2013) and Boshart and Van Cook (2004), seasonal freshening effects from the south are assumed to have a minimal effect in terms of classifying high and low freshwater impact areas.

Also of interest is the relatively high degree of fluctuation in mean salinity related to siphon operation and observed throughout the study area, but especially in high freshwater impact areas. While disturbances are recognized as an intrinsic part of ecosystem dynamics and a source of heterogeneity (Sousa, 1984; Lee and Brown, 2011), studies suggest that thresholds exist, which when reached, usher in ecosystem regime changes representing alternative stable states (Scheffer *et al*., 2001; Carpenter *et al.*, 2011). The observed fluctuation in salinity throughout the study area suggests the possibility that ecosystem regime changes may be occurring based on a freshwater introduction threshold. Intermittent operation of the siphon may be causing alternative stable states that disrupt and undermine the stability of the ecosystem and adversely affect flora and fauna within the study area. Consistent, well informed management strategies for siphon operation are needed to avoid exacerbating ecosystem instability and

wetland degradation and to meet the intended goals of the siphon projects to combat saltwater intrusion and stimulate marsh growth.

Conclusions

Satellite image-based turbidity frequency data can be used to accurately differentiate marsh areas experiencing high and low freshwater impacts associated with siphon operations in coastal Louisiana wetlands. Turbidity reflectance levels can be effectively used as a proxy for freshwater impacts to identify wetland areas most frequently and least frequently exposed to turbid Mississippi River water due to siphon operation. The ability to accurately model relatively high and low freshwater impact areas can aid in identifying optimal sample sites for closer monitoring of possible eutrophication related to freshwater siphon diversions. The results of this study suggest that effective monitoring of freshwater impacts and consistent management of siphon operation are needed to avoid exacerbating ecosystem instability and to aid in promoting the health and vitality of wetland ecosystems receiving introduced freshwater.

References

Allen, Y.C.; Constant, G.C., and Couvillion, B.R., 2008. Preliminary classification of water areas within the Atchafalaya Basin Floodway System by using Landsat imagery: U.S. Geological Survey Open-File Report 2008-1320, 14p. URL: http://pubs.usgs.gov/of/2008/1320/

ASTM-International, 2003. D1889-00 Standard test method for turbidity of water. In A. International (Ed.), Annual Book of ASTM Standards, Water and Environmental Technology. Pennsylvania: West Conshohocken.

Barras, J.A.; Beville, S.; Britsch, D.; Hartley, S.; Hawes, S.; Johnston, J.; Kemp, P.; Kinler, Q.; Martucci, A.; Porthouse, J.; Reed, D.; Roy, K.; Sapkota, S., and Suhayda, J., 2003. Historical and projected coastal Louisiana land changes: 1978-2050. U.S. Geological Survey Open-File Report 03-334, 39p.

Barras, J.A., 2009. Land area change and overview of major hurricane impacts in coastal Louisiana, 2004-08. Scientific Investigations Map 3080. Reston, Virginia: U.S. Geological Survey, scale 1:250,000, 6 sheets.

Bethel, M.B.; Brien, L.F.; Danielson, E.J.; Laska, S.B.; Troutman, J.P.; Boshart, W.M.; Giordino, M.J., and Maurice A. Phillips, 2011. Blending Geospatial Technology and Traditional Ecological Knowledge to Enhance Coastal Restoration Decision-Support Processes in Coastal Louisiana. Journal of Coastal Research, 27(3), 555-571.

Boshart, W.M., and Van Cook 2004. 2004 Operations, Maintenance, and Monitoring Report for West Pointe a la Hache Siphon Construction (BA-04), Louisiana Department of Natural Resources, Coastal Restoration Division, New Orleans, Louisiana. 18p.

Boshart, W.M., and Van Cook, P.E., 2007. 2005 Operations, Maintenance, and Monitoring Report for West Pointe a la Hache Siphon Construction (BA-04). Louisiana Department of Natural Resources, Coastal Restoration Division and Coastal Engineering Division, New Orleans, Louisiana. 18p.

Boustany, R.G., 2010. Estimating the benefits of freshwater introduction into coastal wetland ecosystems in Louisiana: Nutrient and sediment analyses. Ecological Restoration, 28(2), 160-174.

Carpenter, S.R.; Cole, J.J.; Pace, M.L.; Batt, R.; Brock, W.A.; Cline, T.; Coloso, J.; Hodgson, J.R.; Kitchell, J.F.; Seekell, D. A.; Smith, L., and Weidel, B., 2011. Early warnings of regime shifts: a whole-ecosystem experiment. Science, 332, 1079-1082.

Cloern, E.C., 2001. Our evolving conceptual model of the coastal eutrophication problem. Marine Ecology Progress Series, 210, 223-253.

Conner, W.H. and Day, J.W. Jr., (ed.), 1987. The Ecology of Barataria Basin, Louisiana: an Estuarine Profile. Coastal Ecology Institute, Center for Wetland Resources, Louisiana State University, Baton Rouge, Louisiana, Biological Report 85, 7-13.

Darby. F.A. and Turner, R.E., 2008(a). Below- and aboveground Spartina alterniflora production in a Louisiana salt marsh. Estuaries and Coasts, 31, 223-231.

Darby, F.A. and Turner, R.E., 2008 (b). Effects of eutrophication on salt marsh root and rhizome biomass accumulation. Marine Ecology Progress Series, 363, 63-70.

Day, J.W.; Cable, J.E.; Cowan, J.H., Jr.; DeLaune, R.; de Mutsert, K.; Fry, B.; Mashriqui, H.; Justic, D.; Kemp, P.; Lane, R.R.; Rick, J.; Rick, S.; Rozas, L. P.; Sneddens, G; Swenson, E.; Twilley, R.R., and Wissel, B., 2009 (a). The impacts of pulsed reintroduction of river water on a Mississippi delta coastal basin. The Journal of Coastal Research, 54, 225-243.

Day, J.; Lane, R.; Moerschbaecher, M.; DeLaune, R; Twilley, R.; Mendelssohn, I., and Baustian, J., 2009 (b). The impact of the Caernarvon diversion on above and belowground marsh biomass in the Breton Sound Estuary after Hurricane Katrina. Final Report submitted to the Louisiana Department of Natural Resources, Project 2512-07-01.

Doxaran, D.; Ruddick, K.; McKee, D.; Gentili, B.; Tailliez, D.; Chami, M., and Babin, M., 2009 Spectral variations of light scattering by marine particles in coastal waters, from visible to near infrared. Limnology and oceanography, 54(4), 1257.

Fraser, R.N., 1998. Multispectral remote sensing of turbidity among Nebraska Sand Hills lakes. International Journal of Remote Sensing, 19(15), 3011-3016.

Froidefond, J.; Gardel, L.; Guiral, D.; Parra, M., and Ternon, J.F., 2002. Spectral remote sensing reflectances of coastal waters in French Guiana under the Amazon influence. Remote sensing of Environment, 80(2), 225-232.

Güttler, F.N.; Niculescu S., and Gohin, F., 2013. Turbidity retrieval and monitoring of Danube Delta waters using multi-sensor optical remote sensing data: An integrated view from the delta plain lakes to the western–northwestern Black Sea coastal zone. Remote Sensing of Environment, 132, 86-101.

Harrington J.A.; Schiebe, F.R., and Nix, J.F., 1992. Remote sensing of Lake Chicot, Arkansas: monitoring suspended sediments, turbidity, and secchi depth with Landsat MSS data. Remote Sensing of Environment, 39(1), 15-27.

Haywood III, E.L., and Boshart, W.M., 1998. West Pointe a la Hache freshwater Diversion: three-year comprehensive report. Louisiana Department of Natural Resources/Coastal Restoriation Division, Baton Rouge, LA, USA. Monitoring Series No. BA-04-MSTY-0498-1.

Howes, N.C.; FitzGerald, D.M.; Hughes, Z.J.; Georgiou, I.Y.; Kulp, M.A.; Miner, M.D.; Smith, J.M., and Barras, J.A., 2010. Hurricane-induced failure of low salinity wetlands. Proceedings of the National Academy of Sciences of the United States of America, www.pnas.org/cgi/doi/10.1073/pnas.0914582107

Kauth, R.J., and Thomas, G.S., 1976. The tasselled cap-a graphic description of the spectral-temporal development of agricultural crops as seen by Landsat. LARS Symposia, Paper 159.

LaCoast. (2008). CWPPRA Restoration Status. URL: http://www.lacoast.gov/reports/rtc/1997/7.htm

Lane, R., and Day, J., 1999. Water quality analysis of a Freshwater Diversion at Caernarvon, Louisiana. Estuaries, 22(2A), 327-336.

Lee, S., and Brown, M.T., 2011. Understanding self-organization of ecosystems under disturbance using a microcosm study. Ecological Engineering, 37, 1747-1756.

Li, R.R.; Kaufman, Y.J.; Gao, B.C., and Davis, C.O., 2003. Remote sensing of suspended sediments and shallow coastal waters. Geoscience and Remote Sensing, IEEE Transactions on, 41(3), 559-566.

Lillesand, T.M; Kiefer, R.W., and Chipman, J.W., 2004. Remote Sensing and Image Interpretation, 5th edition. Hoboken, NJ: John Wiley and Sons, Inc., 19p.

Lissner, J.; Mendelssohn, I.; Lorenzen, B.; Brix, H.; McKee, K., and Miao, S., 2003. Interactive Effects of Redox Intensity and Phosphate Availability on Growth and Nutrient Relations of Cladium Jamaicense (Cyperaceae). American Journal of Botany, 90(5), 736-748.

Lodhi, M.; Rundquist, D.C.; Han, L., and Kuzila, M.S., 1997. The potential for remote sensing of loess soils suspended in surface waters1." JAWRA Journal of the American Water Resources Association, 33(1), 111-117.

Lopez, J. A., 2009. The Environmental History of Human-Induced Impacts to the Lake Pontchartrain Basin in Southeastern Louisiana since European Settlement – 1718 to 2002. Journal of Coastal Research, 54, 1-11.

Miller, R.L., and McKee, B.A., 2004. Using MODIS Terra 250 m imagery to map concentrations of total suspended matter in coastal waters. Remote sensing of Environment, 93(1), 259-266.

Mitsch, W.; Day, J.; Zhang, L., and Lane, R., 2005. Nitrate-nitrogen retention in wetlands in the Mississippi River Basin. Ecological Engineering, 24, 267-278.

OCPR (Office of Coastal Protection and Restoration), 2010. URL: http://www.ocpr.louisiana.gov/CRM/coastres/project.asp?id=BA-04

Richardi, D.C., 2013. 2012 Operations, Maintenance, and Monitoring Report for West Pointe a la Hache Siphon Construction (BA-04), Coastal Protection and Restoration Authority of Louisiana, New Orleans, Louisiana, 35p.

Scheffer, M.; Carpenter, S.; Foley, J.A.; Folke, C., and Walker, B., 2001. Catastrophic shifts in ecosystems. Nature, 413, 591-596.

Siciliano, E.; Wasson, K.; Potts, D.C., and Olsen, R.C., 2008. Evaluating hyperspectral imaging of wetland vegetation as a tool for detecting estuarine nutrient enrichment. Remote Sensing of Environment, 112, 4020-4033.

Sklar, F., and Browder, J., 1998. Coastal Environmental Impacts Brought About by alterations to Freshwater Flow in the Gulf of Mexico. Environmental Management, 22(4), 547-562.

SONRIS, 2011, 2012. Coastal Protection and Restoration Authority of Louisiana, Louisiana Department of Natural Resources, http://sonlite.dnr.state.la.us/

Sousa, W.P., 1984. The role of disturbance in natural communities. Annual Review of Ecology and Systematics, 15, 353-391.

Turner, R.E.; Howes, B.L.; Teal, J.M.; Milan, C.S.; Swenson, E.M., and Tonerb, D.D., 2009. Salt marshes and eutrophication: An unsustainable outcome. Limnology and Oceanography, 54(5), 1634.

VassarStats: Website for Statistical Computation, 2014. http://vassarstats.net/

Volpe, V.; Silvestri S., and Marani, M., 2011. Remote sensing retrieval of suspended sediment concentration in shallow waters. Remote Sensing of Environment, 115(1), 44-54.

Figure 2.1 Location of the approximately 138 km² study area in the Barataria Basin (adapted from ArcGIS basemap with April 17, 2011 Landsat 5 TM image overlay).

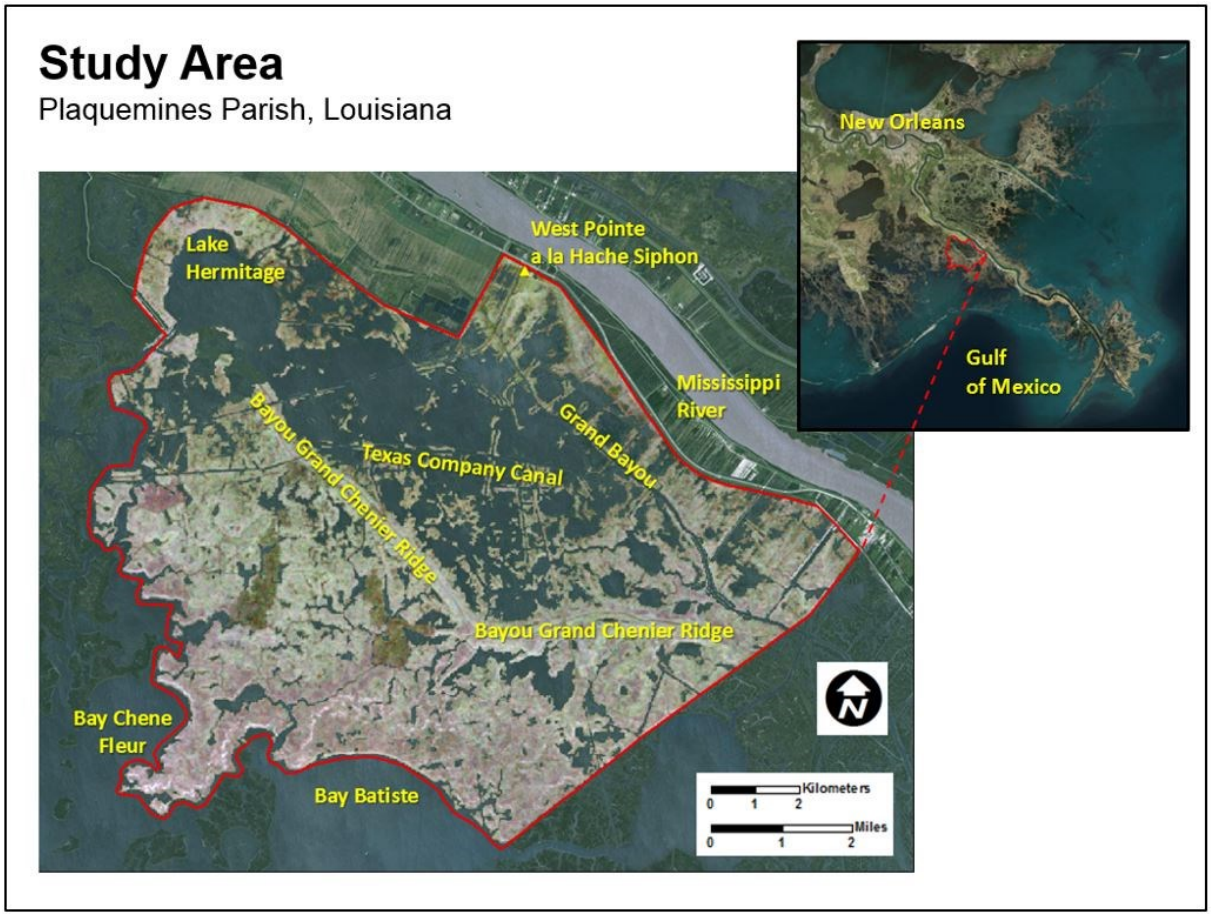

Figure 2.2 Pre-1993 turbidity map adapted from USACE turbidity frequency data.

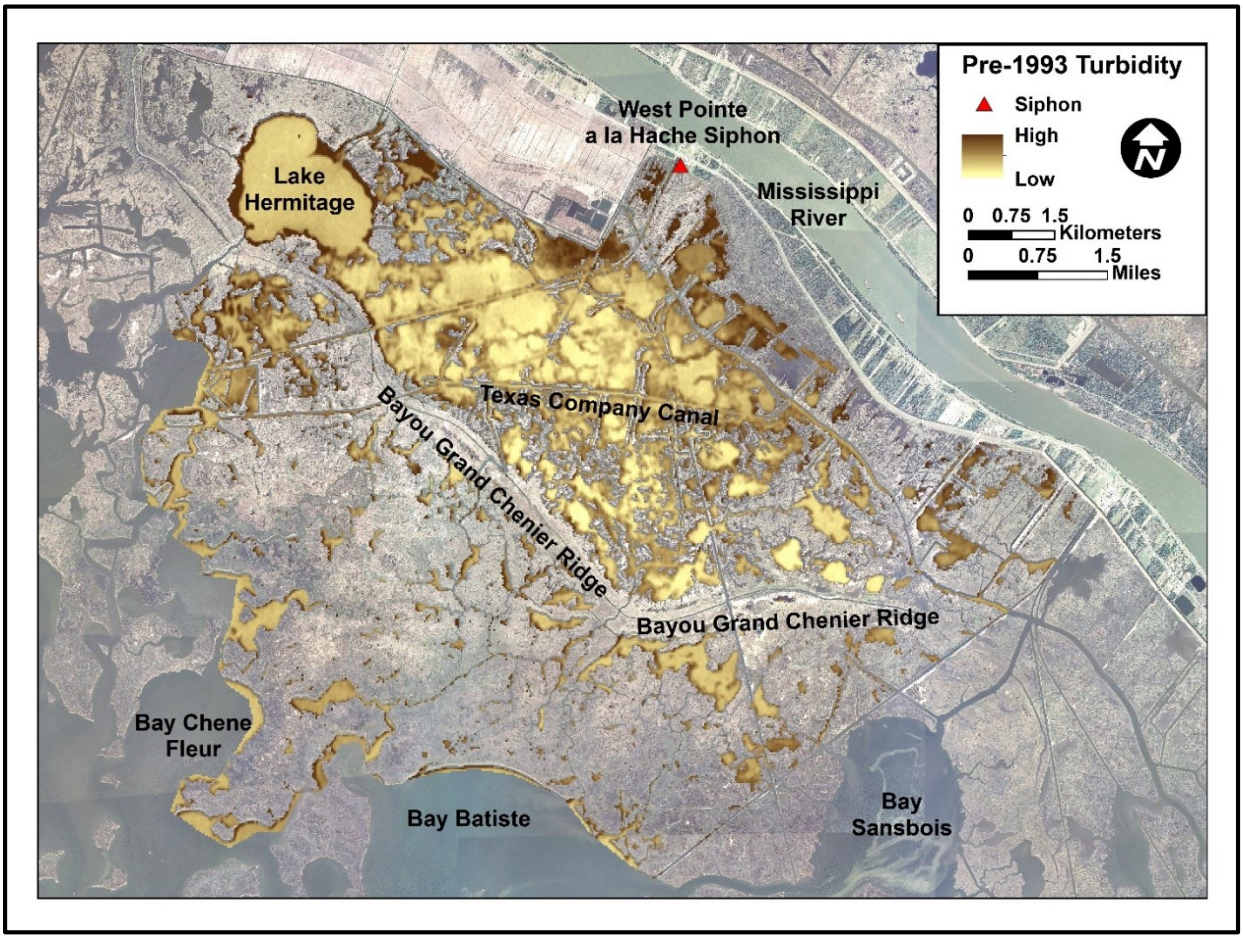

Figure 2.3 Post-1993 turbidity map adapted from USACE turbidity frequency data.

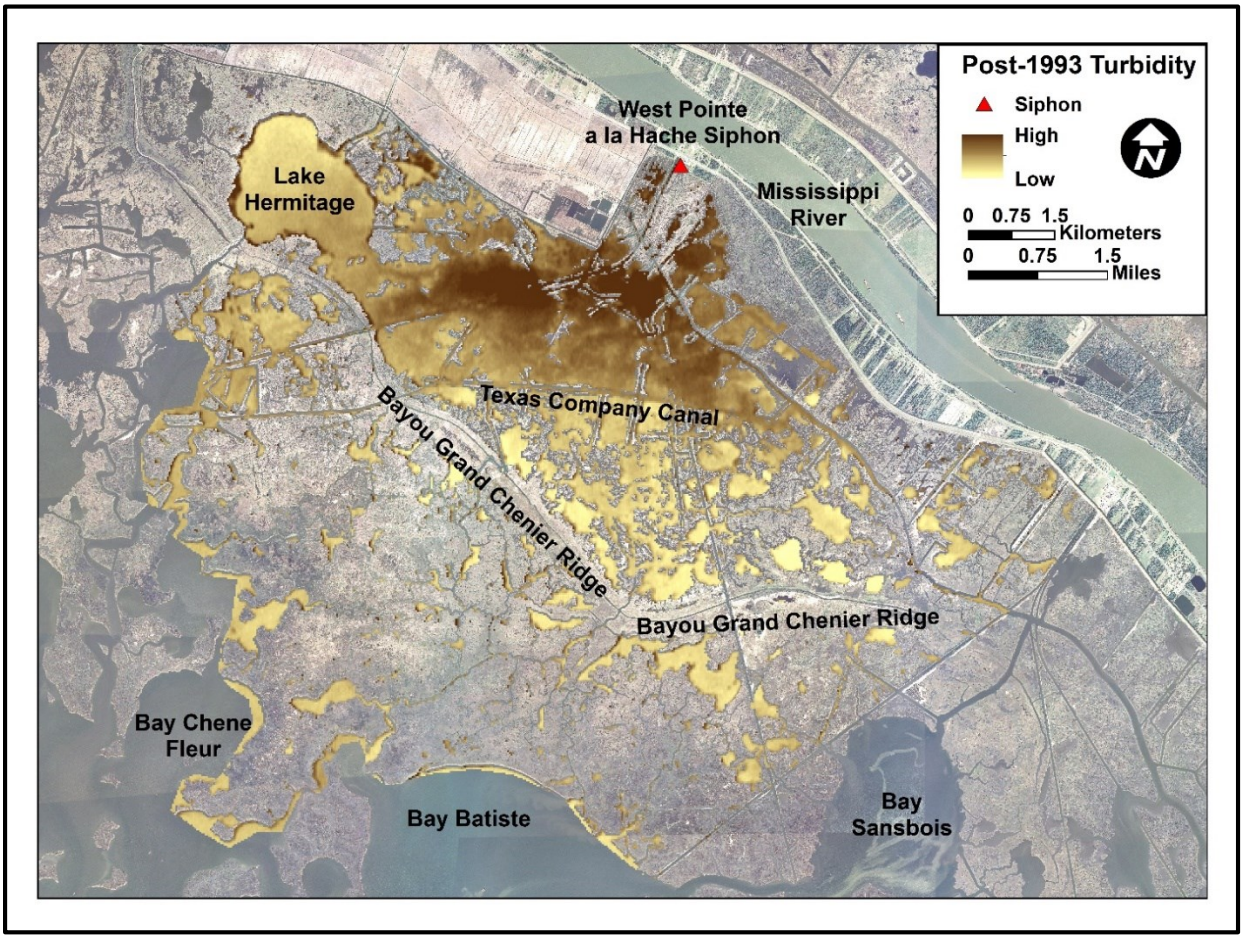

Figure 2.4 Map of study area delineating vegetated marsh areas subject to high and low freshwater impacts.

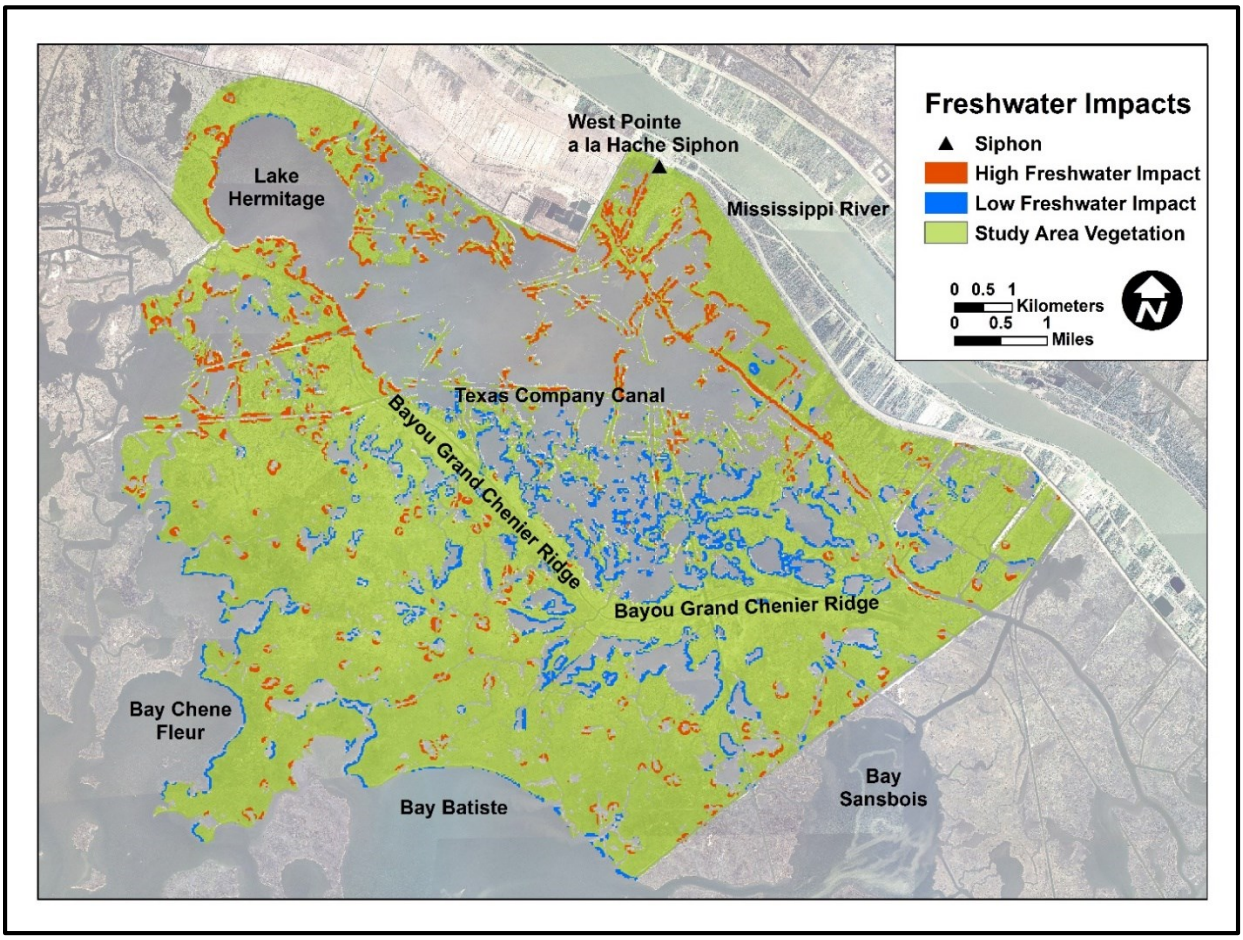

Figure 2.5 Map of study area showing salinity data collection sites in consistently high and low freshwater impact areas.

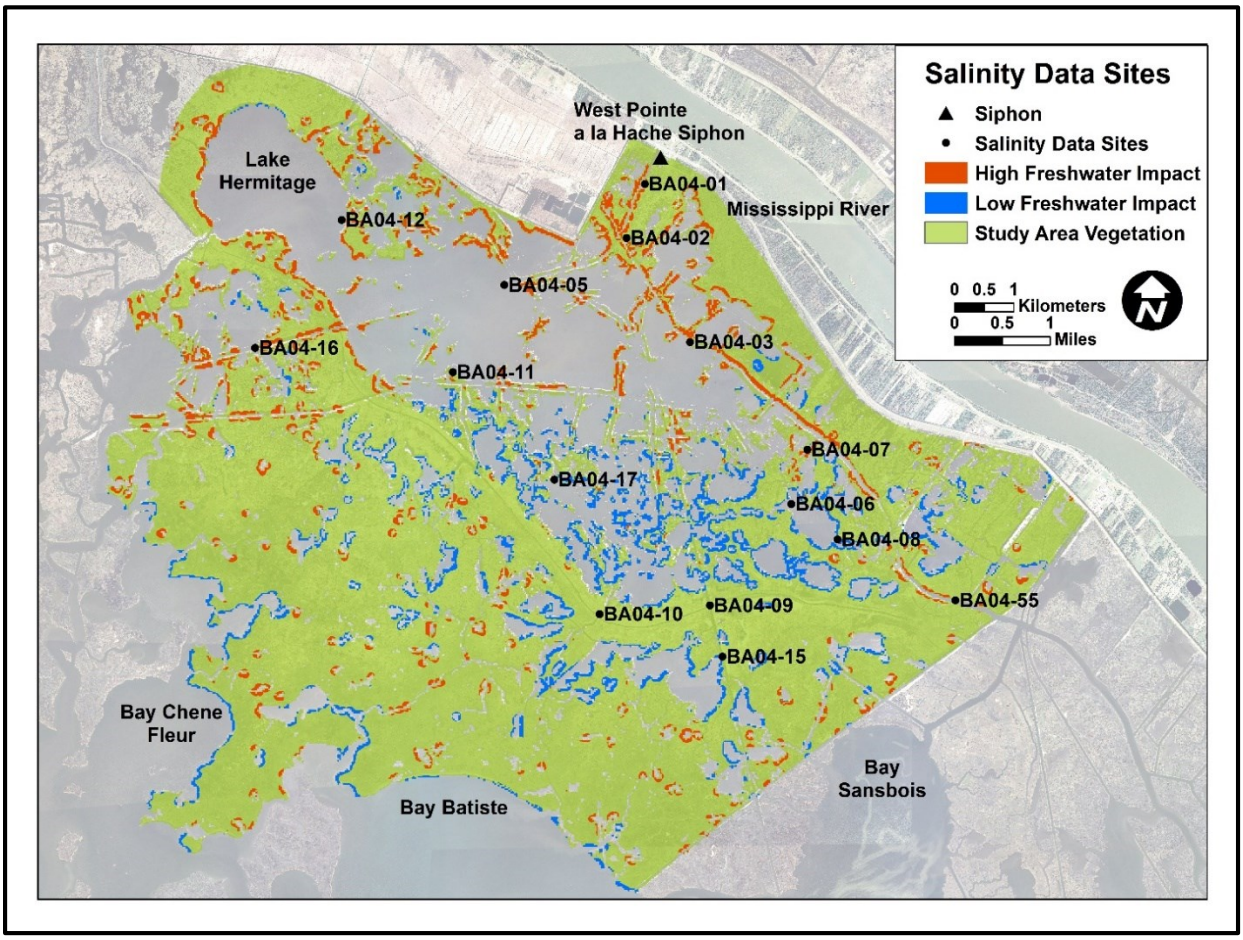

Figure 2.6 Distribution of mean salinity at high and low impact sites during siphon operation and siphon dormancy.

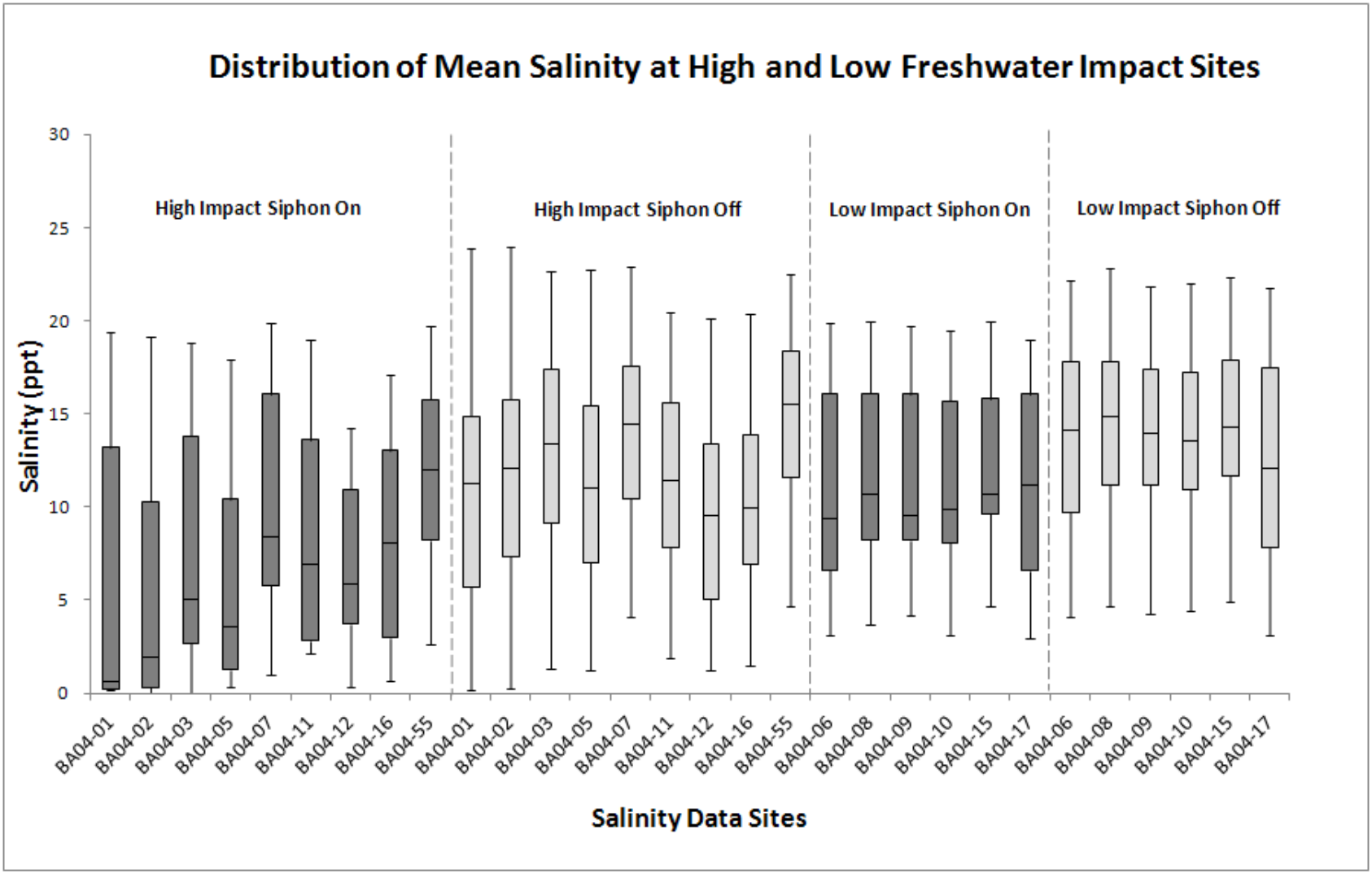

Figure 2.7 Standard deviation of mean salinity at high and low freshwater impact sites during siphon operation and dormancy.

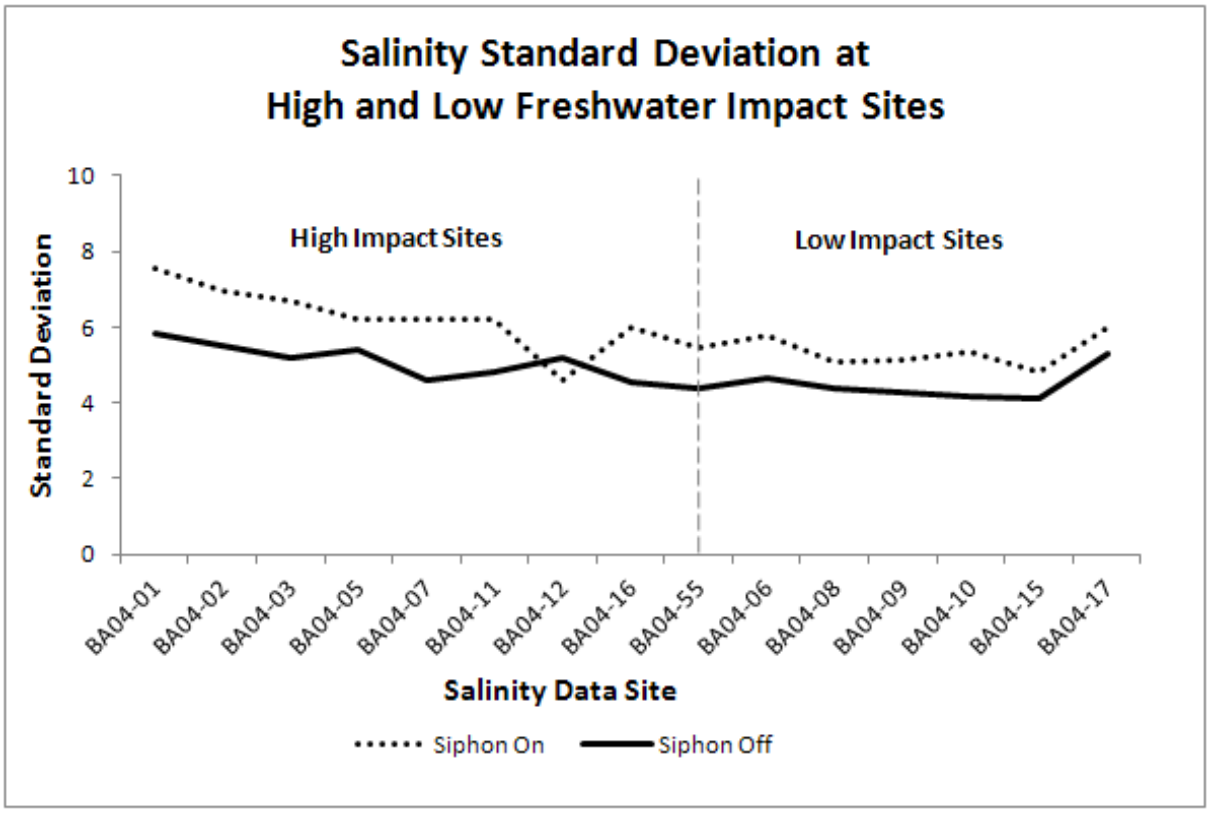

Figure 2.8 Mean salinity at high and low freshwater impact sites during siphon operation and dormancy.

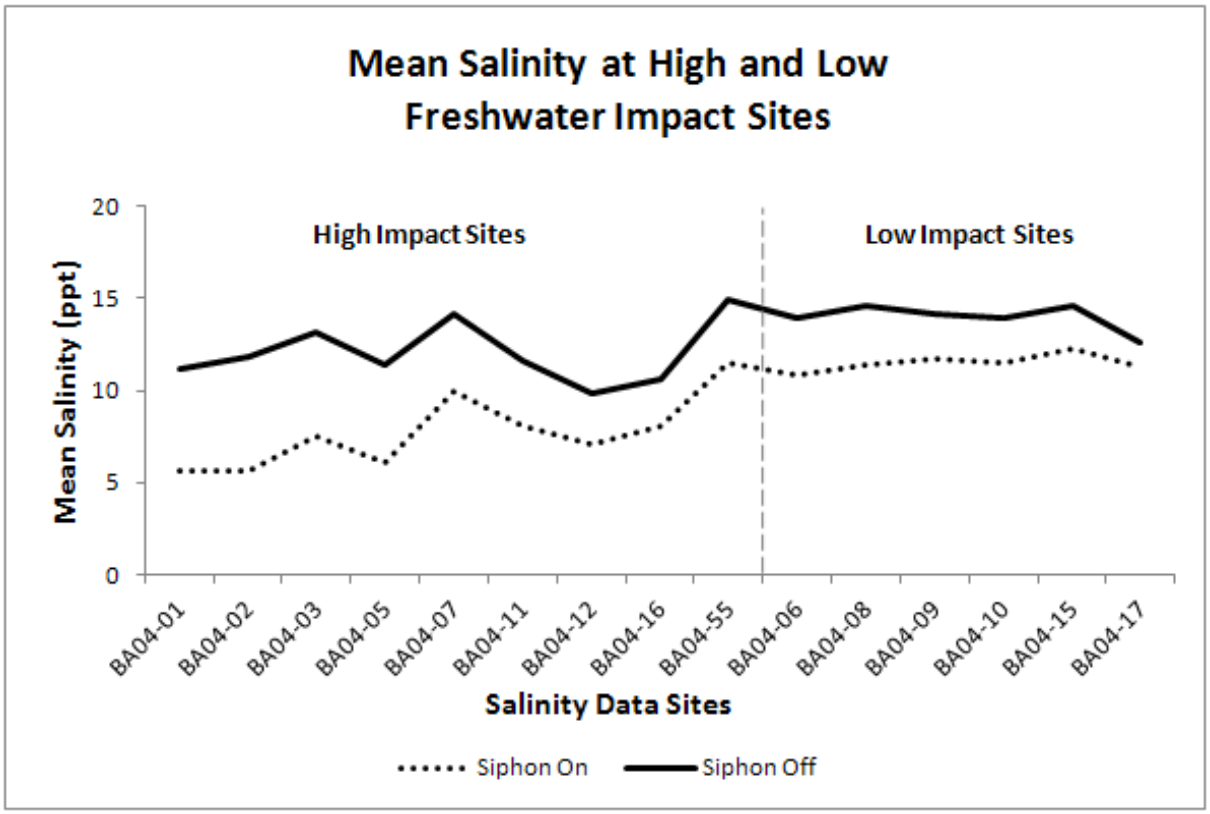

Table 2.1 Pre- and post-siphon operation satellite image dates and associated freshwater flows at WPH siphon diversion project.

Pre-siphon operation (no flow)	Post-siphon operation	
Satellite image dates	Satellite image dates	Freshwater flow (cfs)
04/06/1984	04/02/1994	2023.82
01/19/1985	09/25/1994	118.80
10/08/1987	04/07/1996	1519.67
01/28/1988	02/08/1998	787.01
2/13/1988	02/24/1998	903.08
11/01/1990	01/26/1999	1311.58
11/17/1990	04/18/2000	721.22
03/09/1991	09/17/2000	777.25
02/08/1992	11/20/2000	783.88
10/05/1992	02/27/2002	1327.31
	10/20/2003	1057.15
	02/25/2010	530.66

Table 2.2 Twelve satellite image dates during siphon operation and nearest salinity data dates.

Satellite image dates/ siphon operating	Nearest salinity data dates
04/02/1994	03/29/1994
09/25/1994	09/13/1994
04/07/1996	04/02/1996
02/08/1998	02/17/1998
02/24/1998	02/17/1998
01/26/1999	01/25/1999
04/18/2000	04/18/2000
09/17/2000	09/28/2000
11/20/2000	11/21/2000
02/27/2002	03/07/2002
10/20/2003	10/13/2003
02/25/2010	03/03/2010

Table 2.3 Seventy-one salinity data dates corresponding to no flow periods (siphon not operating for at least 7 days prior to each salinity data date).

No flow dates with available salinity data		
10/11/1994	10/12/1999	01/16/2006
11/09/1994	11/16/1999	02/24/2006
12/07/1994	12/14/1999	03/28/2006
01/04/1995	01/19/2000	04/28/2006
02/15/1995	02/22/2000	05/26/2006
03/14/1995	05/02/2001	06/27/2006
04/10/1995	08/15/2001	07/28/2006
04/26/1995	09/04/2001	08/31/2006
05/23/1995	10/08/2001	09/27/2006
06/06/1995	10/26/2001	10/24/2006
06/07/1995	08/16/2002	08/27/2007
06/22/1995	09/03/2002	10/02/2007
10/17/1995	10/10/2002	11/01/2007
11/02/1995	11/07/2002	11/30/2007
11/14/1995	12/28/2002	12/28/2007
12/12/1995	07/17/2003	08/22/2008
01/17/1996	08/18/2003	09/26/2008
09/16/1997	09/03/2003	10/28/2008
10/21/1997	09/10/2004	12/03/2008
11/17/1997	10/13/2004	01/07/2009
12/16/1997	11/09/2004	02/16/2009
03/16/1999	10/14/2005	10/15/2009
08/25/1999	11/21/2005	10/14/2010
09/16/1999	12/19/2005	

Table 2.4 Mean salinity for high and low freshwater impact sites by siphon flow.

High freshwater impact sites	Low freshwater impact sites	Mean salinity (ppt) (siphon flow)	Mean salinity (ppt) (no siphon flow)
BA04-01	-	5.68	11.13
BA04-02	-	5.59	11.89
BA04-03	-	7.57	13.18
BA04-05	-	6.13	11.38
BA04-07	-	9.90	14.17
BA04-11	-	8.11	11.64
BA04-12		7.07	9.83
BA04-16	-	8.13	10.64
BA04-55	-	11.53	14.91
-	BA04-06	10.85	13.96
-	BA04-08	11.42	14.64
-	BA04-09	11.70	14.16
-	BA04-10	11.49	13.97
-	BA04-15	12.24	14.59
-	BA04-17	11.33	12.59

Chapter 3 - **Optimal DigitalGlobe and Spectroradiometer Band Combinations and Vegetation Indices for Modeling Biophysical Characteristics Related to Nutrient Enrichment of a Coastal Louisiana Marsh**

Abstract

This study was conducted to evaluate the relationships between vegetation biophysical characteristics and spectral reflectance patterns associated with a coastal Louisiana marsh impacted by the introduction of turbid Mississippi River water. The primary goal was to use field spectra and DigitalGlobe WorldView 2 (DG-WV2) satellite image data to identify the bands and vegetation indices most highly correlated with field measurements of vegetation parameters associated with wetland nutrient enrichment. To accomplish this goal, measurements of Leaf Area Index (LAI), plant height, and chlorophyll concentration were collected across vegetation productivity and freshwater impact gradients and correlated with spectral data. The Atmospherically Resistant Vegetation Index (ARVI) using DG-WV2 near infrared image band 8 (860-1040 nm) was optimal for estimating chlorophyll concentration, but no bands or indices correlated well with LAI or plant height. The resulting spatial distribution of estimated chlorophyll concentration was related to proximity to the source of introduced freshwater, with chlorophyll concentration decreasing with increasing distance from the freshwater source. Additionally, areas most consistently impacted by freshwater introduction were associated with high chlorophyll concentration, while least impacted areas were associated with low chlorophyll concentration. These results suggest that remotely sensed imagery combined with field measured vegetation parameters hold promise for effectively identifying freshwater impacted marsh areas vulnerable to eutrophication.

Introduction

Louisiana's coastal wetlands are rapidly degrading and disappearing due to natural and anthropogenic causes. Artificial flood control levees have effectively isolated the Mississippi River from its delta, exacerbating natural subsidence, erosion and storm effects (Lopez, 2009; Day *et al*., 2009a). The construction of extensive networks of canals for oil and gas exploration and the extraction of natural resources have also contributed to subsidence and erosion and promoted saltwater intrusion into Louisiana's freshwater marshes (Lopez, 2009; Day *et al*., 2009a). Over the last half century a major strategy for reducing or reversing wetland loss in Louisiana has been the construction of river diversions designed to reintroduce freshwater from the Mississippi River into wetland ecosystems to combat saltwater intrusion and stimulate marsh growth (Day *et al*., 2009a). During this same period, runoff of fertilizers, pesticides and other pollutants from agricultural and urban areas has increased, adversely affecting water quality in the rivers and streams of the 3 million km^2 Mississippi River Basin (Cloern, 2001; Mitsch, *et al.*, 2005; Siciliano, *et al.*, 2008). Excess nitrogen, in the form of nitrate-nitrogen, is transported in the Mississippi River to coastal areas in Louisiana, where the subtropical climate, associated warm water temperatures, and long growing season facilitate high nutrient uptake and denitrification rates (Mitsch, *et al.,* 2005). Since Louisiana's river diversions introduce nutrient enriched Mississippi River water and sediment into wetland areas, eutrophication is a major concern (Sklar and Browder 1998; Lissner *et al.*, 2003; Lane and Day, 1999; Mitsch *et al.,* 2005; Day *et al*., 2009a). Eutrophication generally refers to gradual nutrient enrichment in water bodies (Christropherson, 2009; Ferreira *et al*., 2011), but when loading rates are very high, nutrients also accumulate in soils and vegetation (Dettmann, 2001; Kamer *et al.*, 2001). In the

presence of excessive nutrient loadings, wetland ecosystem processes are altered, resulting in measurable changes in plant productivity, including increases in net primary productivity (U.S. EPA, 2002; Ferreira *et al*., 2011). Functional indicators of eutrophication include increased biomass production and stem height, and increased leaf nitrogen and phosphorus content (U.S. EPA, 2002), all of which are associated with increased chlorophyll content. Additionally, Haboudane *et al*. (2002) found that estimates of chlorophyll concentration based on leaf and canopy spectra can provide a proxy measurement of N content. Several studies have shown however, that despite increased above ground biomass, excess nutrient loading in salt marshes reduces below ground plant growth, root and rhizome biomass, and carbon accumulation, decreasing geomorphic stability and causing significant loss in marsh elevation (Darby and Turner, 2008a, 2008b; Turner *et al.*, 2009; Turner, 2010; Deegan *et al.*, 2012). Day *et al.* (2009a) challenged Darby and Turner's (2008a; 2008b) results based on a synthesis of previous studies showing that the loading rates they used far exceeded nutrient loading rates in the outfall area of the Caernarvon, Louisiana river diversion. Day *et al.* (2009b) also reported finding high belowground biomass in marshes impacted by the river diversion at Caernarvon, Louisiana. Yet, Howes *et al.* (2010) reported preferential erosion in response to Hurricanes Katrina and Rita in Louisiana marshes that received diverted freshwater for 18 years prior to those storm events. Despite the lack of consensus, studies of the effects of river diversions on nutrient enrichment and eutrophication of Louisiana's wetlands have been limited (Day *et al.*, 2009a; Boustany, 2010).

One strategy for detecting and monitoring nutrient enrichment of wetland ecosystems is to characterize nutrient dynamics through periodic water sampling performed weekly or monthly, a strategy that may not fully capture the effects of nutrient pulsing (Siciliano, *et al.*,

2008). Since estuarine plant tissues integrate the nutrient regime over time, another approach is to harvest plant tissues seasonally to examine nutrient content as an indicator of eutrophication (Boyer and Fong, 2005; Cohen and Fong, 2006; Siciliano, *et al.*, 2008). When applied over large areas in wetland environments, both strategies are resource intensive and often impractical in terms of safety and accessibility (Siciliano, *et al.*, 2008; Bethel, *et al*., 2011). Since data are generally collected from the most easily accessible sites during a limited number of campaigns, the value of the data may be limited both spatially and temporally, often requiring interpolation over large areas and extended time periods (Siciliano, *et al.*, 2008; Volpe *et al.,* 2011).

Remote sensing offers a practical, but underutilized approach for monitoring nutrient enrichment and eutrophication of coastal Louisiana marshes. Analysis of spectral reflectance data has proven useful for assessing vegetation biophysical characteristics, including biomass and nutrient content (Hardisky *et al.*, 1984; Hardisky *et al*., 1986; Guo and Price, 2000; Rundquist *et al.*, 2001; Siciliano, *et al.*, 2008). Working in a wetland environment Hardisky *et al*. (1984) found that biomass estimates based on *in situ* indices were comparable to estimates from traditional harvest techniques. In a 1986 study of salt marsh vegetation, Hardisky *et al.* again used field spectroradiometer data to find that biomass and plant canopy height were significantly correlated with red and near infrared (NIR) spectral reflectance of salt marsh vegetation species, replicating earlier findings of high correlation between spectral data and green biomass. A 1998 study by Jensen *et al*. found that non-intrusive *in situ* LAI measurements of salt marsh vegetation were significantly correlated with *in situ* above-ground biomass measurements, suggesting that field sampling of biomass can be obtained using non-destructive means. Results of a 2002 study by Jensen *et al*. again found that the NIR band and selected vegetation indices, including the Normalized Difference Vegetation Index (NDVI), were highly

correlated with biomass, LAI, and chlorophyll concentration in an estuarine salt marsh. In support of these findings, strong correlations between NDVI and plant primary productivity, NDVI and biomass, and NDVI and LAI have been reported in the literature (Tucker and Sellers, 1986; Justice *et al*., 1998, and Wang *et al*., 2004).

The utility of NDVI is based on the difference between low red reflectance and high NIR reflectance of healthy vegetation (Gitelson *et al*., 1996; Gitelson 2004). Once red reflectance saturates at its lowest level, however, there is little change in NDVI even as NIR reflectance increases (Gitelson *et al*., 1996; Gitelson, 2004). The result is reduced sensitivity to changes in green biomass when vegetation density is moderate to high (Gitelson, 2004). Other indices developed in response to the observed saturation of NDVI and of particular interest for wetland vegetation studies include the Green Normalized Difference Vegetation Index (GNDVI), developed by Gittelson *et al*. (1996), the Wide Dynamic Range Vegetation Index (WDRVI), developed by Gittelson (2004), and the Atmospherically Resistant Vegetation Index (ARVI), developed by Kaufman and Tanre (1992). The GNDVI, which replaces the green band for the red band in the NDVI, has been used to successfully assess biomass variation (Gittelson *et al*., 1996; Vigier *et al*., 2004). The WDRVI enhances the dynamic range of the NDVI using a weighting parameter based on vegetation density characteristics within a study area (Gittelson, 2004). The ARVI has been shown to be slightly more sensitive to vegetation changes and less sensitive to atmospheric and soil affects than other indices in the presence of moderate to high vegetation cover (Qi *et al*., 1994). Each of these indices has been used to successfully characterize spatial patterns of salt marsh biomass (Gitelson *et al.*, 1996; Zhang *et al*., 1997; Gitelson, 2004), suggesting their utility for delineating regions of high marsh biomass relative to introduced nutrient rich freshwater based on remotely sensed data.

Research to develop effective methods for assessing and monitoring nutrient enrichment of Louisiana's coastal wetlands is needed. This study was conducted to evaluate the relationships between vegetation biophysical characteristics and spectral reflectance patterns associated with a coastal Louisiana marsh receiving freshwater from the Mississippi River. The primary goal was to use field spectra and satellite image data to identify bands and vegetation indices most highly correlated with field measurements of vegetation parameters that respond rapidly to nutrient enrichment. The ability to accurately map potentially eutrophic and relatively unenriched wetland areas allows for more informed and efficient sample collection protocols and contributes to effective assessment and monitoring of eutrophication associated with freshwater introduction into Louisiana's wetland ecosystems.

Study Area

The study area (Figure 3.1) is an approximately 138 km^2 portion of the Barataria Basin in Lower Plaquemines Parish, Louisiana. The Barataria Basin is an interdistributary estuarine wetland system of the Mississippi Delta severely impacted by wetland degradation and loss, having experienced some of the highest rates of land loss in Louisiana's coastal zone (Conner and Day, 1987; Bethel *et al*., 2011). Within the Barataria Basin, wetland vegetation is characterized by a progression of fresh, brackish, intermediate and salt marshes, moving to open water (Conner and Day, 1987). The study area within the basin is bordered by the Mississippi River to the east and stretches beyond the Bayou Grand Chenier ridge toward the open waters of Barataria Bay to the west. It incorporates both highly degraded and fragmented marsh areas north and northeast of Bayou Grand Chenier Ridge, as well as relatively intact core marsh west and southwest of the ridge, a juxtaposition allowing compelling comparisons. Land within the study area is generally characterized by high density marsh vegetation. It is generally dominated

by salt tolerant species, such as *Spartina alterniflora, Spartina patens,* and *Distichlis spicata*, although fresher species, such as *Ipomoea sagitatta, Vigna luteola,* and *Schoenoplectus pungens*, are also found within the study area.

The West Pointe a la Hache Siphon Diversion Project is located within the study area and has been operational since 1993. The project was designed to introduce freshwater and sediment for marsh restoration and land building (OCPR, 2010; LaCoast, 2008). It is a relatively low-flow diversion consisting of eight 1.8 m diameter steel siphon pipes that cross over the levee, run underground, then discharge river water into an outfall pond. Four channels radiate southward from the pond to distribute freshwater to the surrounding marsh (Richardi, 2013). Although maximum discharge for the siphons is estimated as 2144 ft^3s^{-1} (61 m^3s^{-1}), based on high river stage and all siphons in full operation, freshwater flow at WPH typically ranges between 500-1000 ft^3s^{-1} (14-28 m^3s^{-1}) when the siphon is operational (Richardi, 2013). It is estimated that the siphon has operated approximately 60% of the time since flow began in January, 1993 (Richardi, 2013). Although the siphons at WPH have had some effect in reducing salinities, land loss is still occurring in the project area (Boshart and Van Cook, 2007; Richardi, 2013).

Methods

Landsat 5 Thematic Mapper Satellite Image Data

Water Turbidity Frequency Datasets

Water turbidity frequency datasets were produced for this study by the U.S. Army Corps of Engineers (USACE) based on a technique developed by Allen *et al*. (2008) and outlined in Appendix A. The datasets are based on time series cloud-free Landsat images captured between 1984 and 2010 and corresponding to periods of pre- and post-siphon operation of the WPH diversion project. Satellite image specifications are provided in Table 3.1. For the post-siphon

operation time period, optimal Landsat image dates were chosen to coincide with siphon freshwater flow based on records obtained from Louisiana Coastal Protection and Restoration Authority (CPRA) Strategic Online Natural Resources Information System (SONRIS, 2011). Pre- and post-siphon operation satellite image dates and associated freshwater flows are provided in Table 3.2.

The USACE datasets consist of two turbidity frequency maps, adapted versions of which are provided in Figures 3.2 and 3.3. The pre-1993 turbidity map (Figure 3.2) depicts the frequency of classification of water pixels as turbid during the pre-siphon time period between 1984 and commencement of siphon operation in 1993. This turbidity frequency dataset was used to estimate baseline turbidity. The post-1993 turbidity map (Figure 3.3) depicts the frequency of classification of water pixels as turbid for image dates captured during periods of siphon operation between 1993 and 2010.

Estimating Highest and Lowest Turbidity Post-Siphon Operation

The USACE turbidity frequency datasets were used to derive an estimate of turbidity attributed to siphon operation. This was accomplished by comparing pre- and post-1993 turbidity. The USACE turbidity frequency datasets were reprojected to UTM, Zone 15, GRS 1980, NAD 83 and checked for consistent alignment. For each turbidity frequency map, five classes of water turbidity were identified using natural breaks in ArcGIS, a geographic information system (GIS) software. The highest turbidity classes in the pre- and post-siphon datasets were compared and areas of intersection were removed from the post-siphon turbidity data. The resulting subset provides a map layer representing areas of highest turbidity associated with freshwater flow during siphon operation, thus indicating locations that consistently received distributions of sediment-laden freshwater from the siphon (Allen *et al*., 2008). This procedure

was repeated for the lowest turbidity classes in the pre- and post-siphon datasets to create a map layer delineating areas of lowest turbidity associated with siphon freshwater flow.

Mapping High and Low Freshwater Impacted Marsh Areas

ArcGIS was used to identify marsh areas subject to relatively high and low freshwater impacts. Landsat 5 TM imagery captured April 17, 2011 was reprojected to UTM, Zone 15, GRS 1980, NAD 83 and checked for consistent alignment with the turbidity frequency maps. The imagery was subset to the study area and a land-water map was developed using a hybrid classification method described by Bethel *et al*. (2011) and outlined in Appendix B. A vegetation-only layer was created from the land-water map by masking pixels representing water and developed land. Restricting subsequent remote sensing and geographic information system processing to vegetation-only pixels minimized the influence of non-vegetation pixels and insured that final results were based solely on analysis of pixels classified as marsh vegetation. The vegetation layer was then included in a GIS with the map layers produced from the turbidity frequency data delineating highest and lowest turbidity associated with freshwater flow during siphon operation.

In the GIS environment 15 m buffers were created around areas of highest and lowest turbidity associated with siphon operation. Those areas within the highest turbidity buffers were classified as high freshwater impact areas and those within the lowest turbidity buffers were classified as low freshwater impact areas. Vegetated areas within the highest turbidity buffers were identified as marsh areas most consistently exposed to freshwater introduction, while vegetated areas within the lowest turbidity buffers were identified as marsh areas least impacted by freshwater introduction. Figure 3.4 shows the resulting freshwater impacts map delineating vegetated marsh areas subject to high and low freshwater impacts.

Accuracy Assessment of Freshwater Impacts Map

Hydrographic salinity data obtained from SONRIS were used to assess the accuracy of the freshwater impact map (SONRIS, 2012). Figure 3.5 shows the locations of salinity data collection sites within areas of high and low freshwater impacts. For salinity estimates during siphon operation, 12 salinity data dates were identified as dates of siphon operation nearest the Landsat image capture dates (Table 3.3). For no flow salinity estimates, 71 salinity data dates were identified for periods in which the siphon had not operated for a minimum of 7 days (Table 3.4). Estimates of mean salinity (ppt) during siphon freshwater flow and no flow periods were calculated for the 9 salinity data collection sites in high freshwater impact areas and for the 6 salinity data collection sites in low freshwater impact areas (Table 3.5). All salinity estimates were based on hourly bottom and surface salinity readings. The Mann-Whitney statistical method was used to test for differences in mean salinity in high and low freshwater impact areas during both freshwater flow and no flow periods (VassarStats, 2014).

Mapping the Vegetation Productivity Gradient

To aid in the identification of appropriate field data collection sites, a map of the study area's vegetation productivity was created. The map was based on an NDVI derived from the Landsat 5 Thematic Mapper (TM) image acquired over the study area on April 17, 2011 and classified into areas of high, medium, and low NDVI values (Figure 3.6).

Field Data

Sample Site Selection

A randomized opportunistic sampling approach was used for field data collection. This allowed the use of preexisting sample sites maintained by Louisiana's Coastal Protection and Restoration Authority (CPRA), many of which include infrastructure in the form of boardwalks

conducive to field sampling in the marsh. Sample sites were selected to insure data collection across vegetation productivity and freshwater impact gradients within the study area. A GIS dataset of existing CPRA sample sites, the NDVI-based Vegetation Productivity Gradient map (Figure 3.6), and the Freshwater Impacts map (Figure 3.4) were co-registered in ArcGIS to derive 6 classes of potential sample sites: low freshwater impact/low NDVI; low freshwater impact/medium NDVI; low freshwater impact/high NDVI; high freshwater impact/low NDVI; high freshwater impact/medium NDVI; and high freshwater impact/high NDVI. Based on the sample site classification a field investigation was conducted to determine the suitability of each potential site for data collection in terms of accessibility and sufficient area of contiguous emergent marsh vegetation. Figure 3.7 shows the 24 sample sites identified with 4 sites representing each of the 6 classes described above. All but 3 of the sample sites chosen were preexisting CPRA sample sites.

Field Data Collection

Field data collection was accomplished during peak growing season on August 2 and August 3, 2011, and included measuring vegetation-based indicators of marsh health and possible nutrient enrichment, including spectral reflectance as an indicator of overall health, chlorophyll concentration as a proxy for leaf nitrogen content, and leaf area index (LAI) and plant stem height as a proxy for above ground biomass (U.S. EPA, 2002; Bethel *et al*., 2011).

All field data were collected within single, approximately 4.0 m^2 plots located at each sample site. The sites were GPS located using a Trimble Nomad 900GLC hand held computer and were accessed by boat. An Ocean Optics USB4000 Field Spectroradiometer (~350-1045 nm at ~ 0.2 nm resolution), mounted on a pole to minimize interference with data collection, was used to simultaneously measure incoming solar radiation and top of canopy (TOC) reflectance at

each sample site. TOC reflectance was measured approximately 0.75 m above the canopy. Reflectance measurements were calibrated once at each site using a white (99% reflectance) Spectrolon calibration panel, after which three reflectance measurements distributed within the sample plot were collected and averaged. A Li-Cor 2000 LAI meter was used to estimate foliage biomass at each of the sample sites. Three sample sequences, each consisting of one above canopy for every four below canopy measurements, were taken at each site and averaged. The above canopy measurements were taken to calibrate the LAI readings for atmospheric conditions (LAI-2000, 1992). Average stem height at each sample site was calculated based on measurements of the five to ten tallest stems of dominant species within each sample plot according to procedures outlined by U.S. EPA (2002). A Field Scout CM1000 chlorophyll meter was used to measure relative leaf chlorophyll concentration. Within each sample plot, average chlorophyll concentration was derived from five CM1000 measurements collected using standard procedures outlined by the CM1000's manufacturer (FieldScout, 2009). The CM1000 senses reflectance at 700 nm, the wavelength absorbed by chlorophyll ***a***, and at 840 nm, a wavelength unaffected by leaf chlorophyll content that serves as an indicator of how much light is reflected due to leaf physical characteristics. The ratio of reflectance at 700 nm to reflectance at 840 nm is multiplied by a constant to derive an index value between 0 and 999, with higher values indicative of higher chlorophyll content (FieldScout, 2009). A study by Murdock, *et al.* (2004) found that the Field Scout, measuring reflectance, rather than transmittance and absorbance, and offering the advantage of canopy measurement rather than single leaf measurement, performed as well as the SPAD 502 chlorophyll meter for obtaining measurements in the field.

All field data were collected at ground level outside the boat whenever possible. When necessary for reasons of safety or adequate access, the boat was positioned adjacent to the shore at the sample site and data were collected from floor level of the boat or from a specially designed platform and ladder apparatus within the boat (Figure 3.8).

Digital Globe WorldView 2 Image Data

Data acquisition, preprocessing, and accuracy assessment

DG-WV2 satellite images were acquired over the study area on August 1 and August 6, 2011 (within 4 days of field data collection). Each image covered the aerial extent of the study area delivered as georeferenced and radiometrically corrected products scaled to absolute spectral reflectance (DigitalGlobe, 2010). Satellite image specifications are provided in Table 3.1. The raw digital numbers (DN) of each image were converted to top-of-atmosphere radiance and an empirical line method was used to relate radiance to band equivalent reflectance (BER) of field spectra as described by Staben, *et al*. (2011). This was accomplished for each image band by extracting values for the brightest and darkest pixels and for pixels corresponding to a random selection of 12 of the field sample sites. The extracted pixel values were used to generate a regression equation for each image band to convert radiance values to reflectance values. Accuracy assessment was based on computing the root mean square error (RMSE) for each image band by comparing the pixel values of the reflectance image to the corresponding BER of field spectra at the sample sites not selected to generate the regression equations. The RMSE represents the average magnitude of error, providing a measure of the spread of the data around the regression line. Analysis of the computed RMSE values revealed that sample site BA01-114 contributed disproportionally to the total error for each band, suggesting that it was an outlier. Examination of field notes and photos taken at the site confirmed that the data point should be

excluded based on the extent of exposed dark soils unique to that sample site. The data point was removed from further analysis and revised regression equations were developed. The regression equations used to produce the final reflectance images and the associated RMSEs are provided in Table 3.6.

Removal of cloud contamination and creation of composite image

Since the two satellite images covered the same areal extent and were captured within a six day period, cloud contamination was removed by creating a composite of the two images. Clouds and cloud shadows were masked from each image using the hybrid classification method described by Bethel *et al*. (2011) and outlined in Appendix B. This procedure was followed by digitization to remove remnant hazy areas. Pixel values were extracted from both images at 400 random points located within intersecting cloud-free areas of the images. The extracted pixel values were used to generate regression equations for each image band to predict the missing values in the cloud-masked August 1 image based on values from the August 6 image. The resulting composite image retained the original reflectance values of the August 1 image at all field sample sites and in all other areas not contaminated by clouds. In areas where cloud contamination had been removed from the August 1 image the composite image incorporated values predicted by the regression equations. Regression equations relating the two images are provided in Table 3.7.

Classification of composite image, classification accuracy assessment, and creation of vegetation indices

The composite image was classified into three classes, water, vegetation, and developed land, using the hybrid classification method described by Bethel *et al*. (2011) and outlined in Appendix B. Developed land consisted of an exceptionally small percentage of the total pixels

in the scene, making accuracy assessment of that class unfeasible. Following close visual inspection developed land was masked from the classification. Accuracy assessment of the resulting water/vegetation classification was performed using 150 stratified random points. The water pixels were then masked from the classified image and vegetation indices were calculated using the vegetation-only data. The indices calculated included the NDVI, GNDVI, WDRVI, and ARVI. Based on vegetation density characteristics within the study area, including moderate to high LAI values, a weighting parameter of 0.2 was used to calculate WDRVI, as recommended by Gitelson (2004). Two of each of the indices were calculated, one using DG-WV2 NIR band 7 (770-895 nm) and one using DG-WV2 NIR band 8 (860-1040 nm). The formulas used to calculate the vegetation indices are provided in Table 3.8.

Statistical Analysis

Estimating biophysical characteristics

Pearson product-moment correlation analysis was used to analyze the linear relationships between biophysical characteristics (LAI, chlorophyll concentration, and average stem height) and field spectra, image bands, and vegetation indices. The resulting correlation coefficients were tested using a two-tail test of significance at the $p \leq 0.05$ level. To test the ability of the most highly significantly correlated spectral data to predict marsh biophysical characteristics, empirical models were developed using regression analysis. The Jackknife Cross Validation approach was used to assess the accuracy of the resulting predictions. This approach was implemented by withholding the data from one sample site and building a regression model using data from the remaining sites. This process was repeated until all sites had been withheld. Each regression model was tested for its ability to predict the withheld value by comparing

actual and predicted values and computing the root mean square error (RMSE) values. Based on correlation and regression results an estimated chlorophyll concentration map was generated.

Testing the correlation between estimated chlorophyll concentration and proximity to the siphon

To investigate the relationship between estimated chlorophyll concentration and proximity to the source of introduced freshwater, an analysis of the spatial distribution of predicted chlorophyll values was conducted. The estimated chlorophyll map was classified into 5 classes using a Jenks natural breaks classification in ArcGIS, after which 29 concentric, non-overlapping buffers, each 500 m wide, were created around the siphon. Within each of the buffers, the percentages were calculated for pixels classified as highest chlorophyll concentration, pixels classified as highest chlorophyll concentration within high freshwater impact areas, and pixels classified as highest chlorophyll concentration within low freshwater impact areas. This procedure was repeated for pixels classified as lowest chlorophyll concentration. The linear relationships between these percentages and distance to the siphon were investigated using Pearson product-moment correlation analysis. The resulting correlation coefficients were tested using a two-tail test of significance at the $p \leq 0.05$ level.

Visual comparison of the estimated chlorophyll concentration map with ancillary data

To further assess its accuracy, the chlorophyll concentration map was compared to two Jenks natural breaks 5 class colorized NDVI maps. The visual comparison was intended to identify any conflicting patterns that might exist between estimated chlorophyll concentration and overall vegetation health. The first NDVI map was derived from the DG-WV2 composite image used to create the chlorophyll map. The second NDVI map was derived from an August 23, 2011 Landsat 5 TM image, captured within 22 days of the images from which the DG-WV2

composite image and the chlorophyll concentration map were created. The estimated chlorophyll map was also compared to a Jenks natural breaks 5 class digital elevation model (DEM) adapted from a 2010 LiDAR-derived DEM (ArcGIS online; LOSCO, LSU, C4G, 2010). Since differences in marsh elevation are known to affect species composition and overall health, thus affecting chlorophyll concentration, this visual comparison was intended to identify any chlorophyll concentration patterns that might be related to differences in elevation. Finally, available Google Earth imagery was examined for evidence of vegetation patterns that conformed or conflicted with the estimated chlorophyll concentration map.

Results

High and Low Freshwater Impacts

The spatial distribution of high and low freshwater impact areas depicted on the freshwater impacts map (Figure 3.4) suggests a general reduction in impact with increasing distance from the siphon diversion along a north to south gradient. The location of the Texas Company Canal coincides with a relatively abrupt change from high freshwater impacts north of the canal to low freshwater impacts to the south. In contrast to this general trend, relatively discontinuous and isolated areas of high turbidity were found distant from the siphon to the south and southwest between Bayou Grand Chenier Ridge and Bays Chene Fleur, Batiste, and Sansbois.

Greater fluctuation in mean salinity was observed among high freshwater impact sites compared to low impact sites (Figure 3.9). With the exception of site BA04-12, both high and low freshwater impact sites exhibited greater variation in mean salinity during periods of siphon operation compared to siphon dormancy (Figure 3.10). During siphon flow periods both high and low freshwater impact sites had significantly lower mean salinity ($Z = -3.09$, $P = 0.001$ and

Z = -2.8, P = 0.003, respectively) compared to no-flow periods (Figure 3.11). Although no significant difference was found between high and low freshwater impact sites during periods of siphon dormancy, mean salinity during siphon operation was significantly lower at high freshwater impact sites compared to low impact sites (Z = -2.65, P = 0.004). The results suggest that siphon operation freshens water throughout the study area, but that water is freshened to a greater extent in areas classified as high freshwater impact areas as compared to areas classified as low impact areas. Furthermore, when salinity data for all dates (freshwater flow and no flow periods) were tested, this finding was replicated. That is, high impact sites were found to be statistically significantly lower in mean salinity than low freshwater impact sites (Z= -2.42, P = 0.008), suggesting that the overall effect of the siphon is to freshen the high impact areas significantly more than the low impact areas and also suggesting that this effect may extend beyond siphon operation periods.

Image processing, classification, and accuracy assessment

Conversion of the satellite images to reflectance was judged acceptable based on the resulting RMSE values (Table 3.6) and guidelines outlined by Staben, *et al*. (2001). The water/vegetation classification of the composite image yielded an overall accuracy of 98% with an overall Kappa statistic of 0.96. For the water class, producer's and user's accuracies were 98.65% and 97.33%, respectively. For the vegetation class, producer's and user's accuracies were 97.37% and 98.67%, respectively.

Field spectra correlation analysis

The strongest statistically significant correlations between field spectra and chlorophyll were positive correlations found in the near infrared (NIR) region of the spectrum, with the highest r value of 0.79 found at 749.9 nm. Regression using the first polynomial yielded an r^2 of

0.64. Correlations between field spectra and LAI and between field spectra and stem height were weak. The strongest correlation for LAI was found in the near infrared region (r = 0.49 at 896 nm), while the strongest correlation for stem height was found in the red edge region (r = 0.59 at 705.9 nm). Figure 3.12 provides a graph representing the resulting correlation coefficients.

Image bands and vegetation indices correlation analysis

Figures 3.13 and 3.14 show the correlation plots depicting the strength and direction of the relationships between the tested vegetation indices and the biophysical variables and between the image bands and the biophysical variables, respectively. Correlation values representing relationships between vegetation parameters and image bands and between vegetation parameters and vegetation indices are provided in Table 3.9. As indicated in Figure 3.13, the strongest statistically significant correlation was a positive relationship between chlorophyll concentration and ARVI using DG-WV2 near infrared band 8 (860-1040 nm) ($r = 0.88$, $p < 0.05$). Figure 3.14 illustrates the positive correlation found between chlorophyll concentration and DG-WV2 near infrared band 8 (860-1040 nm) ($r = 0.76$, $p < 0.05$) and the negative correlation found between chlorophyll concentration and DG-WV2 red band 5 (630-690 nm) ($r = -0.76$, $p < 0.05$.) No bands or indices correlated well with LAI or plant height and those parameters were removed from further analysis.

Regression analysis and predicted chlorophyll concentration

The ARVI using NIR image band 8 was optimal for estimating chlorophyll concentration ($r^2 = 0.77$), performing slightly better than the NDVI using DG-WV2 near infrared band 8 (860-1040 nm) ($r^2 = 0.74$) and the WDRVI using DG-WV2 near infrared band 8 (860-1040 nm) ($r^2 = 0.74$). Figures 3.15 (a) and (b) provide graphs of the regression model used to develop the

predicted chlorophyll concentration map and the associated 95% confidence intervals, respectively. Based on an index of 0 to 999, the relative chlorophyll concentration values measured in the field ranged from 89 to 472, with a mean of 234.61. Jackknife Cross Validation of the predictive equation yielded a root mean square error (RMSE) of 42.96 (Table 3.10). The 5 class estimated chlorophyll map is provided in Figure 3.16 and a map classifying the level of confidence associated with predicted chlorophyll concentration is provided in Figure 3.17.

Spatial analysis of predicted chlorophyll concentration

The chlorophyll concentration map with an overlay of 29 concentric, non-overlapping 500 m buffers is provided in Figure 3.18. The spatial distribution of predicted chlorophyll values indicates that estimated chlorophyll concentration is related to proximity to the siphon. A statistically significant negative correlation was found between the percentage of total vegetation pixels in the highest chlorophyll concentration class and distance to the siphon ($r = -0.83$; $p < 0.0001$), indicating decreasing chlorophyll concentration with increasing distance to the siphon. Within areas most highly impacted by freshwater introduction an even stronger statistically significant negative correlation was found ($r = -0.91$; < 0.0001). No statistically significant correlation was found between the percentage of highest chlorophyll pixels and distance to the siphon within areas of low freshwater impact.

In contrast, a statistically significant positive correlation was found between the percentage of total vegetation pixels in the lowest chlorophyll concentration class and distance to the siphon, indicating that low chlorophyll concentration and distance to siphon vary together. This relationship was evident throughout the study area ($r = 0.87$; $p < 0.0001$) and within low freshwater impact areas ($r = 0.83$; $p < 0.0001$), while a slightly weaker correlation was found within high freshwater impact areas ($r = 0.71$; $p < 0.0001$). Graphs depicting the relationships

between predicted chlorophyll concentration and distance to the source of freshwater are provided in Figures 3.19, 3.20, and 3.21. Correlation coefficients (r-values) relating distance to siphon with percentage of pixels in highest and lowest chlorophyll classes by level of freshwater impact are provided in Table 3.11.

Visual comparison of the estimated chlorophyll concentration map with NDVI maps and LiDAR-based DEM

Visual comparisons of the estimated chlorophyll map with the DG-WV2-based and Landsat 5 TM-based NDVI maps suggest a high level of agreement in their depiction of vegetation condition. The chlorophyll map reveals areas of interest exhibiting high levels of chlorophyll concentration southwest of the siphon beyond the Bayou Grand Chenier Ridge that are also evident on both NDVI maps (Figures 3.22 b and c). Although differences in marsh elevation are known to affect species composition and overall health, thus affecting chlorophyll concentration, there are no corresponding patterns evident in the LiDAR-based DEM (Figure 3.22 d). This suggests that high chlorophyll concentration in the areas of interest may not be explained by differential effects of elevation on marsh vegetation. Examination of Google Earth imagery from various dates did not reveal a discernible difference in the appearance of vegetation within the areas of interest compared to surrounding areas. The patterns evident in the chlorophyll and NDVI maps, therefore, were not apparent in the Google Earth imagery, underscoring the need for further research to understand these areas of interest.

Discussion

The lack of a statistically significant link between vegetation spectral response and LAI and stem height measurements respectively, prevented the use of those parameters for predicting vegetation productivity within the study area. The relative lack of variation among the sample

sites in LAI and in plant stem height, especially when compared to variation in chlorophyll, suggests a high degree of homogeneity of vegetation type throughout the study area (Table 3.12). In contrast, the relatively high degree of variation in chlorophyll content among the sample sites suggests a significant gradient exists for vegetation condition, allowing an acceptable degree of accuracy in predicting chlorophyll concentration throughout the study area. As indicated in Figure 3.15 (b), at the 95% level, confidence in the accuracy of predicted chlorophyll concentration is greatest for values in the mid-range. The map based on the 95% confidence interval for predicting chlorophyll concentration indicates that, with the exception of a very limited area of extremely high chlorophyll content nearest the siphon, the model can be used most confidently to assess chlorophyll concentrations closer to the WPH siphon.

Measurable differences in plant productivity, as evidenced by differences in chlorophyll concentration, were found to be spatially related to the location of the Pointe a la Hache siphon diversion, the source of introduced freshwater. Plant productivity appears to be greatest nearest the siphon and to decrease with increasing distance from the siphon, suggesting that introduced freshwater is positively impacting plant productivity. This impact appears strongest in regions that have most consistently received introduced freshwater and weakest in areas that have least consistently received introduced freshwater, suggesting that plants within high freshwater impact areas are photosynthesizing at a rate different from vegetation within low freshwater impact areas. Results of the chlorophyll concentration map are supported by the digital elevation model that suggests that nutrient enriched freshwater flows from the higher elevation siphon to lower elevation areas south and west of the siphon. Flow rate is assumed to decrease as introduced freshwater moves away from confined areas near the siphon and into more open areas south and west of the siphon, causing nutrient enriched sediment to settle out and potentially enrich

vegetation. The spatial distribution of predicted chlorophyll concentration suggests the higher elevation Bayou Grand Chenier Ridge then acts as a natural barrier to the flow of freshwater to areas south and west of the Chenier. The spoil banks created in the dredging of the Texas Company Canal may function similarly to slow or block the flow of freshwater, thereby helping to explain the spatial distribution of areas of highest and lowest freshwater impacts and the corresponding differences in chlorophyll concentration.

Areas of unusually high chlorophyll concentration are apparent between 7500 and 9500 m southwest of the siphon (Figures 3.16, 3.18, and 3.22 a). Vegetation within those areas exhibit consistently higher NDVI values for both Landsat- and DG-WV2-derived NDVI maps (Figure 3.22 b and c). Although this suggests possible differences in elevation or in vegetation species composition, close examination of the DEM (Figure 3.22 d), satellite imagery, and Google Earth imagery from various dates did not reveal visual clues to support either possibility. The patterns of natural streams near the regions in question suggest hydrological influences that may account for differences in chlorophyll concentration and NDVI values. Additional detailed analysis of vegetation and hydrology may be necessary to further understand the evident vegetation differences.

Conclusions

Remotely sensed imagery and field measured vegetation parameters were used to successfully identify spectral bands and vegetation indices most highly correlated with vegetation characteristics suggestive of wetland nutrient enrichment. High correlation between ARVI using near infrared image band 8 and field measured chlorophyll content allowed the prediction of estimated chlorophyll content across the study area. The resulting spatial distribution of estimated chlorophyll concentration was related to proximity to the source of

introduced freshwater, with chlorophyll concentration decreasing with increasing distance from the West Pointe a la Hache siphon diversion. Additionally, areas most consistently impacted by freshwater introduction were associated with the highest levels of chlorophyll concentration, while least impacted areas were associated with the lowest levels of chlorophyll concentration. These results suggest that remotely sensed imagery combined with field measured vegetation parameters can be used to accurately identify freshwater impacted marsh areas vulnerable to eutrophication.

References

Allen, Y.C.; Constant, G.C., and Couvillion, B.R., 2008. Preliminary classification of water areas within the Atchafalaya Basin Floodway System by using Landsat imagery: U.S. Geological Survey Open-File Report 2008-1320, 14p. URL: http://pubs.usgs.gov/of/2008/1320/

ArcGIS online, LOSCO, LSU, C4G, 2010. http://www.esri.com/software/arcgis/arcgisonline

Bethel, M.B.; Brien, L.F.; Danielson, E.J.; Laska, S.B.; Troutman, J.P.; Boshart, W.M.; Giordino, M.J., and Maurice A. Phillips, 2011. Blending Geospatial Technology and Traditional Ecological Knowledge to Enhance Coastal Restoration Decision-Support Processes in Coastal Louisiana. Journal of Coastal Research, 27(3), 555-571.

Boshart, W.M., and Van Cook, P.E., 2007. 2005 Operations, Maintenance, and Monitoring Report for West Pointe a la Hache Siphon Construction (BA-04). Louisiana Department of Natural Resources, Coastal Restoration Division and Coastal Engineering Division, New Orleans, Louisiana. 18p.

Boustany, R.G., 2010. Estimating the benefits of freshwater introduction into coastal wetland ecosystems in Louisiana: Nutrient and sediment analyses. Ecological Restoration, 28(2), 160-174.

Boyer, K.E., and P. Fong, 2005. Macroalgal-mediated transfers of water column nitrogen to intertidal sediments and salt marsh plants. Journal of Experimental Marine Biology and Ecology, 321, 59-69.

Christopherson, R.W., 2009. Geosystems, 7th Edition. Upper Saddle River, NJ: Pearson Prentice Hall, 639p.

Cloern, E.C., 2001. Our evolving conceptual model of the coastal eutrophication problem. Marine Ecology Progress Series, 210, 223-253.

Cohen, R.A., and Fong, P., 2006. Using opportunistic green macroalgae as indicators of nitrogen supply and sources to estuaries. Ecological Applications, 16(4), 1405-1420.

Conner, W.H. and Day, J.W. Jr., (ed.), 1987. The Ecology of Barataria Basin, Louisiana: an Estuarine Profile. Coastal Ecology Institute, Center for Wetland Resources, Louisiana State University, Baton Rouge, Louisiana, Biological Report 85, 7-13.

Darby. F.A. and Turner, R.E., 2008(a). Below- and aboveground Spartina alterniflora production in a Louisiana salt marsh. Estuaries and Coasts, 31, 223-231.

Darby, F.A. and Turner, R.E., 2008 (b). Effects of eutrophication on salt marsh root and rhizome biomass accumulation. Marine Ecology Progress Series, 363, 63-70.

Day, J.W.; Cable, J.E.; Cowan, J.H., Jr.; DeLaune, R.; de Mutsert, K.; Fry, B.; Mashriqui, H.; Justic, D.; Kemp, P.; Lane, R.R.; Rick, J.; Rick, S.; Rozas, L. P.; Sneddens, G; Swenson,

E.; Twilley, R.R., and Wissel, B., 2009 (a). The impacts of pulsed reintroduction of river water on a Mississippi delta coastal basin. The Journal of Coastal Research, 54, 225-243.

Day, J.; Lane, R.; Moerschbaecher, M.; DeLaune, R; Twilley, R.; Mendelssohn, I., and Baustian, J., 2009 (b). The impact of the Caernarvon diversion on above and belowground marsh biomass in the Breton Sound Estuary after Hurricane Katrina. Final Report submitted to the Louisiana Department of Natural Resources, Project 2512-07-01.

Deegan, L.A.; Johnson, D.S.; Warren, R.S.; Peterson, B.J.; Fleeger, J.W.; Fagherazzi, S., and W.M. Wollheim, 2012. Coastal eutrophication as a driver of salt marsh loss. Nature, 490(7420), 388-392.

Dettmann, E.H., 2001. Effect of water residence time on annual export and denitrification of nitrogen in estuaries: A model analysis. Estuaries, 24(4), 481-490.

DigitalGlobe, Inc., 2010. Technical Note 2010-11-01. Radiometric Use of WorldView-2 Imagery.

Ferreira, J.G.; Andersen, J.H.; Borja, A.; Bricker, S.B.; Camp, J.; Cardoso da Silva, M.; Garces, E.; Heiskanen, A.; Humborg, C.; Ignatiades, L.; Lancelot, C.; Menesguen, A.; Tett, P.; Hoepffner, N., and Claussen, U., 2011. Overview of eutrophication indicators to assess environmental status within the European Marine Strategy Framework Directive. Estuarine, Coastal and Shelf Science, 93, 117-131.

Fieldscout CM1000 Chlorophyll Meter Product Manual, 2009. Spectrum Technologies, Inc. URL: http://www.specmeters.com/assets/1/22/2950CM1000.pdf

Gitelson, A.A.; Kaufman, Y.J., and Merzlyak, M.N., 1996. Use of a green channel in remote sensing of global vegetation from EOS-MODIS. Remote Sensing of the Environment, 58, 289-298.

Gitelson, A.A., 2004. Wide dynamic range vegetation index for remote quantification of biophysical characteristics of vegetation. Journal of Plant Physiology, 161, 165-173.

Guo, X., and Price, K.P., 2000. Modeling Biophysical Factors for Grasslands in Eastern Kansas using Landsat TM Data. Transactions of the Kansas Academy of Science (1903), 122-138.

Haboudane, D; Miller, J.R.; Tremblay, N.; Zarco-Tejada, P.J., and Dextraze, L., 2002. Integrated narrow-band vegetation indices for prediction of crop chlorophyll content for application in precision agriculture. Remote Sensing of Environment, 81, 416-426.

Hardisky, M.A.; Daiber, F.C.; Roman, C.T., and Klemas, V., 1984. Remote Sensing of Biomass and Annual Net Aerial Primary Productivity of a Salt Marsh. Remote Sensing of Environment, 16, 91-106.

Hardisky, M.A.; Gross, M.F., and Klemas, V., 1986. Remote Sensing of Coastal Wetlands. BioScience, 36(7), 453-460.

Howes, N.C.; FitzGerald, D.M.; Hughes, Z.J.; Georgiou, I.Y.; Kulp, M.A.; Miner, M.D.; Smith, J.M., and Barras, J.A., 2010. Hurricane-induced failure of low salinity wetlands. Proceedings of the National Academy of Sciences of the United States of America, www.pnas.org/cgi/doi/10.1073/pnas.0914582107

Jensen, J.R., Coombs, C.; Porter, D.; Jones, B.; Schill, S., and White, D., 1998. Extraction of Smooth Cordgrass (Spartina alterniflora) Biomass and Leaf Area Index Parameters from High Resolution Imagery. Geocarto International, 13(4), 25-34.

Jensen, J.R.; Oldon, G.; Schill, S.R.; Porter, D.E., and Morris, J., 2002. Remote Sensing, Leaf-Area-Index, and Chlorophyll a and b Content in the ACE Basin National Estuarine Research Reserve Using Sub-meter digital Camera Imagery. Geocarto International, 17(3), 27-36.

Justice, D.; Hall, D.; Salomonson, V.; Privette, J.; Riggs, G.; Strahler, A.; Lucht, W.; Myeni, R.B.; Knyazikhin, Y.; Running, S.W.; Nemani, R.R.; Wan, Z.; Huete, A.R.; van Leeuwen, W.; Wolfe, R.E.; Giglio, L.; Muller, J.; Lewis, P., and Barnsley, M.J., 1998. The Moderate Resolution Imaging Spectroradiometer (MODIS): Land remote sensing for global change research. IEEE Transactions on Geoscience and Remote Sensing, 36(4) 1228-1249.

Kamer, K.; Boyle, K.A., and Fong, P., 2001. Macroalgal bloom dynamics in a highly eutrophic southern California estuary. Estuaries, 24(4), 623-635.

Kauth, R.J., and Thomas, G.S., 1976. The tasselled cap-a graphic description of the spectral-temporal development of agricultural crops as seen by Landsat. LARS Symposia, Paper 159.

Kaufman, Y.J., and Tanre, D., 1992. Atmospherically resistance vegetation index (ARVI) for EOS-MODIS, IEEE Trans. Geosci. Remote Sens., 30, 261-270.

LaCoast. (2008). CWPPRA Restoration Status. URL: http://www.lacoast.gov/reports/rtc/1997/7.htm

LAI-2000 Plant Canopy Analyzer, 1992. Instruction Manual, Lincoln, Nebraska: LI-COR, Inc.

Lane, R., and Day, J., 1999. Water quality analysis of a Freshwater Diversion at Caernarvon, Louisiana. Estuaries, 22(2A), 327-336.

Lissner, J.; Mendelssohn, I.; Lorenzen, B.; Brix, H.; McKee, K., and Miao, S., 2003. Interactive Effects of Redox Intensity and Phosphate Availability on Growth and Nutrient Relations of Cladium Jamaicense (Cyperaceae). American Journal of Botany, 90(5), 736-748.

Lopez, J. A., 2009. The Environmental History of Human-Induced Impacts to the Lake Pontchartrain Basin in Southeastern Louisiana since European Settlement – 1718 to 2002. Journal of Coastal Research, 54, 1-11.

Mitsch, W.; Day, J.; Zhang, L., and Lane, R., 2005. Nitrate-nitrogen retention in wetlands in the Mississippi River Basin. Ecological Engineering, 24, 267-278.

Murdock, L.; Call, D., and James, J., 2004. Comparison and Use of Chlorophyll Meters on Wheat (Reflectance vs. Transmittance/Absorbance). Cooperative extension service, University of Kentucky-College of Agriculture, AGR-181.

OCPR (Office of Coastal Protection and Restoration), 2010. URL: http://www.ocpr.louisiana.gov/CRM/coastres/project.asp?id=BA-04

Qi, J.; Chehbouni, A.; Huete, A.R., and Kerr, Y.H., 1994. Modified Soil Adjusted Vegetation Index (MSAVI). Remote Sensing of the Environment, 48, 119-126.

Richardi, D.C., 2013. 2012 Operations, Maintenance, and Monitoring Report for West Pointe a la Hache Siphon Construction (BA-04), Coastal Protection and Restoration Authority of Louisiana, New Orleans, Louisiana, 35p.

Rundquist, D.C.; Narumalani, S., and Narayanan, R.M., 2001. A Review of Wetlands Remote Sensing and Defining New Considerations. Remote Sensing Reviews, 20, 207-226.

Siciliano, E.; Wasson, K.; Potts, D.C., and Olsen, R.C., 2008. Evaluating hyperspectral imaging of wetland vegetation as a tool for detecting estuarine nutrient enrichment. Remote Sensing of Environment, 112, 4020-4033.

Sklar, F., and Browder, J., 1998. Coastal Environmental Impacts Brought About by alterations to Freshwater Flow in the Gulf of Mexico. Environmental Management, 22(4), 547-562.

SONRIS, 2011, 2012. Coastal Protection and Restoration Authority of Louisiana, Louisiana Department of Natural Resources, http://sonlite.dnr.state.la.us/

Staben, G.W.; Pfitzner, K.; Bartolo, R., and Lucieer, A, 2011. Calibration of WorldView-2 Satellite Imagery to Reflectance Data Using an Empirical Line Method. Proceedings of the 34th International Symposium on Remote Sensing of Environment – The GEOSS Era: Towards Operational Environmental Monitoring, Sydney, Australia, http://www.isprs.org/proceedings/2011/ISRSE-34/index.html

Tucker, C.J., and Sellers, P.J., 1986. Satellite remote sensing of primary production. International Journal of Remote Sensing, 7(11), 1395-1416.

Turner, R.E.; Howes, B.L.; Teal, J.M.; Milan, C.S.; Swenson, E.M., and Tonerb, D.D., 2009. Salt marshes and eutrophication: An unsustainable outcome. Limnology and Oceanography, 54(5), 1634.

Turner, R.E., 2010. Beneath the Salt Marsh Canopy: Loss of Soil Strength with Increasing Nutrient Loads. Estuaries and Coasts, 34(5), 1084-1093.

US EPA, 2002. Methods for Evaluating Wetland Condition: Vegetation-Based Indicators of Wetland Nutrient Enrichment. Office of Water, U.S. Environmental Protection Agency, Washington, DC. EPA-822-R-02-024.

USGS, 2011. http://landsat.usgs.gov/band_designations_landsat_satellites.php

VassarStats: Website for Statistical Computation, 2014. http://vassarstats.net/

Vigier, B.J.; Pattey, E., and Strachan, I.B., 2004. Narrowband Vegetation Indexes and Detection of Disease Damage in Soybeans. IEEE Geoscience and Remote Sensing Letters, 1(4), 255-259.

Volpe, V.; Silvestri S., and Marani, M., 2011. Remote sensing retrieval of suspended sediment concentration in shallow waters. Remote Sensing of Environment, 115(1), 44-54.

Wang, J. P., M. Rich, K. P. Price, and W. D. Kettle. (2004). Relations between NDVI and tree productivity in the central Great Plains. International Journal of Remote Sensing, 25:6, 3127-3138.

Zhang, M., S. L. Ustin, E. Rejmankova, and E. W. Sanderson. (1997). Monitoring Pacific Salt Marshes using Remote Sensing. Journal of Ecological Applications, 7:3, pp. 1039-1053.

Figure 3.1 Location of the approximately 138 km² study area in the Barataria Basin (adapted from ArcGIS basemap with April 17, 2011 Landsat 5 TM image overlay).

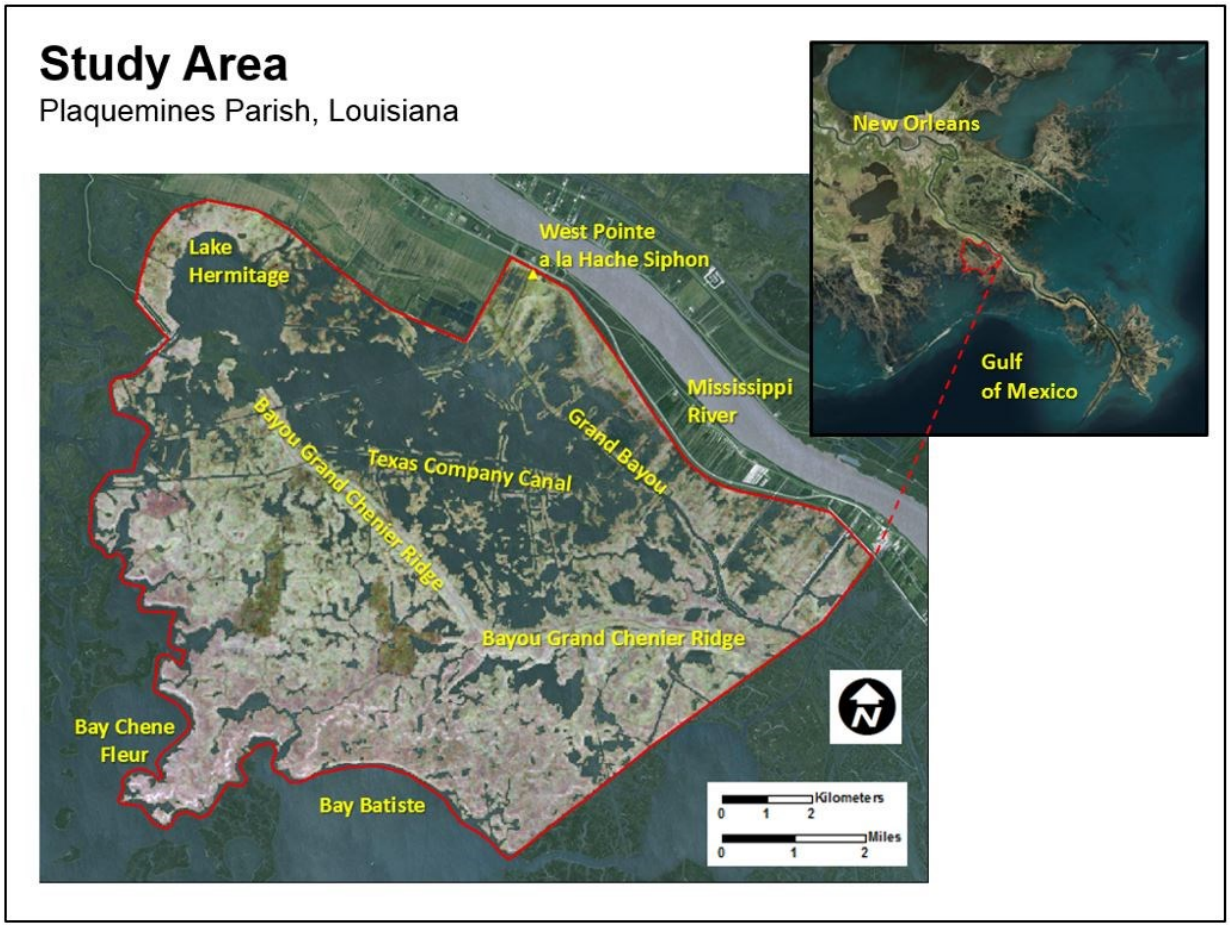

Figure 3.2 Pre-1993 turbidity map adapted from USACE turbidity frequency data.

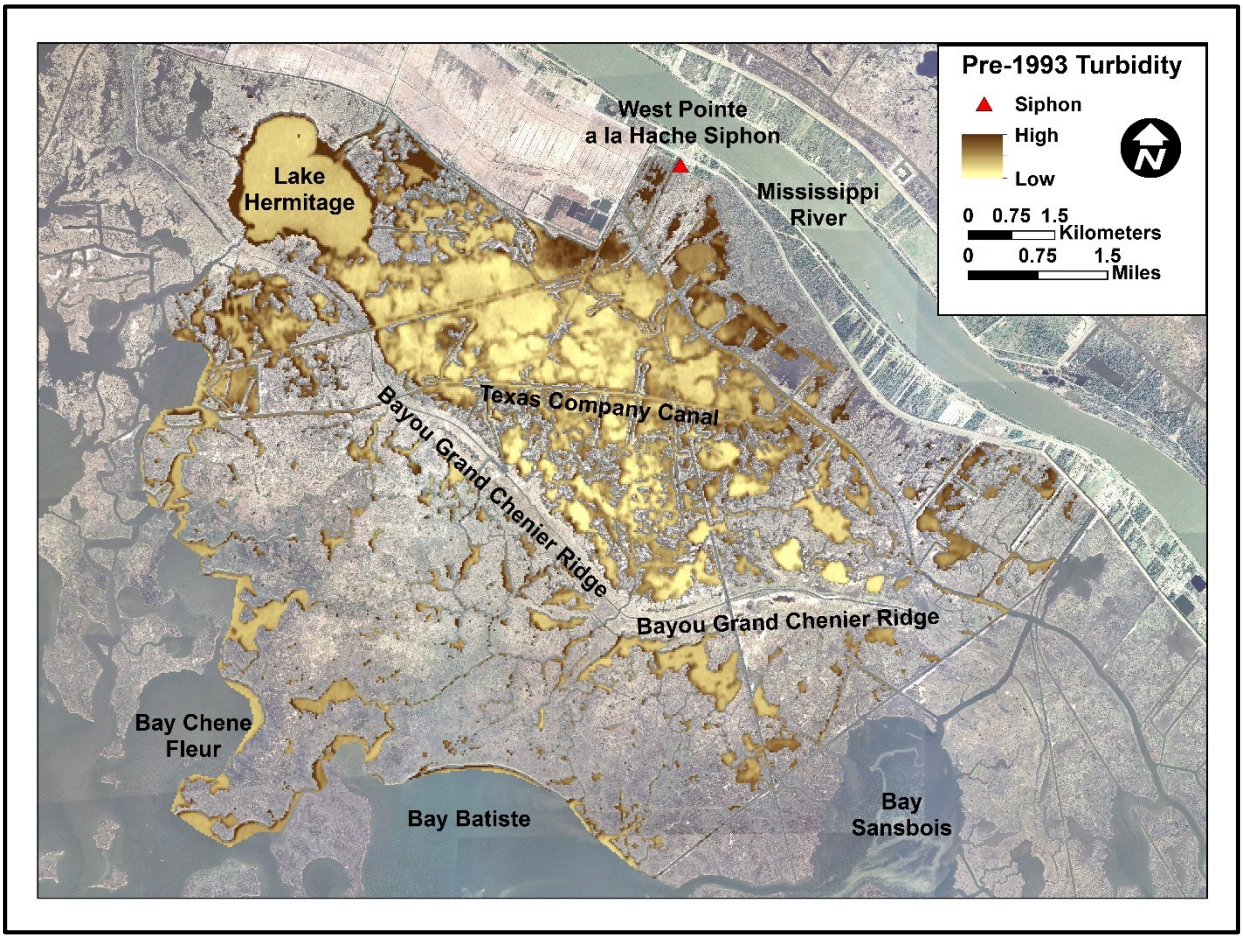

Figure 3.3 Post-1993 turbidity map adapted from USACE turbidity frequency data.

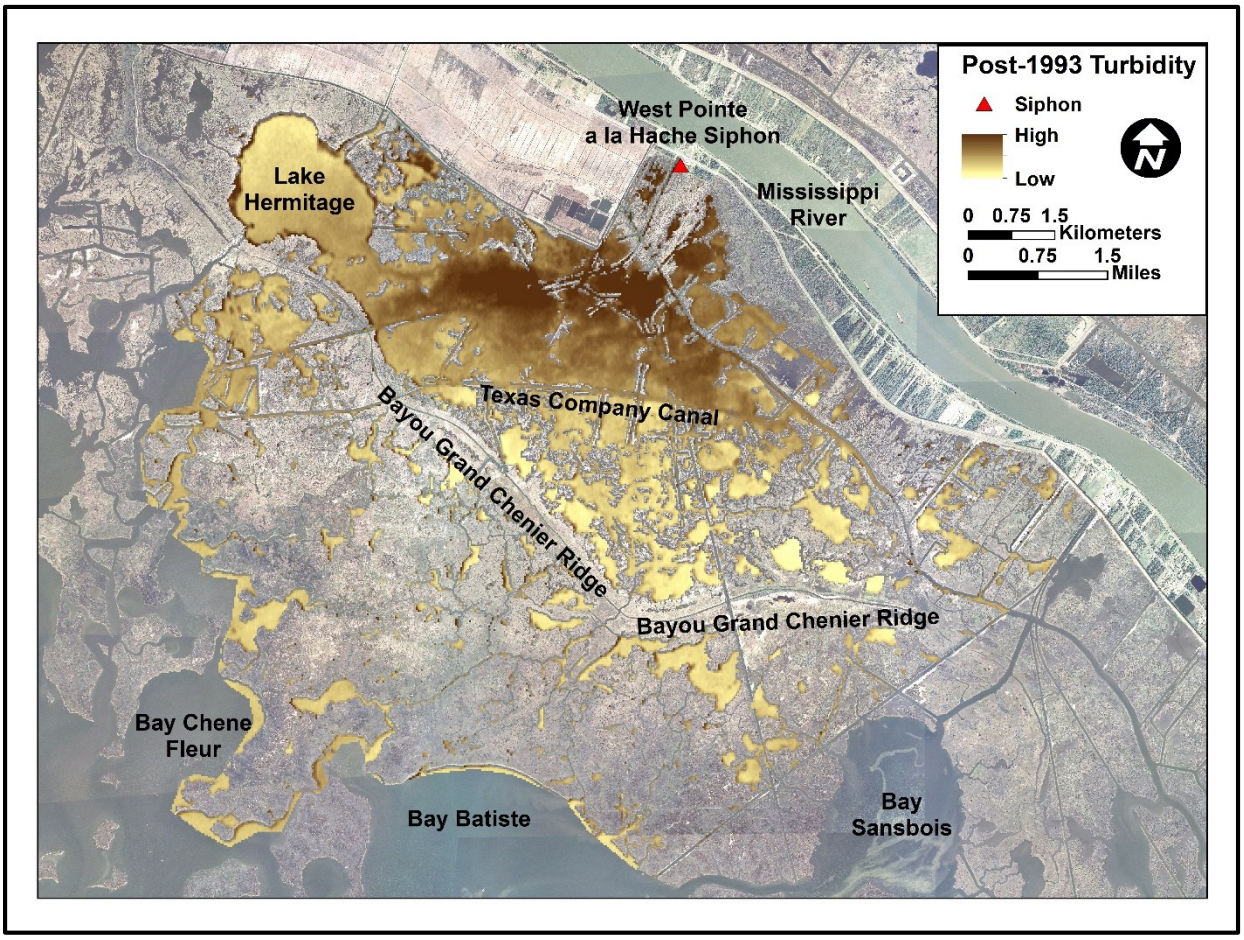

Figure 3.4 Map of study area delineating vegetated marsh areas subject to high and low freshwater impacts.

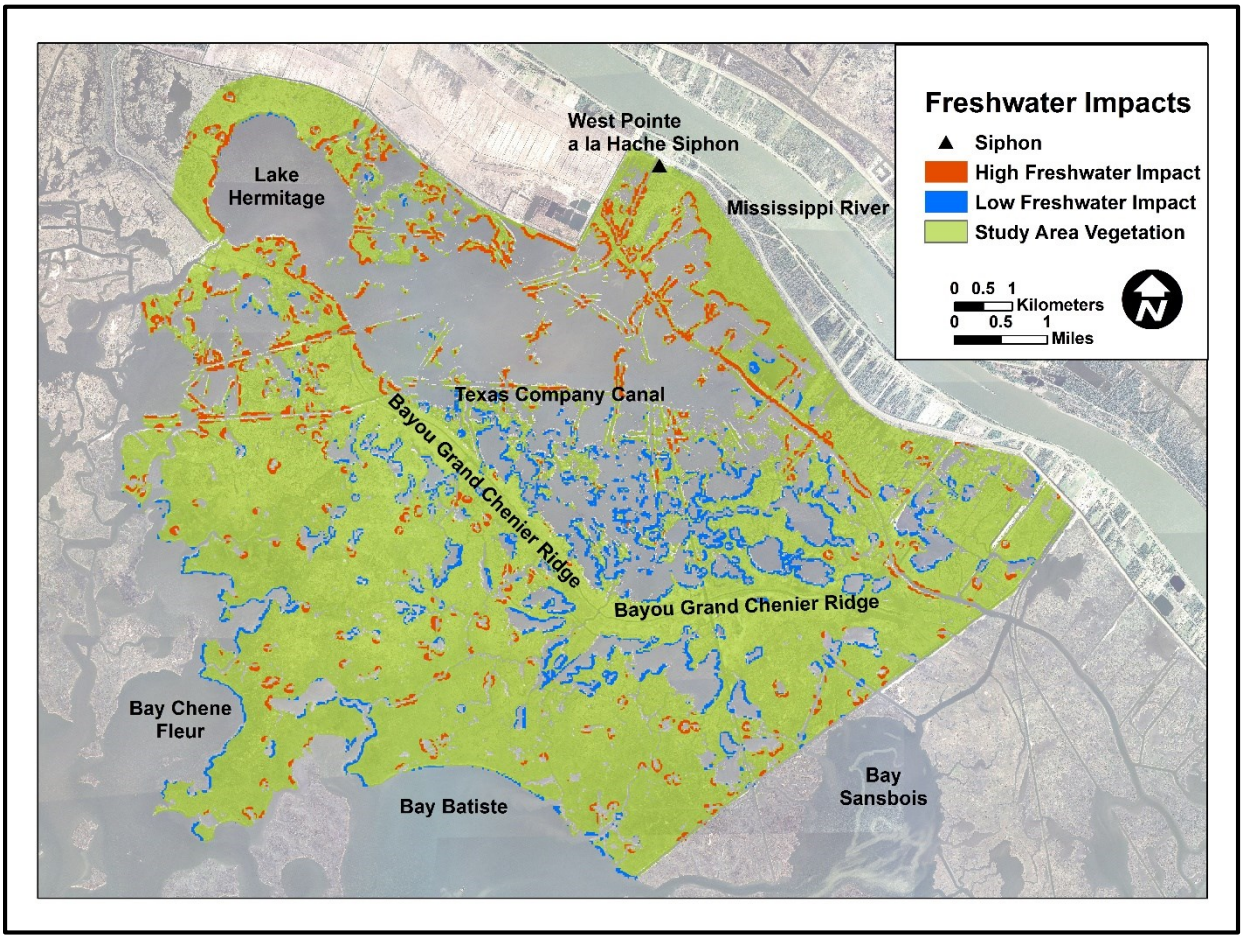

Figure 3.5 Map of study area showing salinity data collection sites in consistently high and low freshwater impact areas.

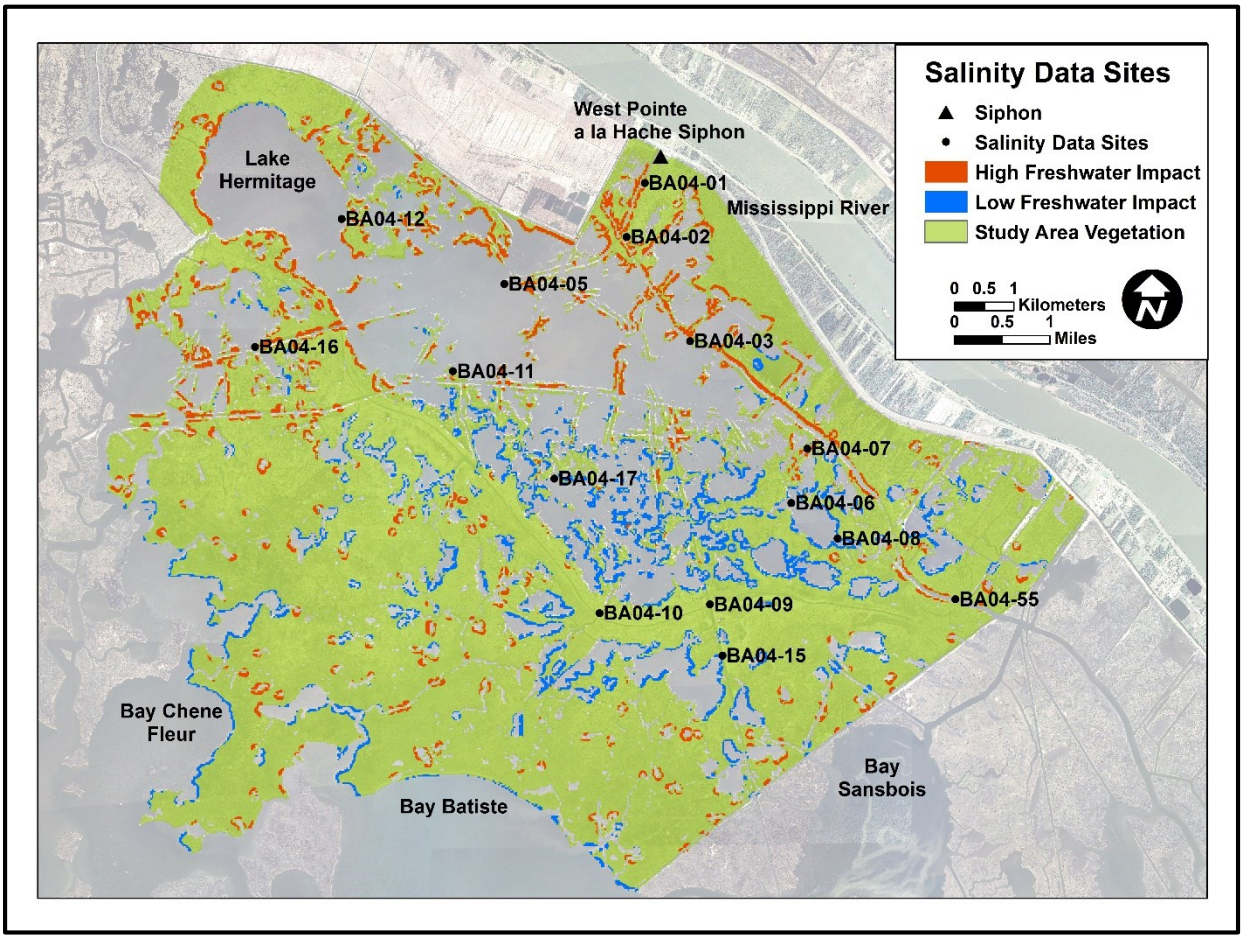

Figure 3.6 Map of study area showing areas of high, medium, and low NDVI values.

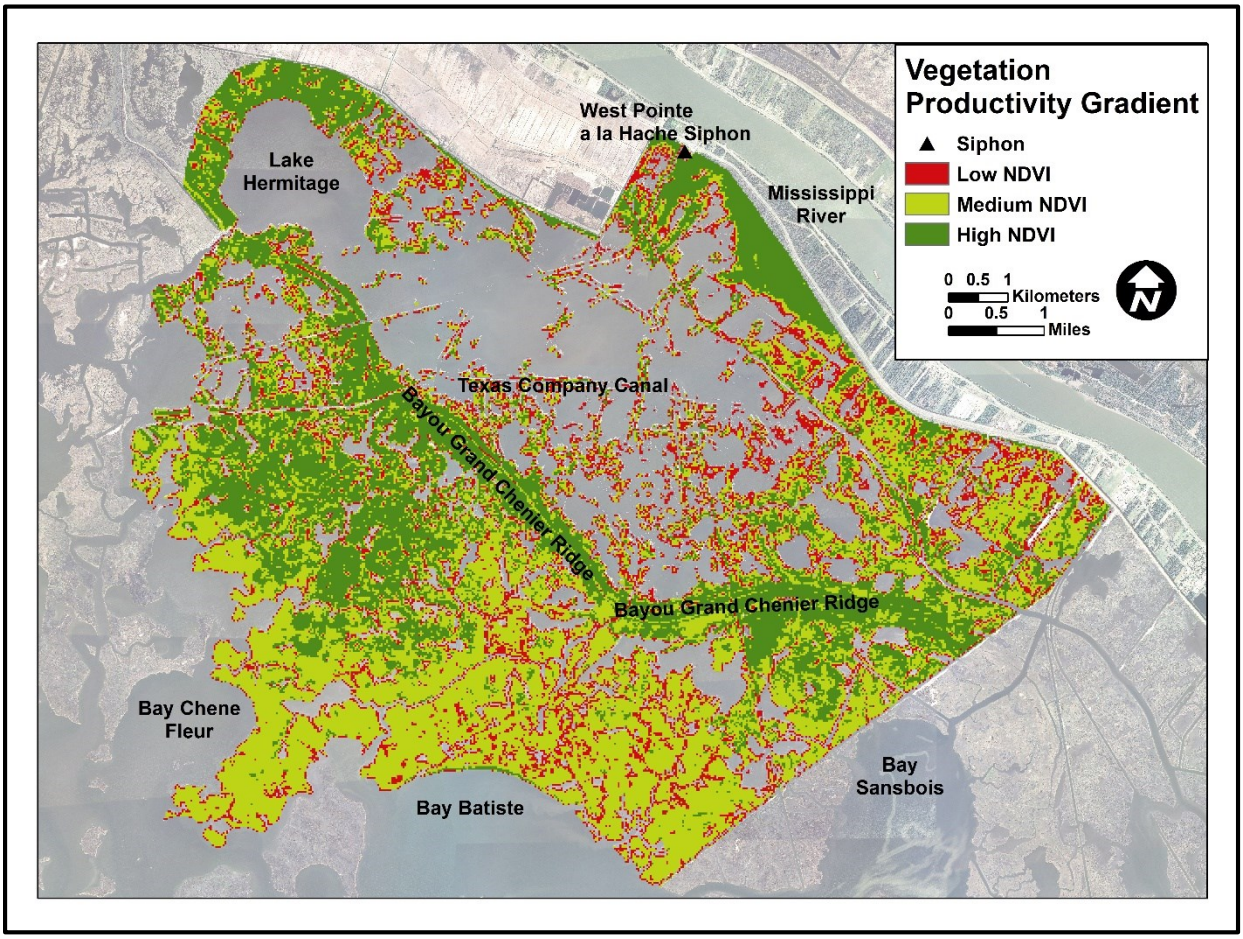

Figure 3.7 Sample sites across vegetation productivity and freshwater impact gradients.

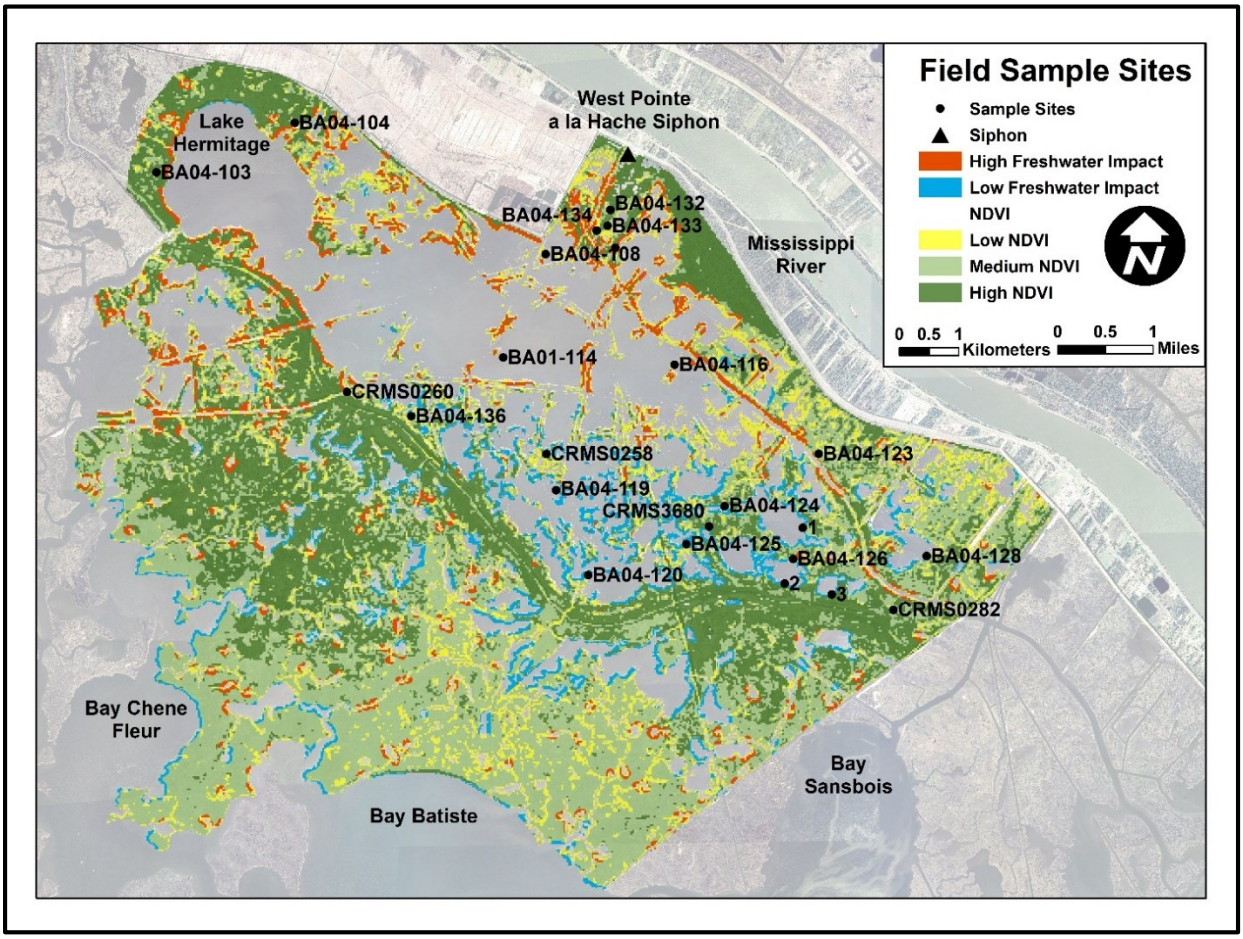

Figure 3.8 (a) Platform and ladder apparatus for data collection from the boat; (b) Computer for spectroradiometer data collection; (c) Improved vantage point for collection of vegetation survey data; (d) Data collection with the Ocean Optics USB4000 spectroradiometer system; (e) Data collection with the LAI-2000 Plant Canopy Analyzer.

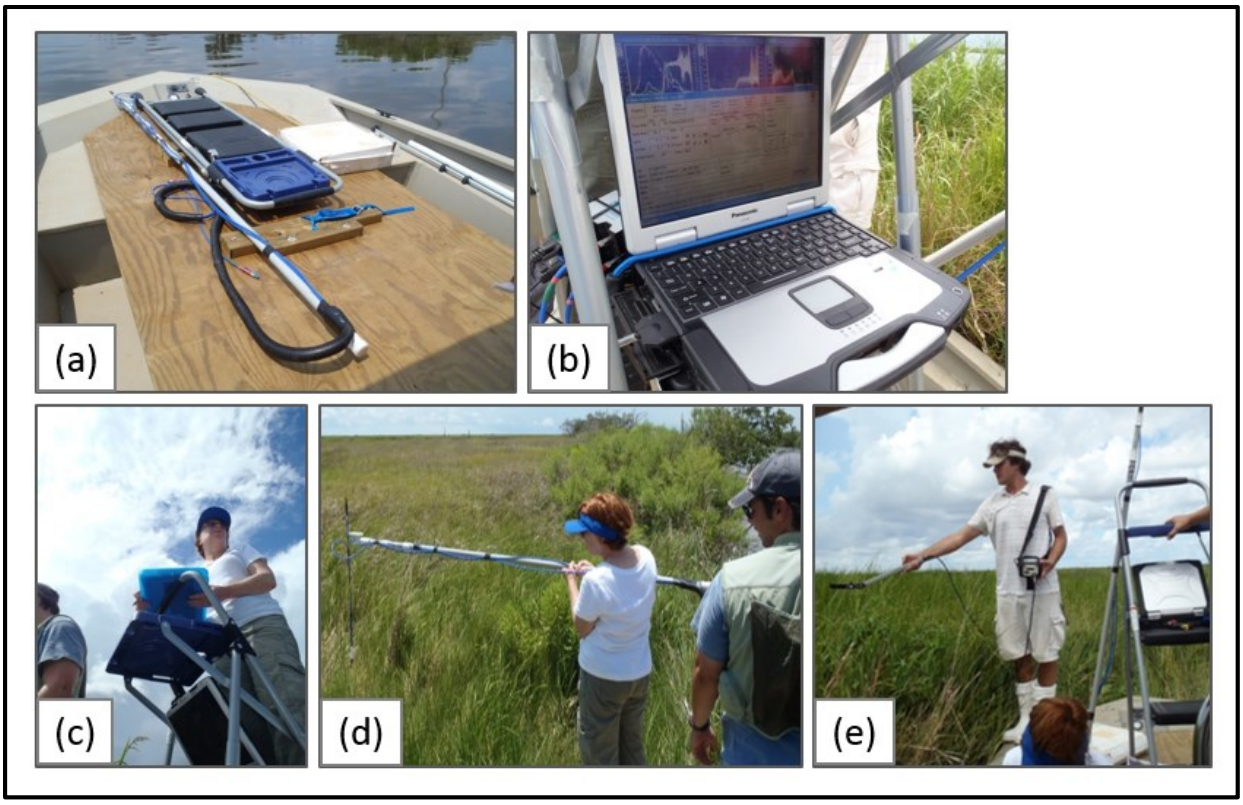

Figure 3.9 Distribution of mean salinity at high and low impact sites during siphon operation and siphon dormancy.

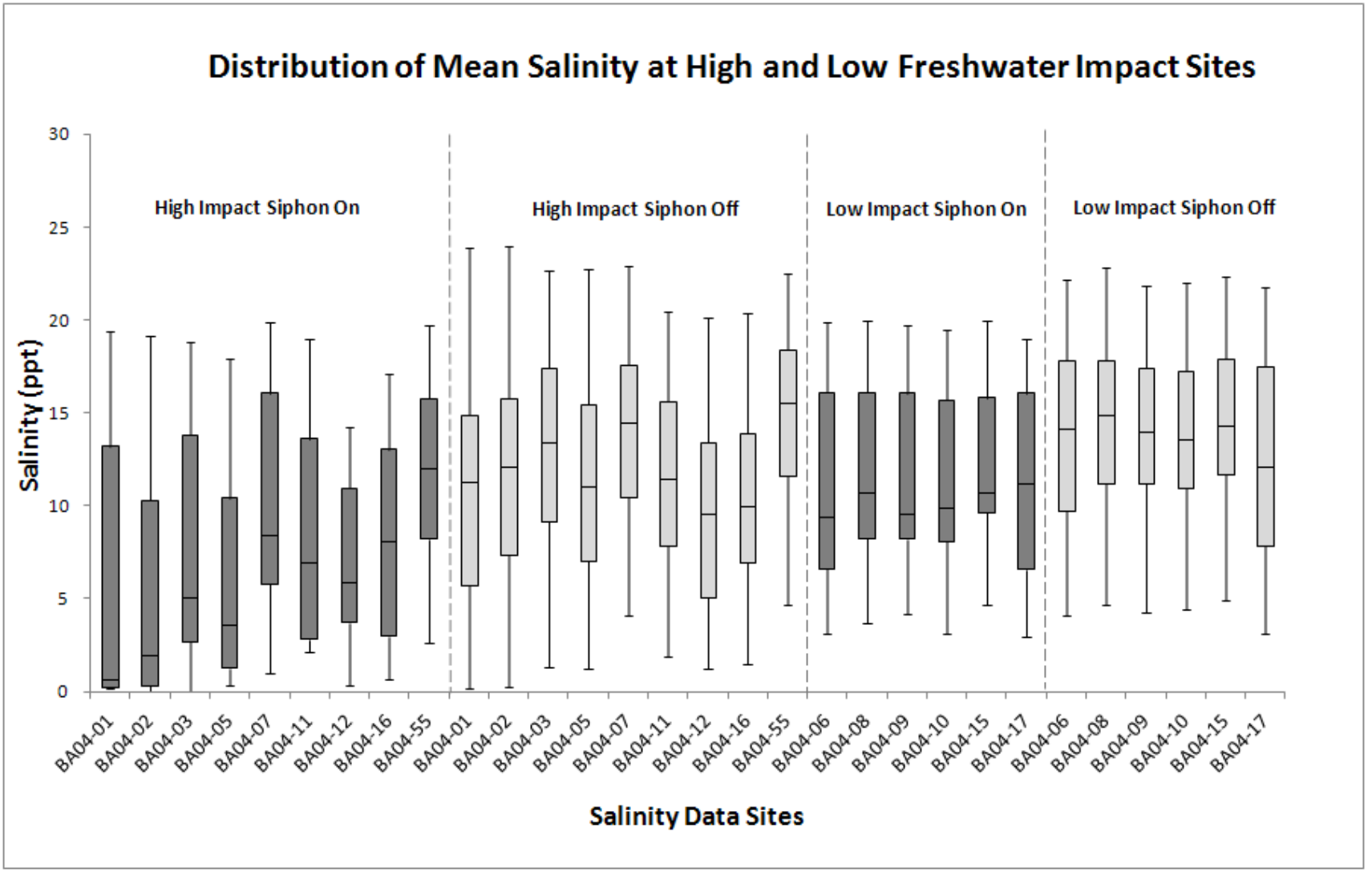

Figure 3.10 Standard deviation of mean salinity at high and low freshwater impact sites during siphon operation and dormancy.

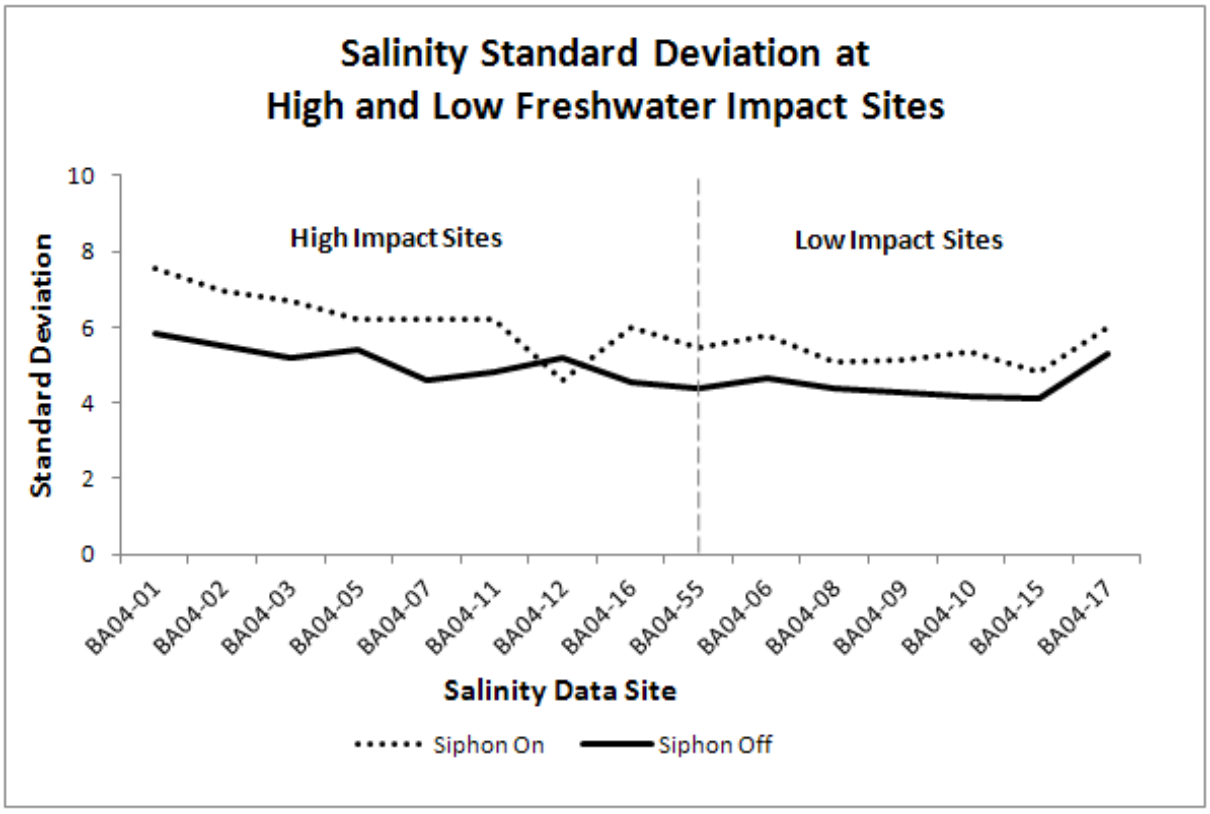

Figure 3.11 Mean salinity at high and low freshwater impact sites during siphon operation and dormancy.

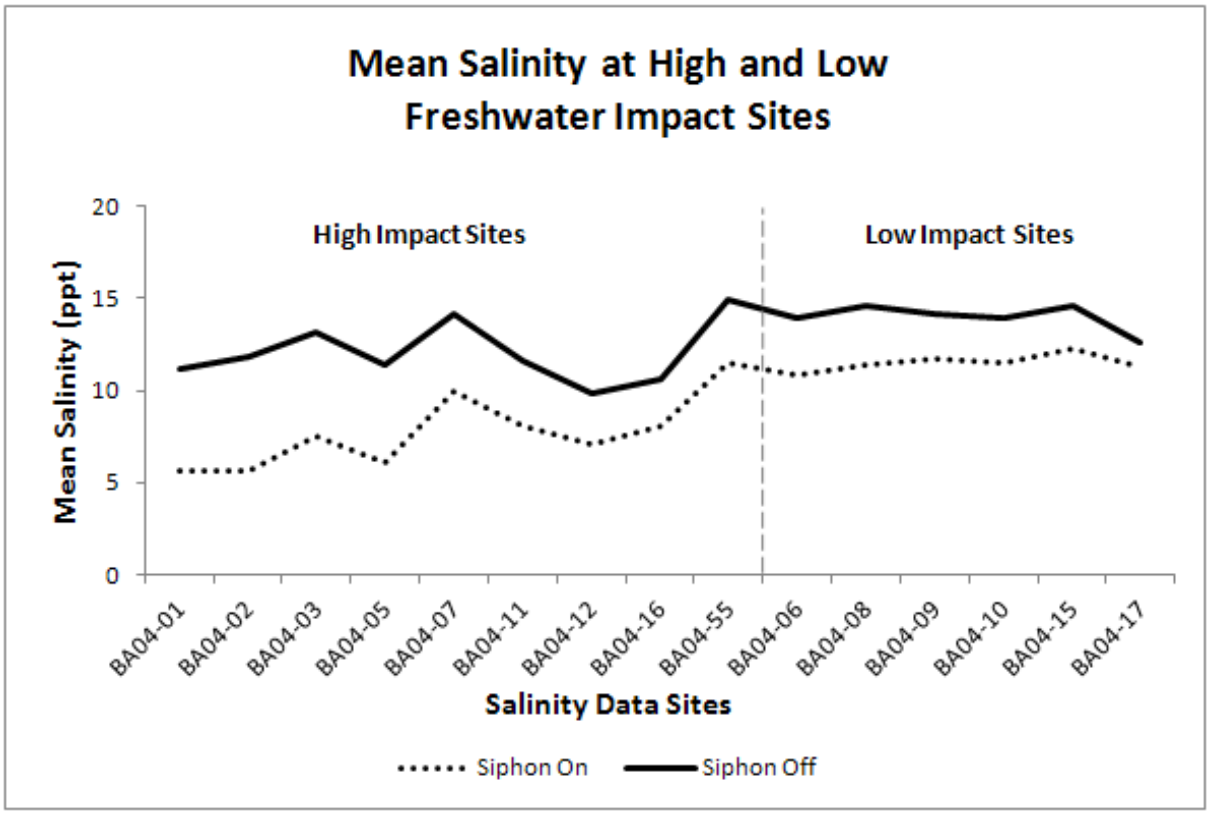

Figure 3.12 Correlation coefficients for relationships between field spectra (every 10th band between 400 and 900 nm) and vegetation biophysical parameters.

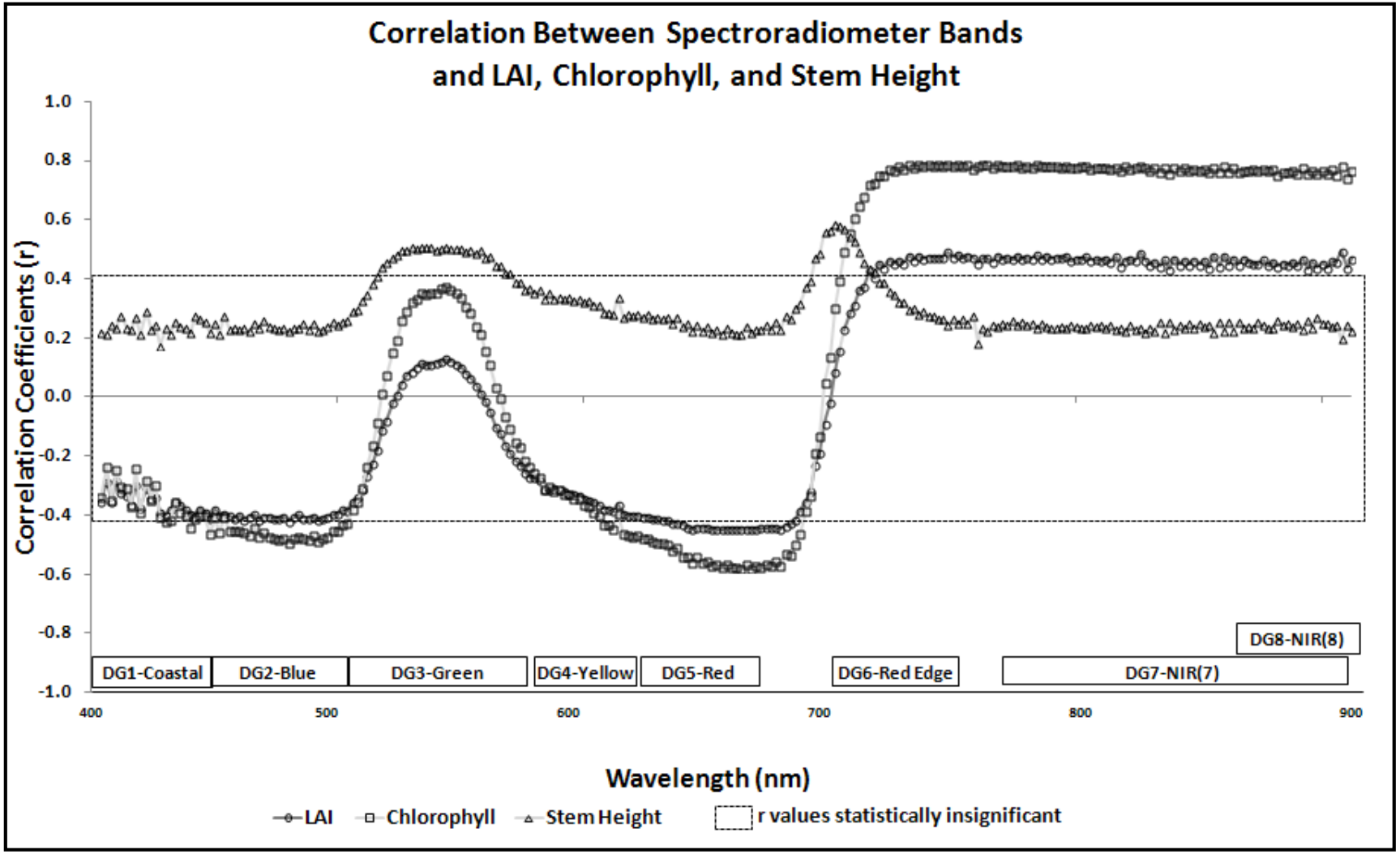

Figure 3.13 Correlation coefficients for relationships between vegetation indices and vegetation biophysical parameters.

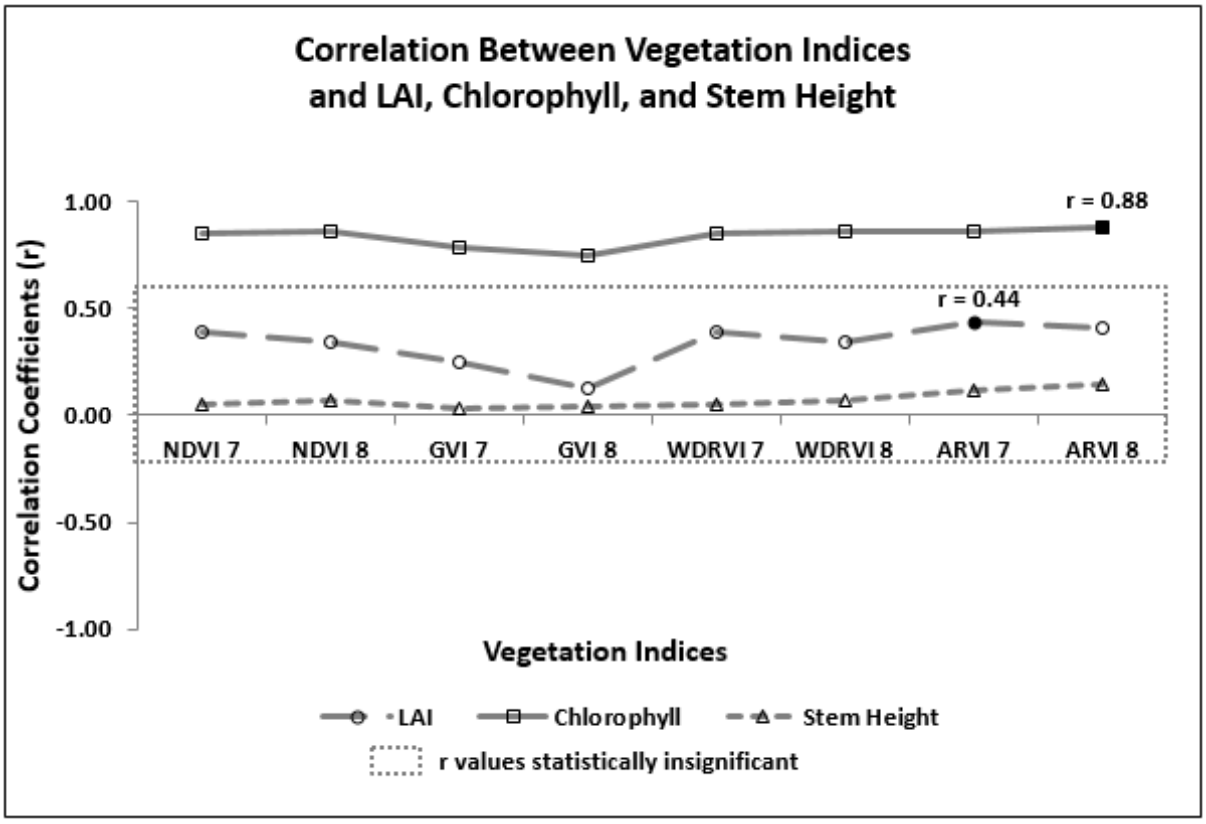

Figure 3.14 Correlation coefficients for relationships between DG-WV2 image bands and vegetation biophysical parameters.

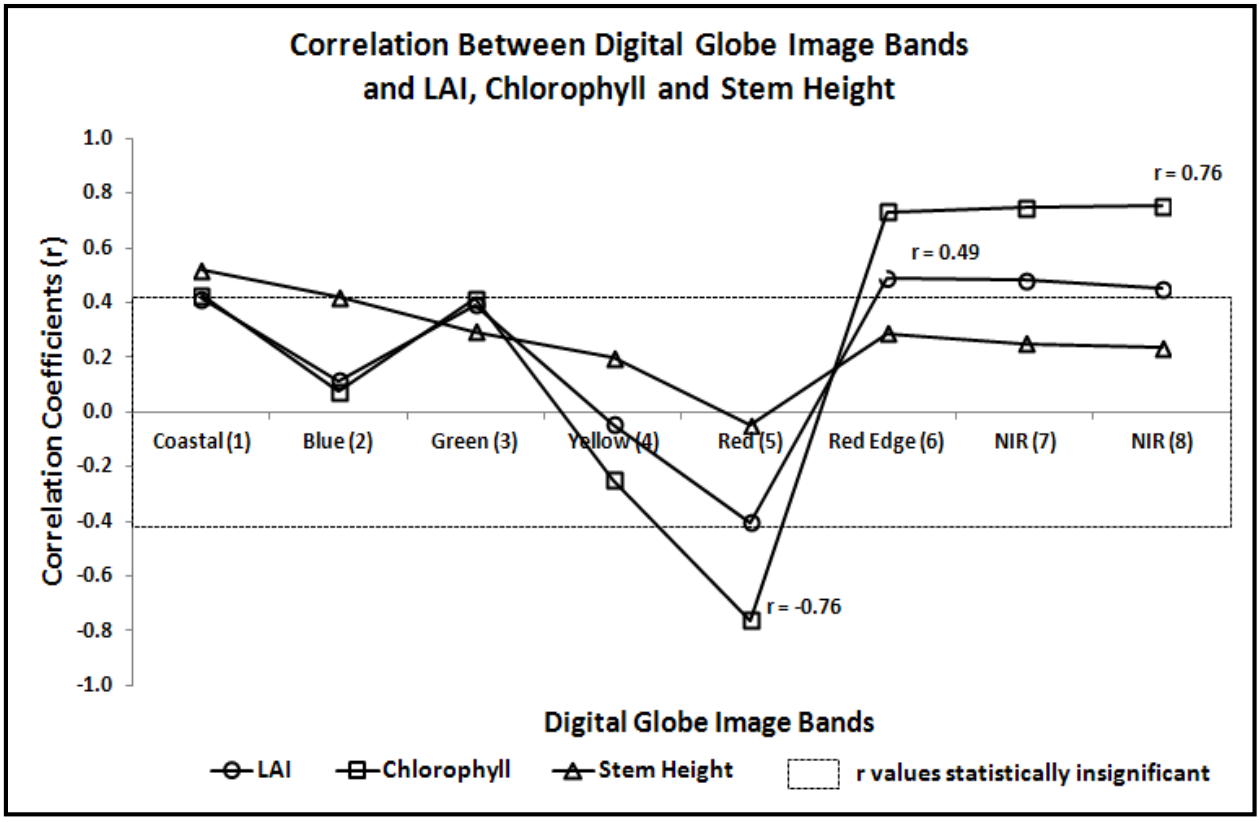

Figure 3.15 (a) Optimal regression model for predicting chlorophyll concentration. (b) 95% confidence intervals for predicted chlorophyll concentration

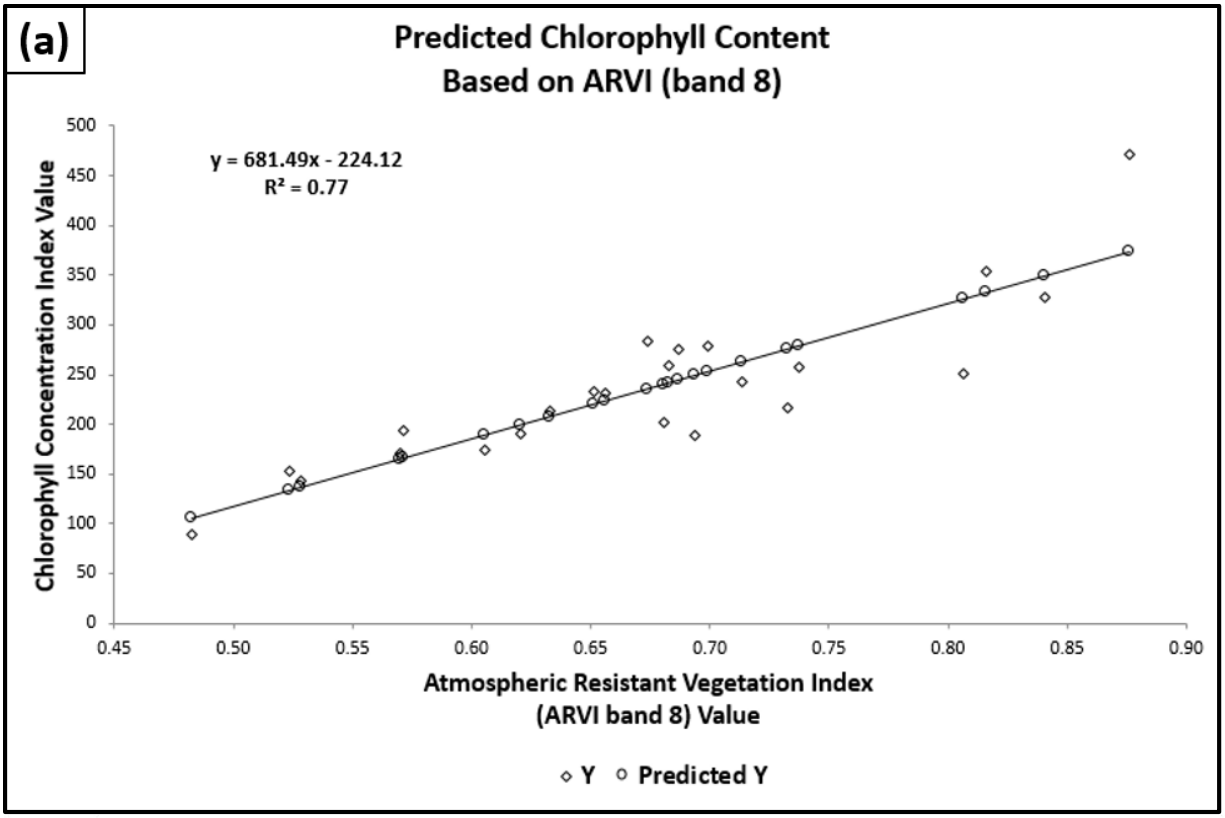

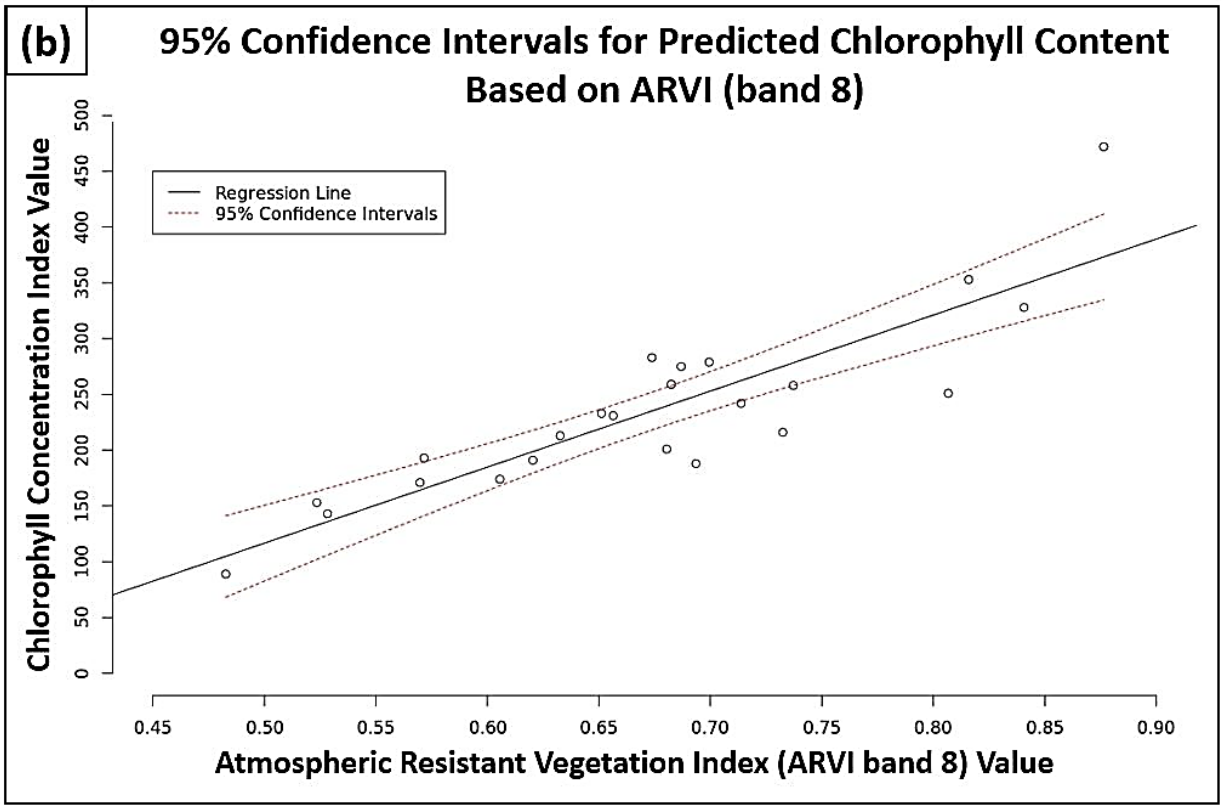

Figure 3.16 Estimated chlorophyll concentration based on ARVI using DG-WV2 near infrared band 8 (860-1040 nm).

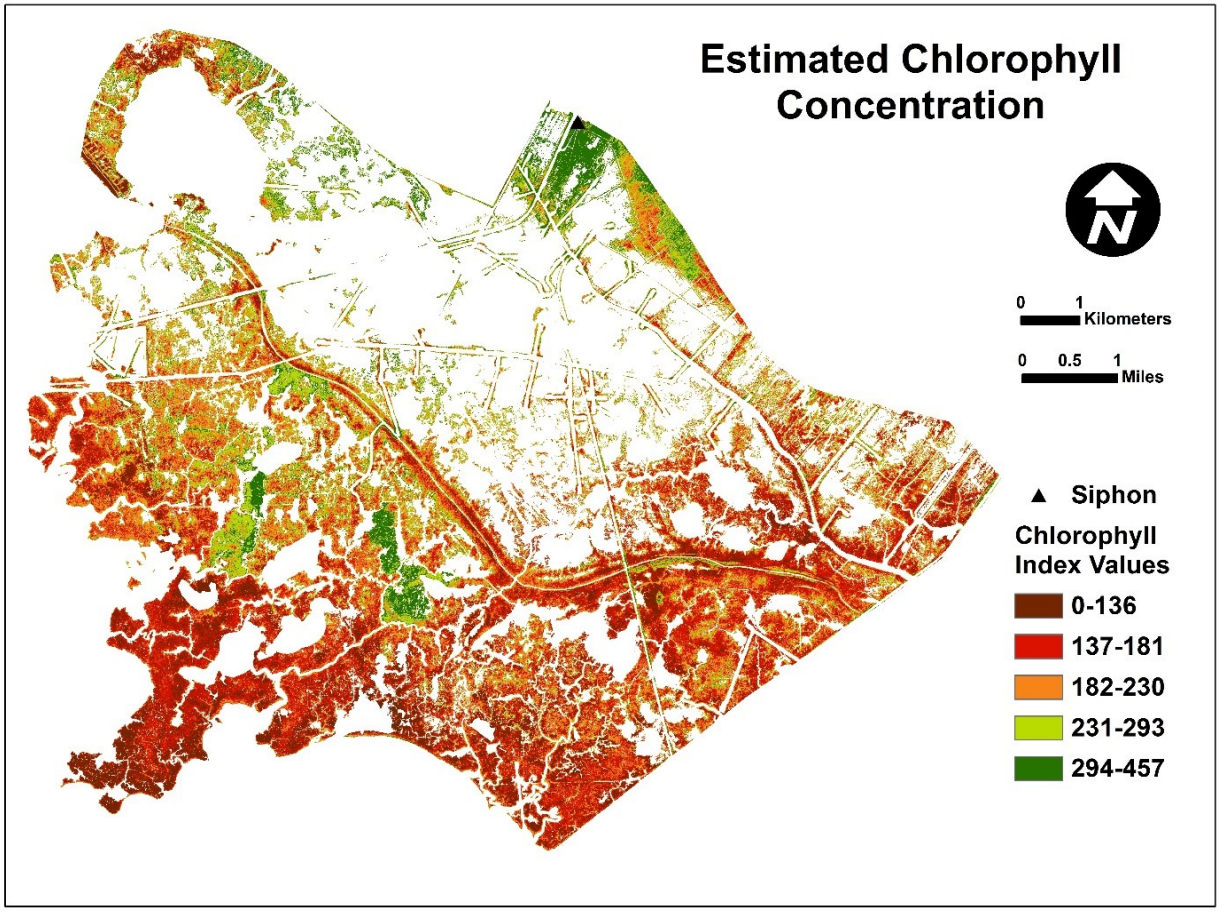

Figure 3.17 Map depicting level of confidence in estimated chlorophyll concentration.

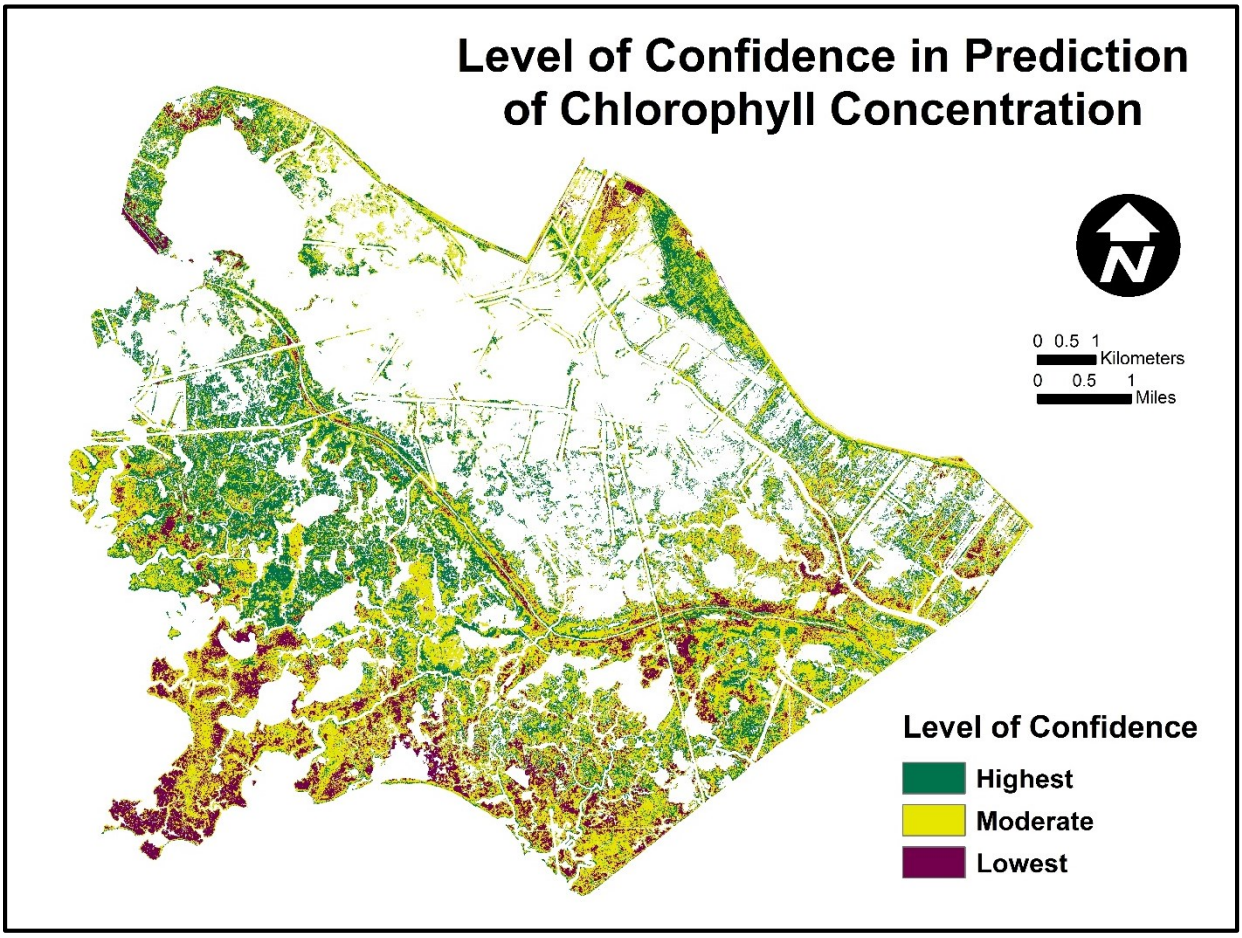

Figure 3.18 Estimated chlorophyll concentration map with 500 m buffers overlaid.

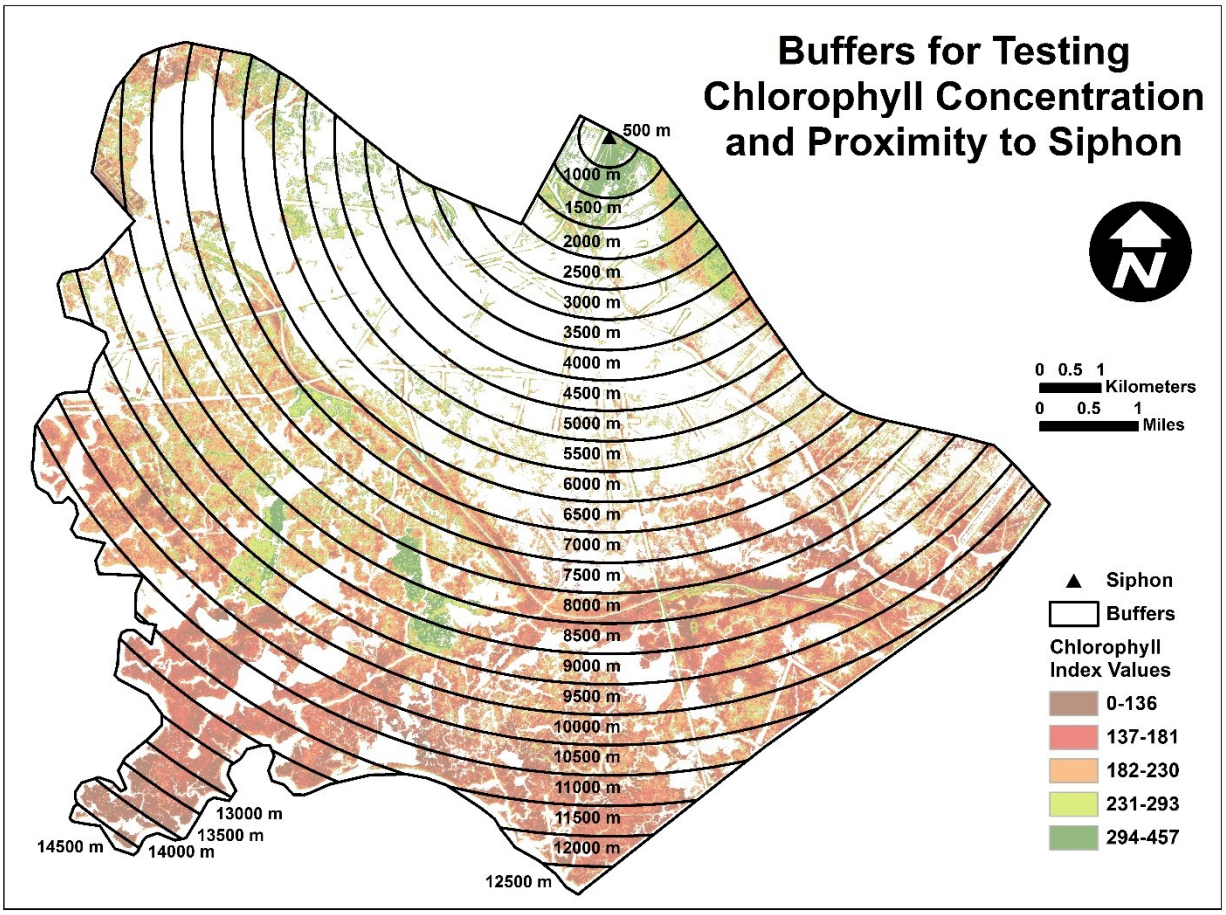

Figure 3.19 Graph depicting the relationship between highest and lowest chlorophyll concentration and distance to the siphon.

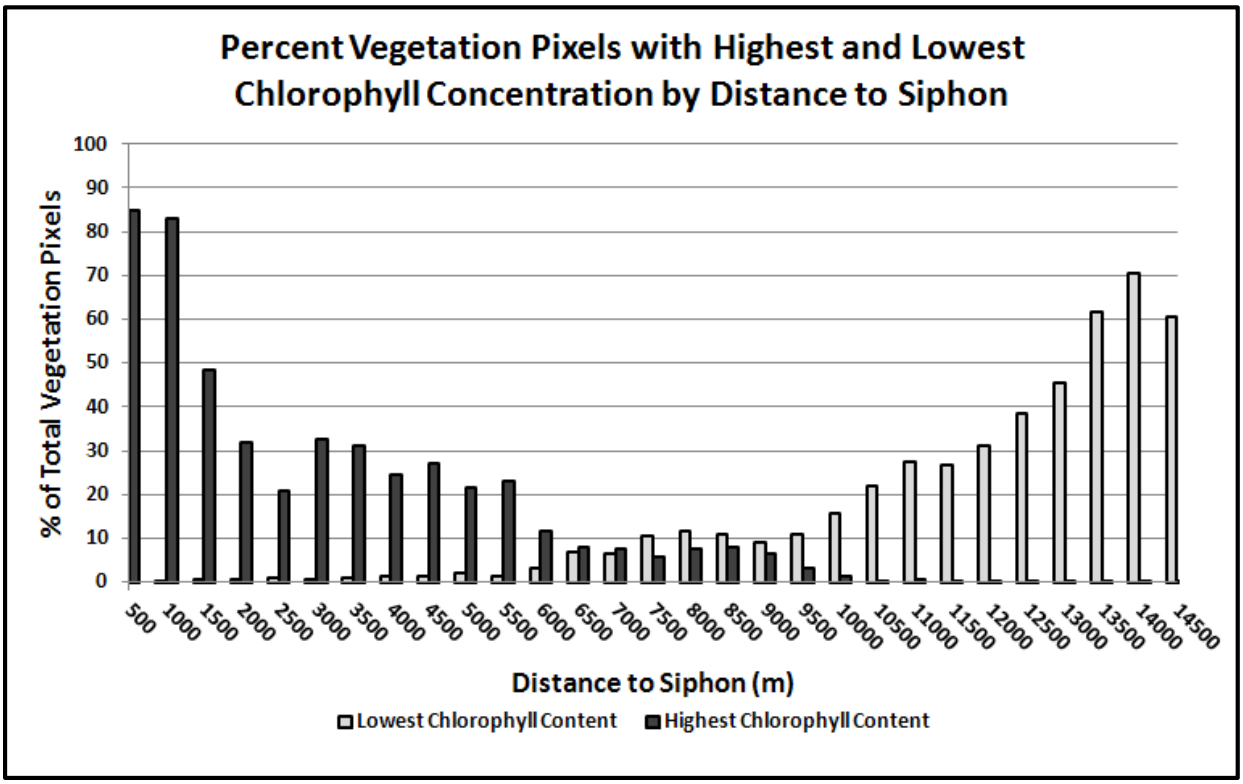

Figure 3.20 Graph depicting the relationship between highest and lowest chlorophyll concentration within high freshwater impact areas and distance to the siphon.

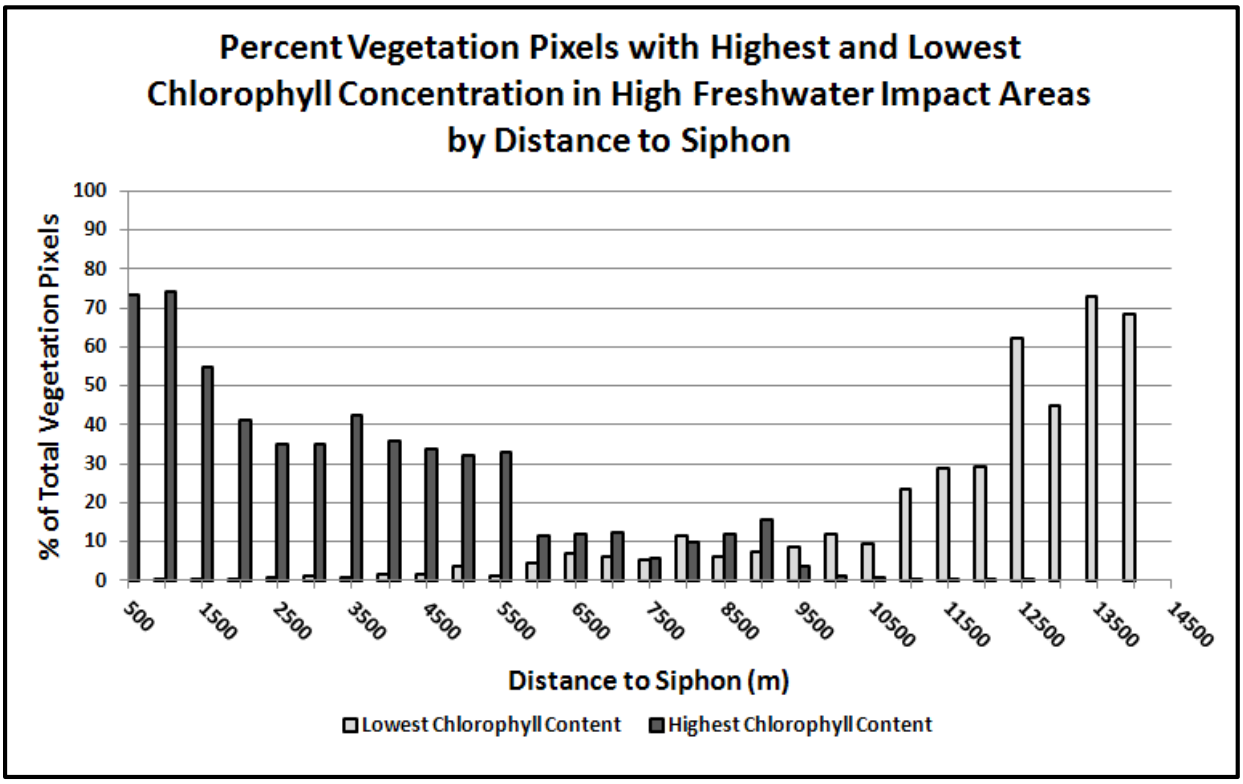

Figure 3.21 Graph depicting the relationship between highest and lowest chlorophyll concentration within low freshwater impact areas and distance to the siphon.

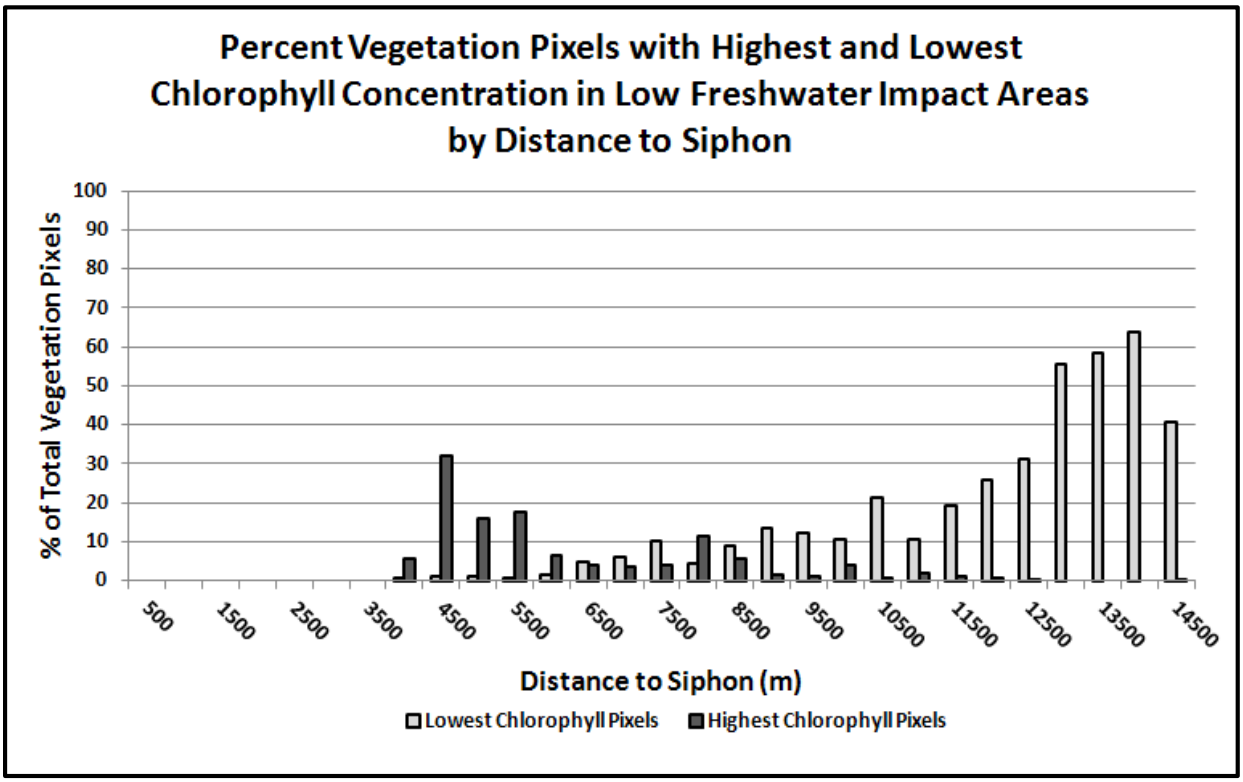

Figure 3.22 Areas of unusually high chlorophyll concentration evident in (a) the estimated chlorophyll concentration map, (b) the DG-WV2 composite NDVI map, and (c) the Landsat 5 TM NDVI map, are not evident in (d) the LiDAR-derived DEM.

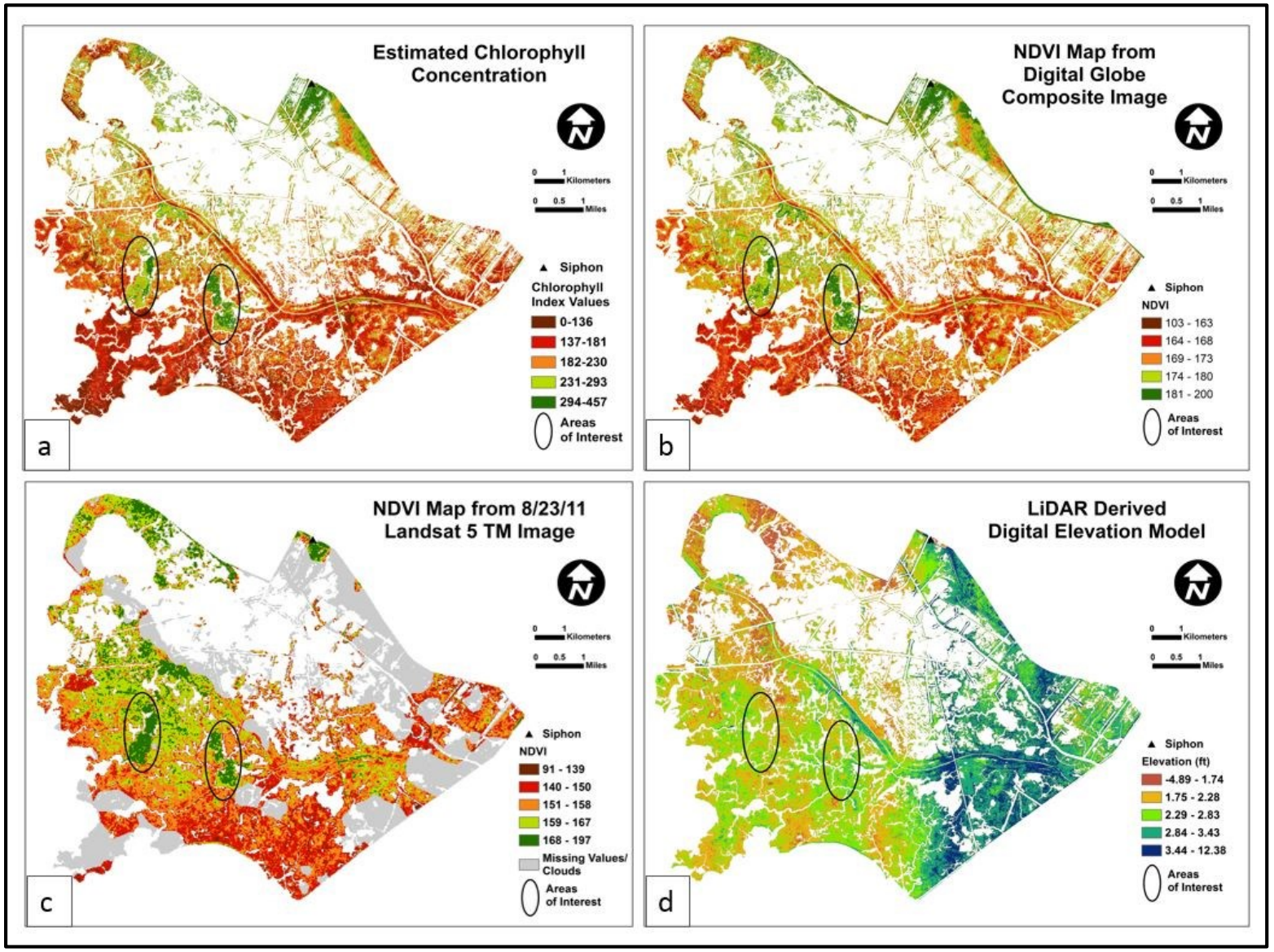

Table 3.1 Satellite image data specifications.

	Band	Wavelength (nm)	Nominal Spectral Location
DigitalGlobe WorldView2	1	400-450	Coastal
Bands 1-8, 2 m	2	450-510	Blue
Panchromatic 0.5 m	3	510-580	Green
	4	585-625	Yellow
	5	630-690	Red
	6	705-745	Red Edge
	7	770-895	NIR1
	8	860-1040	NIR2
	pan	450-800	Panchromatic
Landsat 5 TM	1	450-520	Blue
Bands 1-5 and 7, 30 m	2	520-600	Green
Band 6, 120 m	3	630-690	Red
	4	760-900	NIR
	5	1550-1750	MIR
	6	10400-12500	Thermal
	7	2080-2350	MIR

(Adapted from DigitalGlobe, 2009 and USGS, 2011)

Table 3.2 Pre- and post-siphon operation satellite image dates and associated freshwater flows at WPH siphon diversion project.

Pre-siphon operation (no flow)	Post-siphon operation	
Satellite image dates	Satellite image dates	Freshwater flow (cfs)
04/06/1984	04/02/1994	2023.82
01/19/1985	09/25/1994	118.80
10/08/1987	04/07/1996	1519.67
01/28/1988	02/08/1998	787.01
2/13/1988	02/24/1998	903.08
11/01/1990	01/26/1999	1311.58
11/17/1990	04/18/2000	721.22
03/09/1991	09/17/2000	777.25
02/08/1992	11/20/2000	783.88
10/05/1992	02/27/2002	1327.31
	10/20/2003	1057.15
	02/25/2010	530.66

Table 3.3 Twelve satellite image dates during siphon operation and nearest salinity data dates.

Satellite image dates/ siphon operating	Nearest salinity data dates
04/02/1994	03/29/1994
09/25/1994	09/13/1994
04/07/1996	04/02/1996
02/08/1998	02/17/1998
02/24/1998	02/17/1998
01/26/1999	01/25/1999
04/18/2000	04/18/2000
09/17/2000	09/28/2000
11/20/2000	11/21/2000
02/27/2002	03/07/2002
10/20/2003	10/13/2003
02/25/2010	03/03/2010

Table 3.4 Seventy-one salinity data dates corresponding to no flow periods (siphon not operating for at least 7 days prior to each salinity data date).

No flow dates with available salinity data		
10/11/1994	10/12/1999	01/16/2006
11/09/1994	11/16/1999	02/24/2006
12/07/1994	12/14/1999	03/28/2006
01/04/1995	01/19/2000	04/28/2006
02/15/1995	02/22/2000	05/26/2006
03/14/1995	05/02/2001	06/27/2006
04/10/1995	08/15/2001	07/28/2006
04/26/1995	09/04/2001	08/31/2006
05/23/1995	10/08/2001	09/27/2006
06/06/1995	10/26/2001	10/24/2006
06/07/1995	08/16/2002	08/27/2007
06/22/1995	09/03/2002	10/02/2007
10/17/1995	10/10/2002	11/01/2007
11/02/1995	11/07/2002	11/30/2007
11/14/1995	12/28/2002	12/28/2007
12/12/1995	07/17/2003	08/22/2008
01/17/1996	08/18/2003	09/26/2008
09/16/1997	09/03/2003	10/28/2008
10/21/1997	09/10/2004	12/03/2008
11/17/1997	10/13/2004	01/07/2009
12/16/1997	11/09/2004	02/16/2009
03/16/1999	10/14/2005	10/15/2009
08/25/1999	11/21/2005	10/14/2010
09/16/1999	12/19/2005	

Table 3.5 Mean salinity for high and low freshwater impact sites by siphon flow.

High freshwater impact sites	Low freshwater impact sites	Mean salinity (ppt) (siphon flow)	Mean salinity (ppt) (no siphon flow)
BA04-01	-	5.68	11.13
BA04-02	-	5.59	11.89
BA04-03	-	7.57	13.18
BA04-05	-	6.13	11.38
BA04-07	-	9.90	14.17
BA04-11	-	8.11	11.64
BA04-12		7.07	9.83
BA04-16	-	8.13	10.64
BA04-55	-	11.53	14.91
-	BA04-06	10.85	13.96
-	BA04-08	11.42	14.64
-	BA04-09	11.70	14.16
-	BA04-10	11.49	13.97
-	BA04-15	12.24	14.59
-	BA04-17	11.33	12.59

Table 3.6 Regression equations and resulting r^2 and RMSE values by DigitalGlobe WorldView2 (DG-WV2) image band.

08/01/11 Image			
Band	r^2	Equation	RMSE
1 (Coastal)	.99	Band1 = (0.381859*$n1_080111_radiance(1)) - 32.6621	0.78
2 (Blue)	.99	Band2 = (0.269234723*$n1_080111_radiance(2)) - 21.4367225	0.81
3 (Green)	.99	Band3 = (0.268849236*$n1_080111_radiance(3)) - 13.51864027	0.82
4 (Yellow)	.99	Band4 = (0.316101915*$n1_080111_radiance(4)) - 12.32399846	1.05
5 (Red)	.99	Band5 = (0.298159806*$n1_080111_radiance(5)) - 8.4834054	0.96
6 (Red Edge)	.96	Band6 = (0.371882565*$n1_080111_radiance(6)) - 1.80636633	2.20
7 (NIR1)	.90	Band7 = (-0.0009*($n1_080111_radiance(7)**2) + 0.6552*$n1_080111_radiance(7)) - 7.6661	4.84
8 (NIR2)	.88	Band8 = (-0.002*($n1_080111_radiance(8)**2) + 0.9774*$n1_080111_radiance(8)) - 1.2164	4.40
08/06/11 Image			
Band	r^2	Equation	RMSE
1 (Coastal)	.99	Band1 = (0.330643144*$n1_080611radiance(1)) - 23.19931939	0.73
2 (Blue)	.99	Band2 = (0.234535754*$n1_080611 _radiance(2)) - 14.34778922	0.34
3 (Green)	.99	Band3 = (0.254956446*$n1_080611 _radiance(3)) - 8.98327148	0.68
4 (Yellow)	.99	Band4 = (0.294879488*$n1_080611 _radiance(4)) - 7.432270408	0.95
5 (Red)	.99	Band5 = (0.261416983*$n1_080611 _radiance(5)) - 3.773811245	1.07
6 (Red Edge)	.97	Band6 = (-0.0004*($n1_080611_radiance(6)**2) + 0.4568*$n1_080611_ radiance(6)) - 3.949	3.27
7 (NIR1)	.90	Band7 = (-0.0008*($n1_080611 _radiance(7)**2) + 0.597*$n1_080611_radiance(7)) - 4.775	5.73
8 (NIR2)	.91	Band8 = (-0.0018*($n1_080611_ radiance(8)**2) + 0.8807*$n1_080611_ radiance(8)) + 1.625	6.97

Table 3.7 Regression equations and resulting r^2 values for composite image predicted values.

Band	r^2	Equation
1 (Coastal)	0.05	Band 1 = 2.295 + 0.187 x
2 (Blue)	0.24	Band 2 = 1.393 + 0.477 x
3 (Green)	0.65	Band 3 = 1.086 + 0.762 x
4 (Yellow)	0.70	Band 4 = 0.943 + 0.785 x
5 (Red)	0.72	Band 5 = 0.657 + 0.834 x
6 (Red Edge)	0.89	Band 6 = 6.373 + 0.675 x
7 (NIR1)	0.89	Band 7 = 5.938 + 0.811 x
8 (NIR2)	0.90	Band 8 = 7.663 + 0.799 x

Table 3.8 Vegetation indices and equations

Vegetation Index	Equation
Normalized Difference Vegetation Index	NDVI = *(NIR-red)/(NIR+red)*
Green NDVI	GNDVI = *(NIR-green)/(NIR+green)*
Wide Dynamic Range Vegetation Index	WDRVI = *(a*NIR-red)/(a*NIR+red)* (where a = a weighting parameter based on vegetation density characteristics*)
Atmospherically Resistant Vegetation Index	ARVI = *[NIR-(2.0*red-blue)]/ [NIR-(2.0*red+blue)]*

* Based on vegetation density characteristics within the study area, a weighting parameter of 0.2 was used to calculate WDRVI, as recommended by Gitelson (2004).

Table 3.9 Correlation coefficients (r-values) relating satellite image bands and vegetation indices with vegetation parameters (*$P < 0.05$, **$P < 0.01$).

	LAI	Chlorophyll	Stem Height
DG1	0.413	0.426*	0.521*
DG2	0.115	0.075	0.421*
DG3	0.391	0.414*	0.294
DG4	-0.045	-0.251	0.198
DG5	-0.405	-0.763**	-0.048
DG6	0.489*	0.733**	0.287
DG7	0.482*	0.749**	0.251
DG8	0.450*	0.755**	0.234
ARVI (band 7)	0.437*	0.862**	0.117
ARVI (band 8)	0.407	0.877**	0.144
GNDVI (band 7)	0.252	0.780**	0.032
GNDVI (band 8)	0.127	0.748**	0.038
NDVI (band 7)	0.386	0.851**	0.049
NDVI (band 8)	0.343	0.862**	0.070
WDRVI (band 7)	0.386	0.851**	0.049
WDRVI (band 8)	0.343	0.862**	0.070

Table 3.10 Predictive value of chlorophyll model.

Site	Chlorophyll		Difference	(Difference)²	Absolute Value of Difference
	Actual	Predicted			
1	174	189.58	-15.58	242.76	15.58
2	171	163.49	7.51	56.36	7.51
3	143	134.81	8.19	67.07	8.19
BA04-103	188	251.38	-63.38	4017.13	63.38
BA04-104	216	278.77	-62.77	3940.13	62.77
BA04-108	242	263.40	-21.40	458.16	21.40
BA04-112	328	352.95	-24.95	622.30	24.95
BA04-116	259	240.16	18.84	355.04	18.84
BA04-119	258	279.61	-21.61	467.04	21.61
BA04-120	89	108.82	-19.82	392.79	19.82
BA04-123	283	232.90	50.10	2509.84	50.10
BA04-124	233	219.04	13.96	195.01	13.96
BA04-125	191	199.13	-8.13	66.17	8.13
BA04-126	231	222.87	8.13	66.15	8.13
BA04-128	193	162.74	30.26	915.77	30.26
BA04-132	472	344.58	127.42	16235.69	127.42
BA04-133	251	335.95	-84.95	7215.84	84.95
BA04-134	353	328.65	24.35	592.78	24.35
BA04-136	279	251.26	27.74	769.71	27.74
CRMS0258	201	241.33	-40.33	1626.73	40.33
CRMS0260	213	206.68	6.32	39.91	6.32
CRMS0282	275	242.57	32.43	1051.68	32.43
CRMS3680	153	129.33	23.67	560.23	23.67
Minimum value		89			
Maximum value		472			
Mean		234.61			
Standard deviation		79.27			
Mean absolute error (MAE)		32.25			
Root mean square error (RMSE)		42.96			

Table 3.11 Correlation coefficients (r-values) relating distance to siphon with percentage of pixels in highest and lowest chlorophyll classes by freshwater impact.

Relationship between distance to siphon and:	Correlation coefficient (r)	Significance (*P*)
% of pixels in highest chlorophyll class	-0.83	<0.0001
% of pixels in highest chlorophyll class in highest freshwater impact areas	-0.91	<0.0001
% of pixels in highest chlorophyll class in lowest freshwater impact areas	-0.19	(not significant)
% of pixels in lowest chlorophyll class	0.87	<0.0001
% of pixels in lowest chlorophyll class in highest freshwater impact areas	0.71	<0.0001
% of pixels in lowest chlorophyll class in lowest freshwater impact areas	0.83	<0.0001

Table 3.12 Summary of field data measurements for vegetation parameters.

Sample site	Average stem height (cm)	Average chlorophyll concentration	LAI
1	181	174	4.12
2	155	171	3.54
3	188	143	3.79
BA04-103	151	188	4.03
BA04-104	166	216	3.73
BA04-108	173	242	5.1
BA04-112	167	328	6.97
BA04-116	169	259	3.45
BA04-119	170	258	2.89
BA04-120	197	89	2.18
BA04-123	174	283	2.29
BA04-124	166	233	4.38
BA04-125	176	191	4.45
BA04-126	183	231	3.72
BA04-128	200	193	5.41
BA04-132	216	472	6.25
BA04-133	167	251	4.52
BA04-134	215	353	4.31
BA04-136	167	279	5.63
CRMS 0258	163	201	3.44
CRMS 0260	146	213	2.69
CRMS 0282	171	275	4.3
CRMS 3680	163	153	5.68
Mean	174.96	234.61	4.21
Standard Deviation	18.09	79.27	1.22

Chapter 4 - **Modeling Vulnerability to Eutrophication in a Coastal Louisiana Marsh Using Satellite Imagery and Measures of Historical and Concurrent Marsh Biophysical Characteristics**

Abstract

This study was undertaken to investigate the feasibility of modeling eutrophication vulnerability of a coastal Louisiana marsh receiving turbid Mississippi River water. The major objective was to integrate remotely sensed data with field measurements of vegetation biophysical characteristics and historical ecosystem survey data to delineate landscape patterns suggestive of vulnerability to eutrophication. To accomplish this goal, satellite image data were used in conjunction with measurements of field spectra and vegetation biophysical characteristics. Leaf Area Index (LAI), chlorophyll concentration, average stem height, and vegetation species composition, including percent cover and the presence or absence of nutrient and/or salinity tolerant species, were collected across vegetation productivity and freshwater impact gradients. Historical ecosystem survey data including marsh community type, vegetation species composition, percent cover of herbaceous layer, and average herbaceous plant height were incorporated into the analysis. Image data and vegetation dynamics were analyzed using an agglomerative hierarchical clustering method to classify sample sites as exhibiting higher or lower vulnerability to eutrophication. Pixels associated with the classified sample sites were used as training data in a supervised Maximum Likelihood classification to produce a eutrophication vulnerability map. Assessment of the resulting map using a Jackknife Cross Validation approach yielded an accuracy of 88% for the higher eutrophication vulnerability class and 91% for the lower vulnerability class, with an overall accuracy of 89%. These results suggest that marsh areas within this ecosystem that exhibit relatively higher susceptibility to

eutrophication can be delineated using satellite imagery, marsh vegetation parameters, and historical ecosystem survey data.

Introduction

Louisiana's coastal wetlands, like many throughout the world, are deteriorating and disappearing at an alarming rate due to natural and anthropogenic stressors. Natural subsidence, erosion, and storm effects are exacerbated by artificial flood control levees that have effectively isolated the Mississippi River from its delta, (Lopez, 2009; Day *et al*., 2009a). Extensive networks of canals constructed for oil and gas exploration and the extraction of natural resources have contributed to subsidence and erosion and promoted saltwater intrusion into Louisiana's freshwater marshes (Lopez, 2009; Day *et al*., 2009a). During the past half century, one major strategy for combating saltwater intrusion and stimulating marsh growth has been the construction of Mississippi River diversions designed to reintroduce freshwater into wetland ecosystems (Day *et al*., 2009a). During this same period, an increase in runoff of fertilizers, pesticides and other pollutants from agricultural and urban areas has adversely affected water quality in the rivers and streams of the 3 million km^2 Mississippi River Basin (Cloern, 2001; Mitsch, *et al.*, 2005; Siciliano, *et al.*, 2008). Pollutants transported to coastal zones by sediment laden river water affect nutrient dynamics and phytoplankton productivity (Doxaran *et al*., 2009; Volpe *et al*., 2011; Guttler *et al.,* 2013). The Mississippi River transports excess nitrogen, in the form of nitrate-nitrogen, to coastal areas in Louisiana, where the subtropical climate, warm water temperatures, and long growing season facilitate high nutrient uptake and denitrification rates (Mitsch, *et al.,* 2005). The potential for eutrophication is a major concern, since the diversions introduce nutrient enriched Mississippi River water and sediment into wetland areas (Sklar and Browder 1998; Lissner *et al.*, 2003; Lane and Day, 1999; Mitsch *et al.,* 2005; Day *et al*., 2009a).

Although eutrophication generally refers to gradual nutrient enrichment in water bodies (Christropherson, 2009; Ferreira *et al*., 2011), in the presence of very high loading rates, nutrients also accumulate in soils and vegetation (Dettmann, 2001; Kamer *et al.*, 2001). Excess nutrient loadings alter wetland ecosystem processes and produce measurable changes in plant productivity, including increases in net primary productivity (U.S. EPA, 2002; Ferreira *et al*., 2011). Despite increased above ground biomass, several studies have linked excess nutrient loading in salt marshes to reductions in below ground plant growth, root and rhizome biomass, and carbon accumulation, as well as decreases in geomorphic stability and marsh elevation (Darby and Turner, 2008a, 2008b; Turner *et al.*, 2009; Turner, 2010; Deegan *et al.*, 2012). In contrast to those findings, Day *et al.* (2009b) reported high belowground biomass in marshes impacted by the river diversion at Caernarvon, Louisiana. Based on a synthesis of previous studies Day *et al.* (2009a) also challenged Darby and Turner's (2008a; 2008b) results showing that the nutrient loading rates they used far exceeded rates found in the outfall area of the Caernarvon, Louisiana river diversion. Yet, Howes *et al.* (2010) found storm-related preferential erosion in Louisiana marshes that received diverted freshwater for 18 years prior to Hurricanes Katrina and Rita. This lack of consensus underscores the need to better understand the effects of river diversions on nutrient enrichment of Louisiana's wetlands (Day *et al.*, 2009a; Boustany, 2010).

One strategy for detecting and monitoring nutrient enrichment of wetland ecosystems is to characterize nutrient dynamics through periodic water sampling performed weekly or monthly, a strategy that may not fully capture the effects of nutrient pulsing (Siciliano, *et al.*, 2008). Since estuarine plant tissues integrate the nutrient regime over time another approach is to harvest plant tissues seasonally to examine nutrient content as an indicator of eutrophication

(Boyer and Fong, 2005; Cohen and Fong, 2006; Siciliano, *et al.*, 2008). When applied over large areas in wetland environments, both strategies are resource intensive and often impractical in terms of safety and accessibility (Siciliano, *et al.*, 2008; Bethel, *et al*., 2011). Since data are generally collected from the most easily accessible sites during a limited number of campaigns, the value of the data may be limited both spatially and temporally, often requiring interpolation over large areas and extended time periods (Siciliano, *et al.*, 2008; Volpe *et al.,* 2011).

Another strategy is to examine functional and/or structural indicators of eutrophication to determine whether an ecosystem is eutrophic or unenriched (U.S. EPA, 2002). Functional indicators are associated with high chlorophyll content and include increased biomass production and stem height, and increased leaf nitrogen and phosphorus content (U.S. EPA, 2002). Functional indicators become evident once the ecosystem's threshold of assimilative capacity is exceeded, leading to increased nutrient uptake and increased growth (U.S. EPA, 2002). Ecosystem processes such as decomposition and accumulation of soil organic matter are altered, sometimes resulting in structural indicators of eutrophication, including changes in plant community composition and shifts from nutrient-intolerant to nutrient-tolerant species (U.S. EPA, 2002).

A fourth approach, satellite remote sensing, offers an underutilized tool that can be integrated with more traditional approaches to monitor possible eutrophication from freshwater diversions. Water diverted from the Mississippi River contains high concentrations of suspended particulate matter (SPM) and exhibits significantly higher reflectance than clear water (Froidefond *et al*. 2002; Li *et al*. 2003; Allen *et al*., 2008). Reflectance differences in the near infrared and red wavelengths can be leveraged to map turbidity in river diversion outfall areas, while turbidity frequency mapping can facilitate analysis over time (Harrington and Schiebe,

1992; Miller and McKee, 2004; Allen *et al*., 2008). Furthermore, in addition to being a relative measure of the amount of suspended particulate matter (SPM) in water, turbidity is an important water quality parameter that can also be used as an indicator of eutrophication (Fraser, 1998; Guttler *et al*., 2013).

Remote sensing offers a practical approach for monitoring functional and structural indicators of eutrophication in coastal marshes. Spectral reflectance data are useful for assessing vegetation biophysical characteristics, including biomass and nutrient content (Hardisky *et al.*, 1984; Hardisky *et al*., 1986; Guo and Price, 2000; Rundquist *et al.*, 2001; Siciliano *et al.*, 2008). Wetland biomass estimates based on *in situ* indices were reported by Hardisky *et al*. (1984) to be comparable to estimates from traditional harvest techniques. A subsequent study of salt marsh vegetation found biomass and plant canopy height significantly correlated with red and near infrared (NIR) spectral reflectance (Hardisky *et al*., 1986). Jensen *et al*. (1998) found that non-intrusive *in situ* LAI measurements of salt marsh vegetation were significantly correlated with *in situ* above-ground biomass measurements. Results of a 2002 study by Jensen *et al*. again found that the NIR band and selected vegetation indices, including the Normalized Difference Vegetation Index (NDVI), were highly correlated with biomass, LAI, and chlorophyll concentration in an estuarine salt marsh. In support of these findings, strong correlations between NDVI and plant primary productivity, NDVI and biomass, and NDVI and LAI have been reported in the literature (Tucker and Sellers, 1986; Justice *et al*., 1998, and Wang *et al*., 2004). The utility of NDVI is based on the difference between low red reflectance and high NIR reflectance of healthy vegetation (Gitelson *et al*., 1996; Gitelson 2004). In the presence of moderate to high vegetation density, however, there is a reduction in the sensitivity of NDVI to changes in green biomass due to the saturation of red reflectance at its lowest level (Gitelson *et*

al., 1996; Gitelson, 2004). Other indices developed in response to the observed saturation of NDVI and of particular interest for wetland vegetation studies include the Green Normalized Vegetation Index (GNDVI) (Gittelson *et al*., 1996), the Wide Dynamic Range Vegetation Index (WDRVI) (Gittelson, 2004), and the Atmospherically Resistant Vegetation Index (ARVI), (Kaufman and Tanre, 1992). The GNDVI replaces the green band for the red band in the NDVI and has been used to successfully assess biomass variation (Gittelson *et al*., 1996; Vigier *et al*., 2004). The WDRVI enhances the dynamic range of the NDVI using a weighting parameter based on vegetation density characteristics within a study area (Gittelson, 2004). The ARVI has been shown to be slightly more sensitive to vegetation changes and less sensitive to atmospheric and soil affects than other indices in the presence of moderate to high vegetation cover (Qi *et al*., 1994). Each of these indices has been used to successfully estimate spatial patterns of salt marsh biomass (Gitelson *et al.*, 1996; Zhang *et al*., 1997; Gitelson, 2004), suggesting their utility for delineating regions of high marsh biomass relative to introduced nutrient rich freshwater.

Research to develop effective methods for assessing and monitoring nutrient enrichment of Louisiana's coastal wetlands is needed. This study integrates satellite image data, field measurements of vegetation biophysical data, and historical ecosystem survey data in order to identify functional and structural indicators of eutrophication and to map vulnerability to nutrient enrichment in the West Pointe a la Hache siphon diversion outfall area. The ability to accurately model potentially eutrophic and relatively unenriched wetland areas allows for sound sample collection protocols and contributes to effective assessment and monitoring of eutrophication risks associated with freshwater introduction into Louisiana's wetland ecosystems.

Study Area

The study area (Figure 4.1) is an approximately 138 km^2 portion of the Barataria Basin, an interdistributary estuarine wetland system of the Mississippi Delta located in Plaquemines Parish, Louisiana. Like the larger Barataria Basin, the study area has been severely impacted by wetland degradation and loss, having experienced some of the highest rates of land loss in Louisiana's coastal zone (Conner and Day, 1987; Barras *et al*., 2003; Barras, 2009; Bethel *et al*., 2011). Vegetation within the estuary is characterized by a progression of fresh, intermediate, brackish, and salt marshes, moving to open water (Conner and Day, 1987). Land areas generally support high density marsh vegetation dominated by salt tolerant species, including *Spartina alterniflora* and *Distichlis spicata*. Bordered by the Mississippi River to the east, the study area incorporates both highly degraded and fragmented marsh areas north and northeast of Bayou Grand Chenier Ridge, as well as relatively intact core marsh west and southwest of the ridge, a juxtaposition allowing compelling comparisons.

Located within the study area on the west bank of the Mississippi River at river kilometer 78.7 (mile 48.9) is the West Pointe a la Hache (WPH) Siphon Diversion Project (Haywood and Boshart, 1998). The project is a relatively low-flow diversion designed to provide freshwater and sediment to the marshes for restoration and land building (OCPR, 2010; LaCoast, 2008). The diversion consists of eight 1.8 m diameter steel siphon pipes that cross over the levee, run underground, and then discharge river water into an outfall pond. Four channels radiate southward from the pond to distribute freshwater to the surrounding marsh (Richardi, 2013). Freshwater flow at WPH typically ranges between 500-1000 ft^3s^{-1} (14-28 m^3s^{-1}) when the siphon is operational, although maximum discharge for the siphons is estimated as 2144 ft^3s^{-1} (61 m^3s^{-1}), based on high river stage and all siphons in full operation, (Richardi, 2013). The siphon is estimated to have operated approximately 60% of the time since flow began in January, 1993

(Richardi, 2013). Although WPH siphon has had some effect in reducing salinity in the outfall area, land loss continues in the project area (Boshart and Van Cook, 2007; Richardi, 2013).

Methods

Landsat 5 Thematic Mapper Satellite Image Data

Water Turbidity Frequency Datasets

Water turbidity frequency datasets were produced for this study by the U.S. Army Corps of Engineers (USACE) based on a technique developed by Allen *et al*. (2008) and outlined in Appendix A. The datasets are based on time series cloud-free Landsat images captured between 1984 and 2010 and corresponding to periods of pre- and post-siphon operation of the WPH diversion project. Satellite image specifications are provided in Table 4.1. For the post-siphon operation time period, optimal Landsat image dates were chosen to coincide with siphon freshwater flow based on records obtained from Louisiana Coastal Protection and Restoration Authority (CPRA) Strategic Online Natural Resources Information System (SONRIS, 2011). Pre- and post-siphon operation satellite image dates and associated freshwater flows are provided in Table 4.2.

The USACE datasets consist of two turbidity frequency maps, adapted versions of which are provided in Figures 4.2 and 4.3. The pre-1993 turbidity map (Figure 4.2) depicts the frequency of classification of water pixels as turbid during the pre-siphon time period between 1984 and commencement of siphon operation in 1993. This turbidity frequency dataset was used to estimate baseline turbidity. The post-1993 turbidity map (Figure 4.3) depicts the frequency of classification of water pixels as turbid for image dates captured during periods of siphon operation between 1993 and 2010.

Estimating Highest and Lowest Turbidity Post-Siphon Operation

The USACE turbidity frequency datasets were used to derive an estimate of turbidity attributed to siphon operation. This was accomplished by comparing pre- and post-1993 turbidity. The USACE turbidity frequency datasets were reprojected to UTM, Zone 15, GRS 1980, NAD 83 and checked for consistent alignment. For each turbidity frequency map, five classes of water turbidity were identified using natural breaks in ArcGIS, a geographic information system (GIS) software. The highest turbidity classes in the pre- and post-siphon datasets were compared and areas of intersection were removed from the post-siphon turbidity data. The resulting subset provides a map layer representing areas of highest turbidity associated with freshwater flow during siphon operation, thus indicating locations that consistently received distributions of sediment-laden freshwater from the siphon (Allen *et al*., 2008). This procedure was repeated for the lowest turbidity classes in the pre- and post-siphon datasets to create a map layer delineating areas of lowest turbidity associated with siphon freshwater flow.

Mapping High and Low Freshwater Impacted Marsh Areas

ArcGIS was used to identify marsh areas subject to relatively high and low freshwater impacts. Landsat 5 TM imagery captured April 17, 2011 was reprojected to UTM, Zone 15, GRS 1980, NAD 83 and checked for consistent alignment with the turbidity frequency maps. The imagery was subset to the study area and a land-water map was developed using a hybrid classification method described by Bethel *et al*. (2011) and outlined in Appendix B. A vegetation-only layer was created from the land-water map by masking pixels representing water and developed land. Restricting subsequent remote sensing and geographic information system processing to vegetation-only pixels minimized the influence of non-vegetation pixels and insured that final results were based solely on analysis of pixels classified as marsh vegetation. The vegetation layer was then included in a GIS with the map layers produced from the turbidity

frequency data delineating highest and lowest turbidity associated with freshwater flow during siphon operation.

In the GIS environment 15 m buffers were created around areas of highest and lowest turbidity associated with siphon operation. Those areas within the highest turbidity buffers were classified as high freshwater impact areas and those within the lowest turbidity buffers were classified as low freshwater impact areas. Vegetated areas within the highest turbidity buffers were identified as marsh areas most consistently exposed to freshwater introduction, while vegetated areas within the lowest turbidity buffers were identified as marsh areas least impacted by freshwater introduction. Figure 4.4 shows the resulting freshwater impacts map delineating vegetated marsh areas subject to high and low freshwater impacts.

Accuracy Assessment of Freshwater Impacts Map

Hydrographic salinity data obtained from SONRIS were used to assess the accuracy of the freshwater impact map (SONRIS, 2012). Figure 4.5 shows the locations of salinity data collection sites within areas of high and low freshwater impacts. For salinity estimates during siphon operation, 12 salinity data dates were identified as dates of siphon operation nearest the Landsat image capture dates (Table 4.3). For no flow salinity estimates, 71 salinity data dates were identified for periods in which the siphon had not operated for a minimum of 7 days (Table 4.4). Estimates of mean salinity (ppt) during siphon freshwater flow and no flow periods were calculated for the 9 salinity data collection sites in high freshwater impact areas and for the 6 salinity data collection sites in low freshwater impact areas (Table 4.5). All salinity estimates were based on hourly bottom and surface salinity readings. The Mann-Whitney statistical method was used to test for differences in mean salinity in high and low freshwater impact areas during both freshwater flow and no flow periods (VassarStats, 2014).

Mapping the Vegetation Productivity Gradient

To aid in the identification of appropriate field data collection sites, a map of the study area's vegetation productivity was created. The map was based on an NDVI derived from the Landsat 5 Thematic Mapper (TM) image acquired over the study area on April 17, 2011 and classified into areas of high, medium, and low NDVI values (Figure 4.6).

Field Data

Sample Site Selection

A randomized opportunistic sampling approach was used for field data collection. This allowed the use of preexisting sample sites maintained by Louisiana's Coastal Protection and Restoration Authority (CPRA), many of which include infrastructure in the form of boardwalks conducive to field sampling in the marsh. Sample sites were selected to insure data collection across vegetation productivity and freshwater impact gradients within the study area. A GIS dataset of existing CPRA sample sites, the NDVI-based Vegetation Productivity Gradient map (Figure 4.6), and the Freshwater Impacts map (Figure 4.4) were co-registered in ArcGIS to derive 6 classes of potential sample sites: low freshwater impact/low NDVI; low freshwater impact/medium NDVI; low freshwater impact/high NDVI; high freshwater impact/low NDVI; high freshwater impact/medium NDVI; and high freshwater impact/high NDVI. Based on the sample site classification a field investigation was conducted to determine the suitability of each potential site for data collection in terms of accessibility and sufficient area of contiguous emergent marsh vegetation. Figure 4.7 shows the 24 sample sites identified with 4 sites representing each of the 6 classes described above. All but 3 of the sample sites chosen were preexisting CPRA sample sites.

Field Data Collection

Field data collection was accomplished during peak growing season on August 2 and August 3, 2011, and included measuring vegetation-based indicators of marsh health and possible nutrient enrichment, including spectral reflectance as an indicator of overall health, chlorophyll concentration as a proxy for leaf nitrogen content, and leaf area index (LAI) and plant stem height as a proxy for above ground biomass (U.S. EPA, 2002; Bethel *et al*., 2011). Ocular estimates of vegetation cover were also collected using a modified Daubenmire quadrat technique (Daubenmire, 1959). To insure accurate identification of species, digital images and vegetation samples were collected at each site for subsequent species verification by Louisiana Department of Natural Resources (LDNR) personnel (Boshart, 2011). The resulting survey of vegetation species and associated percent cover were used to assess the presence or absence of nutrient and/or salinity tolerant species and to assign marsh community types.

All field data were collected within single, approximately 4.0 m^2 plots located at each sample site. The sites were GPS located using a Trimble Nomad 900GLC hand held computer and were accessed by boat. An Ocean Optics USB4000 Field Spectroradiometer (~350-1045 nm at ~ 0.2 nm resolution), mounted on a pole to minimize interference with data collection, was used to simultaneously measure incoming solar radiation and top of canopy (TOC) reflectance at each sample site. TOC reflectance was measured approximately 0.75 m above the canopy. Reflectance measurements were calibrated once at each site using a white (99% reflectance) Spectrolon calibration panel, after which three reflectance measurements distributed within the sample plot were collected and averaged. A Li-Cor 2000 LAI meter was used to estimate foliage biomass at each of the sample sites. Three sample sequences, each consisting of one above canopy for every four below canopy measurements, were taken at each site and averaged. The above canopy measurements were taken to calibrate the LAI readings for atmospheric conditions

(LAI-2000, 1992). Average stem height at each sample site was calculated based on measurements of the five to ten tallest stems of dominant species within each sample plot according to procedures outlined by U.S. EPA (2002). A Field Scout CM1000 chlorophyll meter was used to measure relative leaf chlorophyll concentration. Within each sample plot, average chlorophyll concentration was derived from five CM1000 measurements collected using standard procedures outlined by the CM1000's manufacturer (FieldScout, 2009). The CM1000 senses reflectance at 700 nm, the wavelength absorbed by chlorophyll ***a***, and at 840 nm, a wavelength unaffected by leaf chlorophyll content that serves as an indicator of how much light is reflected due to leaf physical characteristics. The ratio of reflectance at 700 nm to reflectance at 840 nm is multiplied by a constant to derive an index value between 0 and 999, with higher values indicative of higher chlorophyll content (FieldScout, 2009). A study by Murdock, *et al.* (2004) found that the Field Scout, measuring reflectance, rather than transmittance and absorbance, and offering the advantage of canopy measurement rather than single leaf measurement, performed as well as the SPAD 502 chlorophyll meter for obtaining measurements in the field.

All field data were collected at ground level outside the boat whenever possible. When necessary for reasons of safety or adequate access, the boat was positioned adjacent to the shore at the sample site and data were collected from floor level of the boat or from a specially designed platform and ladder apparatus within the boat (Figure 4.8).

Assignment of Marsh Community Type Based on Field Data Collection

To determine marsh community type at the time of field data collection, the marsh assignment algorithm used by CPRA to derive community salinity scores and assign marsh types was applied to the field data. Based on the algorithm, marsh at a vegetation cover plot is

classified as fresh, intermediate, brackish, or saline using a community salinity score derived from species composition (Visser and Sasser, 2002; Sasser and Visser, 2008; Sasser, *et al*, 2008; Cretini, *et al*, 2009). To apply the algorithm, the percent cover for each vegetation species found within a plot is multiplied by a predefined value assigned to the species based on the marsh type where the species is most commonly found (Table 4.6). The sum of the resulting products is divided by the total cover to calculate the community salinity score and determine the marsh community type (Visser and Sasser, 2002). Table 4.7 provides the salinity scores for common marsh vegetation species. Table 4.8 lists marsh community assignments by community salinity score and Table 4.9 provides an example of the calculation of community salinity score and assignment of marsh community type. Marsh community scores and community assignments for each sample site for the time period of field data collection are provided in Table 4.10.

Digital Globe WorldView 2 Image Data

Data acquisition, preprocessing, and accuracy assessment

DG-WV2 satellite images were acquired over the study area on August 1 and August 6, 2011 (within 4 days of field data collection). Each image covered the aerial extent of the study area delivered as georeferenced and radiometrically corrected products scaled to absolute spectral reflectance (DigitalGlobe, 2010). Satellite image specifications are provided in Table 4.1. The raw digital numbers (DN) of each image were converted to top-of-atmosphere radiance and an empirical line method was used to relate radiance to band equivalent reflectance (BER) of field spectra as described by Staben, *et al*. (2011). This was accomplished for each image band by extracting values for the brightest and darkest pixels and for pixels corresponding to a random selection of 12 of the field sample sites. The extracted pixel values were used to generate a regression equation for each image band to convert radiance values to reflectance values.

Accuracy assessment was based on computing the root mean square error (RMSE) for each image band by comparing the pixel values of the reflectance image to the corresponding BER of field spectra at the sample sites not selected to generate the regression equations. The RMSE represents the average magnitude of error, providing a measure of the spread of the data around the regression line. Analysis of the computed RMSE values revealed that sample site BA01-114 contributed disproportionally to the total error for each band, suggesting that it was an outlier. Examination of field notes and photos taken at the site confirmed that the data point should be excluded based on the extent of exposed dark soils unique to that sample site. The data point was removed from further analysis and revised regression equations were developed. The regression equations used to produce the final reflectance images and the associated RMSEs are provided in Table 4.11.

Removal of cloud contamination and creation of composite image

Since the two satellite images covered the same areal extent and were captured within a six day period, cloud contamination was removed by creating a composite of the two images. Clouds and cloud shadows were masked from each image using the hybrid classification method described by Bethel *et al*. (2011) and outlined in Appendix B. This procedure was followed by digitization to remove remnant hazy areas. Pixel values were extracted from both images at 400 random points located within intersecting cloud-free areas of the images. The extracted pixel values were used to generate regression equations for each image band to predict the missing values in the cloud-masked August 1 image based on values from the August 6 image. The resulting composite image retained the original reflectance values of the August 1 image at all field sample sites and in all other areas not contaminated by clouds. In areas where cloud contamination had been removed from the August 1 image the composite image incorporated

values predicted by the regression equations. Regression equations relating the two images are provided in Table 4.12.

Classification of composite image, classification accuracy assessment, and creation of vegetation indices

The composite image was classified into three classes, water, vegetation, and developed land, using the hybrid classification method described by Bethel *et al*. (2011) and outlined in Appendix B. Developed land consisted of an exceptionally small percentage of the total pixels in the scene, making accuracy assessment of that class unfeasible. Following close visual inspection developed land was masked from the classification. Accuracy assessment of the resulting water/vegetation classification was performed using 150 stratified random points. The water pixels were then masked from the classified image and vegetation indices were calculated using the vegetation-only data. The indices calculated included the NDVI, GNDVI, WDRVI, and ARVI. Based on vegetation density characteristics within the study area, including moderate to high LAI values, a weighting parameter of 0.2 was used to calculate WDRVI, as recommended by Gitelson (2004). Two of each of the indices were calculated, one using DG-WV2 NIR band 7 (770-895 nm) and one using DG-WV2 NIR band 8 (860-1040 nm). The formulas used to calculate the vegetation indices are provided in Table 4.13.

Historical Data

To analyze vegetation dynamics, including changes in species composition and plant communities over time, historical vegetation data were obtained from SONRIS (CPRA) for the 20 sample sites corresponding to existing vegetation and Coastwide Reference Monitoring System (CRMS) stations. Data for five historical data collection periods between 1997 and 2009 were available for sample sites corresponding to vegetation stations. For sample sites associated

with CRMS stations, data were available for four historical data collection periods between 2007 and 2010. Historical data corresponding to the period prior to commencement of siphon operation were not available. Data for each CPRA vegetation station were collected at a single location, while CPRA CRMS data were collected along transects. Analysis of CRMS historical data was limited to data collected at the latitudinal and longitudinal transect location nearest each GPS-located field sample. Table 4.14 summarizes the data collection periods, associated data collection locations, and types of historical vegetation data analyzed for this study. Table 4.15 lists the marsh community types for each sample site by data collection period. A list of species found at each sample site is provided in Table 4.16.

Estimating Vegetation Nutrient and Salinity Tolerance

The US EPA's *National Database of Wetland Plant Sensitivities to Enrichment and Hydrologic Alteration* was used to estimate the sensitivity to nutrient and salinity increases of all vegetation species catalogued during field data collection and/or in the historical data for each sample site (US EPA, 2012). The database lists wetland species and their known sensitivities and allows access to peer-reviewed published studies relating to the tolerances of specific species to nutrient enrichment and hydrologic modification, including salinity increases (US EPA, 2012). Two indices were derived using the database classification system, one for sensitivity to nutrient increases and one for sensitivity to salinity increases. For each index, intolerant (IT) species were assigned a value of 1, somewhat tolerant (ST) species a value of 2, moderately tolerant (MT) species a value of 3, tolerant species (T) a value of 4, and very tolerant (VT) species a value of 5. Index values were assigned to vegetation species found at each sample site during field data collection, as well as to species found during each historical data collection period.

Table 4.17 lists the index values representing known nutrient and salinity sensitivities of vegetation species found at the sample sites historically and/or during field data collection.

Quantifying Change in Vegetation Characteristics

Changes in Vegetation Species Number and Average Herb Height

To estimate the increase or decrease in species number at each sample site, the difference between the number of species present at the initial historical data collection period and the number present at field data collection was calculated. The absolute value of the difference provides a measure of the net change in species number over time at that location. To estimate the degree of fluctuation at each sample site, the number of times species number changed between sample periods was divided by the total number of possible fluctuations (i.e. by the total number of sample periods minus 1). Data related to changes in species number are provided in Table 4.18.

The historical data provide the average herb height at each sample site. In contrast, field data collection measured the average height of the 5 to 10 tallest stems within each sample plot. For this reason only historical data were included in the assessment of change in average herb height over time. To estimate the increase or decrease in average herb height at each sample site, the difference between average herb height at the initial historical data collection period and average herb height at the last historical data collection period was calculated. The absolute value of the difference provides a measure of the net change in average herb height at that location. To estimate the degree of fluctuation in average herb height at each sample site, the number of times average herb height changed between sample periods was divided by the total number of possible fluctuations (i.e. by the total number of sample periods minus 1). Data related to changes in average herb height are provided in Table 4.19.

Changes in Nutrient and Salinity Tolerance and in Marsh Community Type

For each sample site, a nutrient tolerance score was calculated for each historical data collection period and for the field data. The scores were calculated by averaging the tolerance index values of species present at the site at the time of data collection. To estimate the increase or decrease in nutrient tolerance, the difference between the score for the initial historical data collection period and the score for field data collection was calculated. The absolute value of the difference provides a measure of the net change in nutrient tolerance over time at that location. To estimate the degree of fluctuation in nutrient tolerance at each sample site, the number of times the nutrient tolerance score changed between sample periods was divided by the total number of possible fluctuations (i.e. by the total number of sample periods minus 1). For each sample site the same procedures were used to derive salinity tolerance scores, to estimate the increase or decrease in salinity tolerance and the net change in salinity tolerance over time, and to estimate the degree of fluctuation in salinity tolerance. Data related to changes in nutrient and salinity tolerance are provided in Tables 4.20 and 4.21, respectively.

Values indicative of relative salinity level were assigned to marsh community types, with freshwater marsh assigned a value of 1, intermediate marsh a value of 2, brackish marsh a value of 3, and saline marsh a value of 4. To provide a measure of the net change in marsh community type at each sample site, the absolute value of the difference between the value for community type at the initial historical data collection period and the value at field data collection was calculated. To estimate the degree of fluctuation in marsh community type at each sample site, the number of times marsh community type changed between sample periods was divided by the total number of possible fluctuations (i.e. by the total number of sample periods minus 1). Data related to changes in marsh community type are provided in Table 4.22.

Quantifying Overall Vegetation Dynamics

To summarize and quantify vegetation dynamics within the study area with regard to functional and structural indicators of nutrient enrichment, a series of questions were formulated to transform qualitative observations of vegetation characteristics to binary data (Table 4.23). The questions were designed to determine whether vegetation dynamics associated with a sample site were suggestive of possible eutrophication. Positive responses to the questions were assigned a value of 1 and negative responses were assigned a value of 0.

Classifying Sample Sites by Vulnerability to Nutrient Enrichment using Cluster Analyses

A series of cluster analyses were performed to group sample sites based on characteristics related to structural and functional indicators of nutrient enrichment. The variables included in the cluster analyses are listed in Table 4.24. Several clustering methods were investigated, with Ward's Minimum Variance method judged most appropriate for analyses of the vegetation parameters and the DG-WV2 satellite image data. Ward's method, which has been shown in standard problems to outperform other hierarchical methods, is an agglomerative hierarchical clustering method that calculates the squared Euclidean distance to the cluster means, then sums the distances and joins the clusters in an order that minimizes the overall sum of the squared distances (Khattree and Naik, 2000). Prior to application of the Ward's method, variables measured on different scales were standardized and correlation analysis was performed to rule out multicolinearity among the variables. In the case of the binary data representing the qualitative assessment of vegetation dynamics, the Flexible-Beta method, was judged most appropriate (Khattree and Naik, 2000). This method defines measures of dissimilarity between sample sites by counting the number of agreements and disagreements in the binary data associated with the sites. Clustering of sites is based on application of a beta coefficient

recommended to be negative yet close to 0 (Khattree and Naik, 2000). All clustering analyses were performed using the statistical software, SAS, and the default value of the beta coefficient, -0.25, was applied for the Flexible-Beta method (SAS Institute Inc., 2013).

To aid in the interpretation of clustering results, several statistical measures were calculated for the vegetation parameter clustering and for the satellite image data clustering. One measure of the homogeneity of a cluster is the root means squared standard deviation (RMSSTD), calculated by pooling the standard deviation of all the variables forming a cluster. The semi-partial R-squared (SPRSQ) is also calculated to measure the loss of homogeneity that results as clusters are combined. Low values for RMSSTD and SPRSQ imply that homogenous groups are being clustered. The R-squared (RSQ) measures the extent to which clusters differ from each other, as does the Between Cluster Sum of Squares (BSS) when used in the Ward's method. For both the RSQ and BSS, higher values signify greater differences between clusters.

Results of the clustering analyses were compared to identify consistencies among the groupings. Based on these consistencies, sample sites were classified as exhibiting higher or lower vulnerability to nutrient enrichment or as non-determinant. Sites considered non-determinant were eliminated from further analysis.

Statistical Analyses of Clustering Results

Summary statistics, including mean and standard deviation, were calculated for sites within each vulnerability class for comparison to overall statistics for the study area. The Mann-Whitney statistical method was applied to the vegetation parameters, the DG-WV2 image data, and the vegetation dynamics binary data to test for significant differences between the vulnerability classes (VassarStats, 2014). The Mann-Whitney method was also used to test for

statistically significant differences between conditions measured at initial sampling compared to conditions measured at final sampling for each vulnerability class (VassarStats, 2014).

Creating a Eutrophication Vulnerability Map and Assessing Accuracy

The DG-WV2 composite image was combined with the WDRVI (NIR band 8; 860-1040 nm) and the GNDVI (NIR band 8; 860-1040 nm) images to create a 10 band image. The normality of the image data was verified, after which a supervised Maximum Likelihood classification was performed. Training data for the classification consisted of pixels associated with the sample sites classified through the cluster analyses as having higher or lower vulnerability to eutrophication. The Jackknife Cross Validation approach was used to assess the accuracy of the resulting binary eutrophication vulnerability map. This approach was implemented by withholding the training data from one sample site, performing the supervised classification using the remaining training data, then checking the accuracy of the classification at the withheld sample site based on the percentage of correctly classified pixels at the site. This process was repeated until all sites had been withheld. An estimation of the accuracy of the classified eutrophication vulnerability map was derived by calculating the total percentage of correctly classified pixels associated with the iteratively withheld sample sites. Additionally, as a means of identifying patterns related to elevation differences within the study area, a Jenks natural breaks 5 class digital elevation model (DEM) was adapted from a 2010 LiDAR-derived DEM (ArcGIS online; LOSCO, LSU, C4G, 2010) for visual comparison to the eutrophication vulnerability map.

Results

High and Low Freshwater Impacts

The spatial distribution of high and low freshwater impact areas depicted on the freshwater impacts map (Figure 4.4) suggests a general reduction in impact with increasing distance from the siphon diversion along a north to south gradient. The location of the Texas Company Canal coincides with a relatively abrupt change from high freshwater impacts north of the canal to low freshwater impacts to the south. In contrast to this general trend, relatively discontinuous and isolated areas of high turbidity were found distant from the siphon to the south and southwest between Bayou Grand Chenier Ridge and Bays Chene Fleur, Batiste, and Sansbois.

Greater fluctuation in mean salinity was observed among high freshwater impact sites compared to low impact sites (Figure 4.9). With the exception of site BA04-12, both high and low freshwater impact sites exhibited greater variation in mean salinity during periods of siphon operation compared to siphon dormancy (Figure 4.10). During siphon flow periods both high and low freshwater impact sites had significantly lower mean salinity ($Z = -3.09$, $P = 0.001$ and $Z = -2.8$, $P = 0.003$, respectively) compared to no-flow periods (Figure 4.11). Although no significant difference was found between high and low freshwater impact sites during periods of siphon dormancy, mean salinity during siphon operation was significantly lower at high freshwater impact sites compared to low impact sites ($Z = -2.65$, $P = 0.004$). The results suggest that siphon operation freshens water throughout the study area, but that water is freshened to a greater extent in areas classified as high freshwater impact areas as compared to areas classified as low impact areas. Furthermore, when salinity data for all dates (freshwater flow and no flow periods) were tested, this finding was replicated. That is, high impact sites were found to be

statistically significantly lower in mean salinity than low freshwater impact sites (Z= -2.42, P = 0.008), suggesting that the overall effect of the siphon is to freshen the high impact areas significantly more than the low impact areas and also suggesting that this effect may extend beyond siphon operation periods.

Image processing, classification, and accuracy assessment

Conversion of the DG-WV2 satellite images to reflectance was judged acceptable based on the resulting RMSE values (Table 4.11) and guidelines outlined by Staben, *et al*. (2001). The water/vegetation classification of the composite image yielded an overall accuracy of 98% with an overall Kappa statistic of 0.96. For the water class, producer's and user's accuracies were 98.65% and 97.33%, respectively. For the vegetation class, producer's and user's accuracies were 97.37% and 98.67%, respectively. Summary statistics for the pixel values extracted from the DG-WV2 composite image and vegetation indices at eutrophication vulnerability-classified sample sites are provided in Table 4.24.

Cluster Analyses

Eutrophication Vulnerability Class Assignments

Cluster analyses of the vegetation biophysical data, the DG-WV2 image data, and the vegetation dynamics binary data, each resulted in a two cluster solution that grouped 12 of the 20 sample sites consistently (Table 4.25). It should be noted that although the cluster statistics supported a 3-cluster solution for the DG-WV2 image data, one of those clusters consisted of just two sample sites, making the 2-cluster solution the better option.

For the vegetation biophysical data analysis, the cluster dendrogram, the summary statistics graphs, and the table of summary statistics are provided in Figure 4.12, Figure 4.13, and Table 4.26, respectively. The cluster dendrogram, the summary statistics graphs, and the table of

summary statistics for the DG-WV2 data are provided in Figure 4.14, Figure 4.15, and Table 4.27, respectively. The cluster dendrogram for the vegetation dynamics binary data is provided in Figure 4.16. Based on shared characteristics suggestive of possible eutrophication, the seven sample sites consistently assigned to cluster one were classified as having higher vulnerability to eutrophication. The five sample sites consistently assigned to cluster two were classified as having lower vulnerability to eutrophication. The remaining eight sites were considered indeterminate and eliminated from further analysis.

Differences between Nutrient Enrichment Vulnerability Classes

Summary statistics for the study area and for each vulnerability class, as well as results of the Mann-Whitney tests for significant differences between the vulnerability classes are provided in Table 4.24.

Vegetation species number and average herb height

The mean number of vegetation species was statistically significantly greater for the higher eutrophication vulnerability class at both initial ($Z = 2.6$; $P = 0.005$) and final sampling ($Z = 2.68$; $P = 0.004$). Thirteen species were recorded among the higher vulnerability sites at initial sampling and 12 were recorded at final sampling. This contrasts with 6 species found among lower vulnerability sites at initial sampling and 3 found at final sampling. Still, both the higher and lower vulnerability classes experienced on average a statistically significant decrease in the number of vegetation species from initial to final sampling ($Z = 2.6$; $P = 0.005$ and $Z = 2.68$; $P = 0.004$, respectively). Average net change and average degree of fluctuation were not significantly different for the two classes.

At initial sampling, statistically significantly greater average herb height was recorded for the lower eutrophication vulnerability class ($Z = -1.95$; $P = 0.026$), a difference that was not

evident at final sampling of average herb height. Average net change from initial to final sampling and average fluctuation between sample periods were not significantly different for the two vulnerability classes. Although average herb height did not change significantly from initial to final sampling for the higher vulnerability class, for the lower vulnerability class, a statistically significant loss in average herb height was recorded ($Z = 1.67$; $P = 0.05$).

Nutrient and salinity tolerance and marsh community type

At both initial and final sampling the higher eutrophication vulnerability class exhibited a statistically significantly higher level of average nutrient tolerance than the lower vulnerability class ($Z = 2.35$; $P = 0.009$). Average net change and average degree of fluctuation did not differ significantly between the vulnerability classes. Additionally, neither the higher nor the lower vulnerability class changed significantly in terms of average nutrient tolerance between initial and final sampling.

Initial mean salinity tolerance was statistically significantly lower for the higher eutrophication vulnerability class ($Z = -2.76$; $P = 0.0029$), although no significant difference was evident at final sampling. The vulnerability classes did not differ significantly in terms of change in mean salinity tolerance from initial to final sampling. The degree of average fluctuation, however, was statistically significantly greater for the higher vulnerability class ($Z = 0.003$; $P = 0.006$). For the higher vulnerability class final mean salinity tolerance was statistically significantly greater than initial salinity tolerance ($Z = -2.11$; $P = 0.017$), while no difference was observed between initial and final mean salinity tolerance for the lower vulnerability class.

Marsh community scores and community assignments for each sample site for the time period of field data collection are provided in Table 4.15. At initial sampling there was no significant difference in average marsh community type between higher and lower

eutrophication vulnerability classes. Also, the average change in marsh community type from initial to final sampling was not significant for either vulnerability class. At final sampling, however, the higher vulnerability class exhibited statistically significantly fresher average marsh community type than the lower vulnerability class ($Z = -2.76$; $P = 0.003$). Additionally, the average fluctuation in marsh community type between sample periods was statistically significantly higher for the higher vulnerability class ($Z = 2.03$; $P = 0.021$).

LAI, chlorophyll content, average stem height, and vegetation dynamics binary data scores

No statistically significant differences were found between the higher and lower eutrophication vulnerability classes with regard to mean values of LAI, chlorophyll content, and average stem height measured at final sampling.

The mean scores for qualitative measures of vegetation dynamics were statistically significantly greater for the higher eutrophication vulnerability class compared to the lower vulnerability class ($Z = 2.76$; $P = 0.003$). Higher scores suggest a greater risk of eutrophication.

DG-WV2 image data and vegetation indices

Mean reflectance values for DG-WV2 green band (510-580 nm), red edge band (705-745 nm), NIR1 band (770-895 nm), and NIR2 band (860-1040 nm) were statistically significantly greater for the higher eutrophication vulnerability class compared to the lower vulnerability class ($Z = 2.67$; $P = 0.003$ in all cases). No other bands showed significant differences. For each of the vegetation indices derived from the DG-WV2 image data, mean index values were statistically significantly greater for the higher vulnerability class compared to the lower vulnerability class. This finding suggests that higher vulnerability sites are likely characterized by higher above-ground biomass, chlorophyll content, and plant primary productivity than lower vulnerability sites.

Eutrophication Vulnerability Map and Map Accuracy

The eutrophication vulnerability map resulting from the supervised classification of the 10-band composite image is provided in Figure 4.17. Based on Jackknife Cross Validation, the accuracy is estimated at 88% for the higher vulnerability class and 91% for the lower vulnerability class, with overall accuracy estimated at 89%. Areas of higher eutrophication vulnerability tend to be closer in proximity to the source of introduced freshwater, as well as west and southwest of the siphon. Additionally, visual comparison of the eutrophication vulnerability map and the DEM (Figure 4.18) revealed relatively consistent spatial patterns suggesting that areas of higher vulnerability tend to coincide with lower elevation areas within the study area.

Discussion

Consistent clustering of the sample sites based on DG-WV2 image data, historical ecosystem survey data, and vegetation dynamics binary data was followed by findings of statistically significant differences between several eutrophication vulnerability class parameters. Accurate supervised classification of the DG-WV2 image data using the eutrophication vulnerability classified sites for training suggests that potentially eutrophic vegetated areas within this marsh ecosystem were delineated using the outlined methodology. Of particular interest are significant differences in the spectral reflectance characteristics of the eutrophication vulnerability classes, indicating separability with regard to spectral bands important for vegetation studies, including the DG-WV2 green (510-580 nm), red edge (705-745 nm), NIR1 (770-895 nm), and NIR2 (860-1040 nm) bands. Additionally, statistically significant differences between the vulnerability classes with regard to each of the indices tested (NDVI, GNDVI, WDRVI, and ARVI) suggests that the classes differ in characteristics known to be highly

correlated with red reflectance, near infrared reflectance and vegetation indices, including above-ground biomass and plant primary productivity (Hardisky *et al.*, 1984; Hardisky *et al*., 1986; Tucker and Sellers, 1986; Justice *et al*., 1998; Wang *et al*., 2004; Guo and Price, 2000; Rundquist *et al.*, 2001; Jensen *et al*., 2002; Siciliano *et al.*, 2008).

Significant differences in the mean number of vegetation species at both initial and final sampling also support the separation of the vulnerability classes, with higher vulnerability sites exhibiting greater species diversity. Greater species diversity at higher vulnerability sites at initial and final sampling, although contrary to the expectation of a loss of biodiversity in eutrophic ecosystems, is not unexpected. Within the high freshwater impact regions of this ecosystem, introduced nutrient enriched water allows the survival of less salt tolerant species, thereby supporting biodiversity and counteracting loss of species due to saltwater intrusion. Still, both higher and lower vulnerability sites experienced a statistically significant decline in the mean number of vegetation species, likely due to continuing saltwater intrusion, ecosystem degradation, and loss of land to open water. It must be noted, however, that for each historical data collection period, field data collection may have been performed by different personnel with varying levels of expertise in plant identification, introducing the possibility of species misidentification.

At initial sampling there was no significant difference between the vulnerability classes with regard to average marsh community type. At final sampling, however, the average marsh community type was significantly fresher for the higher vulnerability class. This suggests shifts in vegetation communities and possible structural indicators of eutrophication. This interpretation however, is complicated by noteworthy differences between the vulnerability classes with regard to ecosystem stability. Since a significantly greater degree of fluctuation in

average marsh community type occurred in the higher vulnerability class, the question arises as to whether the differences documented at final sampling are of a relatively permanent nature or if they instead represent cyclical changes within the ecosystem. This question is pertinent also with regard to results showing a lack of significant difference in final mean salinity tolerance and final mean nutrient tolerance, despite significant differences at initial sampling. The relatively greater degree of fluctuation in average marsh community, mean salinity tolerance, and mean nutrient tolerance within the higher vulnerability class suggests that changes may relate to intermittent siphon operation. While disturbances are recognized as an intrinsic part of ecosystem dynamics and a source of heterogeneity (Sousa, 1984; Lee and Brown, 2011), studies suggest that thresholds exist, which when reached, usher in ecosystem regime changes representing alternative stable states (Scheffer *et al*., 2001; Carpenter *et al.*, 2011). The observed greater fluctuations associated with the higher vulnerability class suggest that ecosystem regime changes may be occurring based on a freshwater introduction threshold, possibly leading to alternative stable states that affect flora and fauna within the study area.

The lack of significant differences between the eutrophication vulnerability classes with regard to LAI and chlorophyll content may be due to the relatively uniform abundance of healthy green vegetation across the study sites at the height of growing season. The lack of significant difference in average stem height may be explained by the method of measurement and the species composition of the sample sites. All 3 species found at the lower vulnerability sites were also found at the higher vulnerability sites, raising the possibility that stem height, based on the average of the 5 tallest stems at each site, frequently represented the same species at each site, thereby accounting for a lack of variation. *Spartina alterniflora,* generally one of the tallest herbaceous plants encountered within the sample plots, was found at 9 of the 12 classified

sample sites, supporting this possibility. Additionally, although a significant difference was found at initial sampling, no difference between the vulnerability classes was found at final sampling. This finding, as well as the significant loss in average herb height for the lower vulnerability class from initial to final sampling, may be attributable to differences in species composition and to loss of species over time.

Finally, the significant difference between the vulnerability classes with regard to the vegetation dynamics binary data scores supports the separation of the classes. On average the scores associated with higher vulnerability sites were significantly greater indicating that the vegetation dynamics associated with those sites showed consistencies with functional and structural indicators of nutrient enrichment.

Conclusions

High resolution remotely sensed image data, field measurements of vegetation biophysical characteristics and historical ecosystem survey data were used to model eutrophication vulnerability of a coastal Louisiana marsh impacted by the introduction of turbid Mississippi River water. Cluster analysis of the data resulted in the classification of field sample sites as having higher or lower vulnerability to eutrophication. Statistical analysis of the clustering results revealed significant differences between the vulnerability classes in a majority of the parameters. The eutrophication vulnerability map derived from supervised classification of satellite imagery based on the cluster analysis results had an estimated overall accuracy of 89%. Areas of higher eutrophication vulnerability were generally closer in proximity to the source of introduced freshwater (Figure 4.17). Additionally, visual comparison of the eutrophication vulnerability map and a LiDAR-derived DEM (Figure 4.18) revealed relatively

consistent spatial patterns suggesting that areas of higher vulnerability tend to coincide with lower elevation areas within the study area.

Significantly higher fluctuations in average marsh community type, and in nutrient and salinity tolerance associated with the higher eutrophication vulnerability class suggest that intermittent operation of the siphon diversion may be causing ecosystem regime changes based on a freshwater introduction threshold. As a result, alternative stable states may be disrupting ecosystem stability and adversely affecting flora and fauna especially within higher eutrophication vulnerability regions of the study area.

The results of this study suggest that potentially eutrophic and relatively unenriched wetland areas can be successfully delineated using the described methodology. The ability to accurately model vulnerability to eutrophication allows for sound sample collection protocols and contributes to effective assessment and monitoring of eutrophication risks associated with freshwater introduction into Louisiana's wetland ecosystems.

References

Allen, Y.C.; Constant, G.C., and Couvillion, B.R., 2008. Preliminary classification of water areas within the Atchafalaya Basin Floodway System by using Landsat imagery: U.S. Geological Survey Open-File Report 2008-1320, 14p. URL: http://pubs.usgs.gov/of/2008/1320/

ArcGIS online, LOSCO, LSU, C4G, 2010. http://www.esri.com/software/arcgis/arcgisonline

Barras, J.A.; Beville, S.; Britsch, D.; Hartley, S.; Hawes, S.; Johnston, J.; Kemp, P.; Kinler, Q.; Martucci, A.; Porthouse, J.; Reed, D.; Roy, K.; Sapkota, S., and Suhayda, J., 2003. Historical and projected coastal Louisiana land changes: 1978-2050. U.S. Geological Survey Open-File Report 03-334, 39p.

Barras, J.A., 2009. Land area change and overview of major hurricane impacts in coastal Louisiana, 2004-08. Scientific Investigations Map 3080. Reston, Virginia: U.S. Geological Survey, scale 1:250,000, 6 sheets.

Bethel, M.B.; Brien, L.F.; Danielson, E.J.; Laska, S.B.; Troutman, J.P.; Boshart, W.M.; Giordino, M.J., and Maurice A. Phillips, 2011. Blending Geospatial Technology and Traditional Ecological Knowledge to Enhance Coastal Restoration Decision-Support Processes in Coastal Louisiana. Journal of Coastal Research, 27(3), 555-571.

Boshart, W.M., and Van Cook, P.E., 2007. 2005 Operations, Maintenance, and Monitoring Report for West Pointe a la Hache Siphon Construction (BA-04). Louisiana Department of Natural Resources, Coastal Restoration Division and Coastal Engineering Division, New Orleans, Louisiana. 18p.

Boshart, W.M., 2011. Vegetation species verification via personal communication.

Boustany, R.G., 2010. Estimating the benefits of freshwater introduction into coastal wetland ecosystems in Louisiana: Nutrient and sediment analyses. Ecological Restoration, 28(2), 160-174.

Boyer, K.E., and P. Fong, 2005. Macroalgal-mediated transfers of water column nitrogen to intertidal sediments and salt marsh plants. Journal of Experimental Marine Biology and Ecology, 321, 59-69.

Carpenter, S.R.; Cole, J.J.; Pace, M.L.; Batt, R.; Brock, W.A.; Cline, T.; Coloso, J.; Hodgson, J.R.; Kitchell, J.F.; Seekell, D. A.; Smith, L., and Weidel, B., 2011. Early warnings of regime shifts: a whole-ecosystem experiment. Science, 332, 1079-1082.

Christopherson, R.W., 2009. Geosystems, 7th Edition. Upper Saddle River, NJ: Pearson Prentice Hall, 639p.

Cloern, E.C., 2001. Our evolving conceptual model of the coastal eutrophication problem. Marine Ecology Progress Series, 210, 223-253.

Cohen, R.A., and Fong, P., 2006. Using opportunistic green macroalgae as indicators of nitrogen supply and sources to estuaries. Ecological Applications, 16(4), 1405-1420.

Conner, W.H. and Day, J.W. Jr., (ed.), 1987. The Ecology of Barataria Basin, Louisiana: an Estuarine Profile. Coastal Ecology Institute, Center for Wetland Resources, Louisiana State University, Baton Rouge, Louisiana, Biological Report 85, 7-13.

Cretini, K.F.; Visser, J.M.; Krauss, K.W., and Steyer, G.D., 2009. CRMS Vegetation Analytical Team Framework.

Darby. F.A. and Turner, R.E., 2008(a). Below- and aboveground Spartina alterniflora production in a Louisiana salt marsh. Estuaries and Coasts, 31, 223-231.

Darby, F.A. and Turner, R.E., 2008(b). Effects of eutrophication on salt marsh root and rhizome biomass accumulation. Marine Ecology Progress Series, 363, 63-70.

Daubenmire, R., 1959. A canopy-coverage method of vegetational analysis. Northwest Sci., 33, 43-64.

Day, J.W.; Cable, J.E.; Cowan, J.H., Jr.; DeLaune, R.; de Mutsert, K.; Fry, B.; Mashriqui, H.; Justic, D.; Kemp, P.; Lane, R.R.; Rick, J.; Rick, S.; Rozas, L. P.; Sneddens, G; Swenson, E.; Twilley, R.R., and Wissel, B., 2009 (a). The impacts of pulsed reintroduction of river water on a Mississippi delta coastal basin. The Journal of Coastal Research, 54, 225-243.

Day, J.; Lane, R.; Moerschbaecher, M.; DeLaune, R; Twilley, R.; Mendelssohn, I., and Baustian, J., 2009 (b). The impact of the Caernarvon diversion on above and belowground marsh biomass in the Breton Sound Estuary after Hurricane Katrina. Final Report submitted to the Louisiana Department of Natural Resources, Project 2512-07-01.

Deegan, L.A.; Johnson, D.S.; Warren, R.S.; Peterson, B.J.; Fleeger, J.W.; Fagherazzi, S., and W.M. Wollheim, 2012. Coastal eutrophication as a driver of salt marsh loss. Nature, 490(7420), 388-392.

Dettmann, E.H., 2001. Effect of water residence time on annual export and denitrification of nitrogen in estuaries: A model analysis. Estuaries, 24(4), 481-490.

DigitalGlobe, Inc., 2010. Technical Note 2010-11-01. Radiometric Use of WorldView-2 Imagery.

Doxaran, D.; Ruddick, K.; McKee, D.; Gentili, B.; Tailliez, D.; Chami, M., and Babin, M., 2009 Spectral variations of light scattering by marine particles in coastal waters, from visible to near infrared. Limnology and oceanography, 54(4), 1257.

Ferreira, J.G.; Andersen, J.H.; Borja, A.; Bricker, S.B.; Camp, J.; Cardoso da Silva, M.; Garces, E.; Heiskanen, A.; Humborg, C.; Ignatiades, L.; Lancelot, C.; Menesguen, A.; Tett, P.; Hoepffner, N., and Claussen, U., 2011. Overview of eutrophication indicators to assess environmental status within the European Marine Strategy Framework Directive. Estuarine, Coastal and Shelf Science, 93, 117-131.

Fieldscout CM1000 Chlorophyll Meter Product Manual, 2009. Spectrum Technologies, Inc. URL: http://www.specmeters.com/assets/1/22/2950CM1000.pdf

Fraser, R.N., 1998. Multispectral remote sensing of turbidity among Nebraska Sand Hills lakes. International Journal of Remote Sensing, 19(15), 3011-3016.

Froidefond, J.; Gardel, L.; Guiral, D.; Parra, M., and Ternon, J.F., 2002. Spectral remote sensing reflectances of coastal waters in French Guiana under the Amazon influence. Remote sensing of Environment, 80(2), 225-232.

Gitelson, A.A.; Kaufman, Y.J., and Merzlyak, M.N., 1996. Use of a green channel in remote sensing of global vegetation from EOS-MODIS. Remote Sensing of the Environment, 58, 289-298.

Gitelson, A.A., 2004. Wide dynamic range vegetation index for remote quantification of biophysical characteristics of vegetation. Journal of Plant Physiology, 161, 165-173.

Guo, X., and Price, K.P., 2000. Modeling Biophysical Factors for Grasslands in Eastern Kansas using Landsat TM Data. Transactions of the Kansas Academy of Science (1903), 122-138.

Güttler, F.N.; Niculescu S., and Gohin, F., 2013. Turbidity retrieval and monitoring of Danube Delta waters using multi-sensor optical remote sensing data: An integrated view from the delta plain lakes to the western–northwestern Black Sea coastal zone. Remote Sensing of Environment, 132, 86-101.

Hardisky, M.A.; Daiber, F.C.; Roman, C.T., and Klemas, V., 1984. Remote Sensing of Biomass and Annual Net Aerial Primary Productivity of a Salt Marsh. Remote Sensing of Environment, 16, 91-106.

Hardisky, M.A.; Gross, M.F., and Klemas, V., 1986. Remote Sensing of Coastal Wetlands. BioScience, 36(7), 453-460.

Harrington J.A.; Schiebe, F.R., and Nix, J.F., 1992. Remote sensing of Lake Chicot, Arkansas: monitoring suspended sediments, turbidity, and secchi depth with Landsat MSS data. Remote Sensing of Environment, 39(1), 15-27.

Haywood III, E.L., and Boshart, W.M., 1998. West Pointe a la Hache freshwater Diversion: three-year comprehensive report. Louisiana Department of Natural Resources/Coastal Restoriation Division, Baton Rouge, LA, USA. Monitoring Series No. BA-04-MSTY-0498-1.

Howes, N.C.; FitzGerald, D.M.; Hughes, Z.J.; Georgiou, I.Y.; Kulp, M.A.; Miner, M.D.; Smith, J.M., and Barras, J.A., 2010. Hurricane-induced failure of low salinity wetlands. Proceedings of the National Academy of Sciences of the United States of America, www.pnas.org/cgi/doi/10.1073/pnas.0914582107

Jensen, J.R., Coombs, C.; Porter, D.; Jones, B.; Schill, S., and White, D., 1998. Extraction of Smooth Cordgrass (Spartina alterniflora) Biomass and Leaf Area Index Parameters from High Resolution Imagery. Geocarto International, 13(4), 25-34.

Jensen, J.R.; Oldon, G.; Schill, S.R.; Porter, D.E., and Morris, J., 2002. Remote Sensing, Leaf-Area-Index, and Chlorophyll a and b Content in the ACE Basin National Estuarine Research Reserve Using Sub-meter digital Camera Imagery. Geocarto International, 17(3), 27-36.

Justice, D.; Hall, D.; Salomonson, V.; Privette, J.; Riggs, G.; Strahler, A.; Lucht, W.; Myeni, R.B.; Knyazikhin, Y.; Running, S.W.; Nemani, R.R.; Wan, Z.; Huete, A.R.; van Leeuwen, W.; Wolfe, R.E.; Giglio, L.; Muller, J.; Lewis, P., and Barnsley, M.J., 1998. The Moderate Resolution Imaging Spectroradiometer (MODIS): Land remote sensing for global change research. IEEE Transactions on Geoscience and Remote Sensing, 36(4) 1228-1249.

Kamer, K.; Boyle, K.A., and Fong, P., 2001. Macroalgal bloom dynamics in a highly eutrophic southern California estuary. Estuaries, 24(4), 623-635.

Kaufman, Y.J., and Tanre, D., 1992. Atmospherically resistance vegetation index (ARVI) for EOS-MODIS, IEEE Trans. Geosci. Remote Sens., 30, 261-270.

Kauth, R.J., and Thomas, G.S., 1976. The tasselled cap-a graphic description of the spectral-temporal development of agricultural crops as seen by Landsat. LARS Symposia, Paper 159.

Khattree, R., and Najk, D.N., 2000. Multivariate Data Reduction and Discrimination with SAS® Software, Cary, NC: SAS Institute Inc. 347-441.

LaCoast. (2008). CWPPRA Restoration Status. URL: http://www.lacoast.gov/reports/rtc/1997/7.htm

LAI-2000 Plant Canopy Analyzer, 1992. Instruction Manual, Lincoln, Nebraska: LI-COR, Inc.

Lane, R., and Day, J., 1999. Water quality analysis of a Freshwater Diversion at Caernarvon, Louisiana. Estuaries, 22(2A), 327-336.

Lee, S., and Brown, M.T., 2011. Understanding self-organization of ecosystems under disturbance using a microcosm study. Ecological Engineering, 37, 1747-1756.

Li, R.R.; Kaufman, Y.J.; Gao, B.C., and Davis, C.O., 2003. Remote sensing of suspended sediments and shallow coastal waters. Geoscience and Remote Sensing, IEEE Transactions on, 41(3), 559-566.

Lissner, J.; Mendelssohn, I.; Lorenzen, B.; Brix, H.; McKee, K., and Miao, S., 2003. Interactive Effects of Redox Intensity and Phosphate Availability on Growth and Nutrient Relations of Cladium Jamaicense (Cyperaceae). American Journal of Botany, 90(5), 736-748.

Lopez, J. A., 2009. The Environmental History of Human-Induced Impacts to the Lake Pontchartrain Basin in Southeastern Louisiana since European Settlement – 1718 to 2002. Journal of Coastal Research, 54, 1-11.

Miller, R.L., and McKee, B.A., 2004. Using MODIS Terra 250 m imagery to map concentrations of total suspended matter in coastal waters. Remote sensing of Environment, 93(1), 259-266.

Mitsch, W.; Day, J.; Zhang, L., and Lane, R., 2005. Nitrate-nitrogen retention in wetlands in the Mississippi River Basin. Ecological Engineering, 24, 267-278.

Murdock, L.; Call, D., and James, J., 2004. Comparison and Use of Chlorophyll Meters on Wheat (Reflectance vs. Transmittance/Absorbance). Cooperative extension service, University of Kentucky-College of Agriculture, AGR-181.

OCPR (Office of Coastal Protection and Restoration), 2010. URL: http://www.ocpr.louisiana.gov/CRM/coastres/project.asp?id=BA-04

Qi, J.; Chehbouni, A.; Huete, A.R., and Kerr, Y.H., 1994. Modified Soil Adjusted Vegetation Index (MSAVI). Remote Sensing of the Environment, 48, 119-126.

Richardi, D.C., 2013. 2012 Operations, Maintenance, and Monitoring Report for West Pointe a la Hache Siphon Construction (BA-04), Coastal Protection and Restoration Authority of Louisiana, New Orleans, Louisiana, 35p.

Rundquist, D.C.; Narumalani, S., and Narayanan, R.M., 2001. A Review of Wetlands Remote Sensing and Defining New Considerations. Remote Sensing Reviews, 20, 207-226.

SAS Institute Inc. (2013). http://www.sas.com/

Sasser, C.E., and Visser, J.M., 2008. Coastwide vegetation data collection project: final report: Baton Rouge, La., Louisiana State University Agricultural Center.

Sasser, C.E.; Visser, J.M.; Mouton, E.; Linscombe, J., and Hartley, S.B., 2008. Vegetation types in coastal Louisiana in 2007: U.S. Geological Survey Open-File Report 2008-1224, 1 sheet, scale 1:550,000, http://pubs.usgs.gov/of/2008/1224/, accessed April 2009.

Scheffer, M.; Carpenter, S.; Foley, J.A.; Folke, C., and Walker, B., 2001. Catastrophic shifts in ecosystems. Nature, 413, 591-596.

Siciliano, E.; Wasson, K.; Potts, D.C., and Olsen, R.C., 2008. Evaluating hyperspectral imaging of wetland vegetation as a tool for detecting estuarine nutrient enrichment. Remote Sensing of Environment, 112, 4020-4033.

Sklar, F., and Browder, J., 1998. Coastal Environmental Impacts Brought About by alterations to Freshwater Flow in the Gulf of Mexico. Environmental Management, 22(4), 547-562.

SONRIS, 2011, 2012. Coastal Protection and Restoration Authority of Louisiana, Louisiana Department of Natural Resources, http://sonlite.dnr.state.la.us/

Sousa, W.P., 1984. The role of disturbance in natural communities. Annual Review of Ecology and Systematics, 15, 353-391.

Staben, G.W.; Pfitzner, K.; Bartolo, R., and Lucieer, A, 2011. Calibration of WorldView-2 Satellite Imagery to Reflectance Data Using an Empirical Line Method. Proceedings of the 34th International Symposium on Remote Sensing of Environment – The GEOSS Era: Towards Operational Environmental Monitoring, Sydney, Australia, http://www.isprs.org/proceedings/2011/ISRSE-34/index.html

Tucker, C.J., and Sellers, P.J., 1986. Satellite remote sensing of primary production. International Journal of Remote Sensing, 7(11), 1395-1416.

Turner, R.E.; Howes, B.L.; Teal, J.M.; Milan, C.S.; Swenson, E.M., and Tonerb, D.D., 2009. Salt marshes and eutrophication: An unsustainable outcome. Limnology and Oceanography, 54(5), 1634.

Turner, R.E., 2010. Beneath the Salt Marsh Canopy: Loss of Soil Strength with Increasing Nutrient Loads. Estuaries and Coasts, 34(5), 1084-1093.

US EPA, 2002. Methods for Evaluating Wetland Condition: Vegetation-Based Indicators of Wetland Nutrient Enrichment. Office of Water, U.S. Environmental Protection Agency, Washington, DC. EPA-822-R-02-024.

US EPA, 2012. Database of Wetland Plant Sensitivities to Enrichment and Hydrologic Alteration, http://water.epa.gov/type/wetlands/assessment/publicat.cfm#database1

USGS, 2011. http://landsat.usgs.gov/band_designations_landsat_satellites.php

VassarStats: Website for Statistical Computation, 2014. http://vassarstats.net/

Vigier, B.J.; Pattey, E., and Strachan, I.B., 2004. Narrowband Vegetation Indexes and Detection of Disease Damage in Soybeans. IEEE Geoscience and Remote Sensing Letters, 1(4), 255-259.

Visser, J.M., and Sasser, C.E., 2002. Marsh Assignment Algorithm and CC Score Salinities (provided by William M. Boshart and Danielle Richardi of Louisiana Department of Natural Resources).

Volpe, V.; Silvestri S., and Marani, M., 2011. Remote sensing retrieval of suspended sediment concentration in shallow waters. Remote Sensing of Environment, 115(1), 44-54.

Wang, J. P., M. Rich, K. P. Price, and W. D. Kettle. (2004). Relations between NDVI and tree productivity in the central Great Plains. International Journal of Remote Sensing, 25:6, 3127-3138.

Zhang, M., S. L. Ustin, E. Rejmankova, and E. W. Sanderson. (1997). Monitoring Pacific Salt Marshes using Remote Sensing. Journal of Ecological Applications, 7:3, pp. 1039-1053.

Figure 4.1 Location of the approximately 138 km² study area in the Barataria Basin (adapted from ArcGIS basemap with April 17, 2011 Landsat 5 TM image overlay).

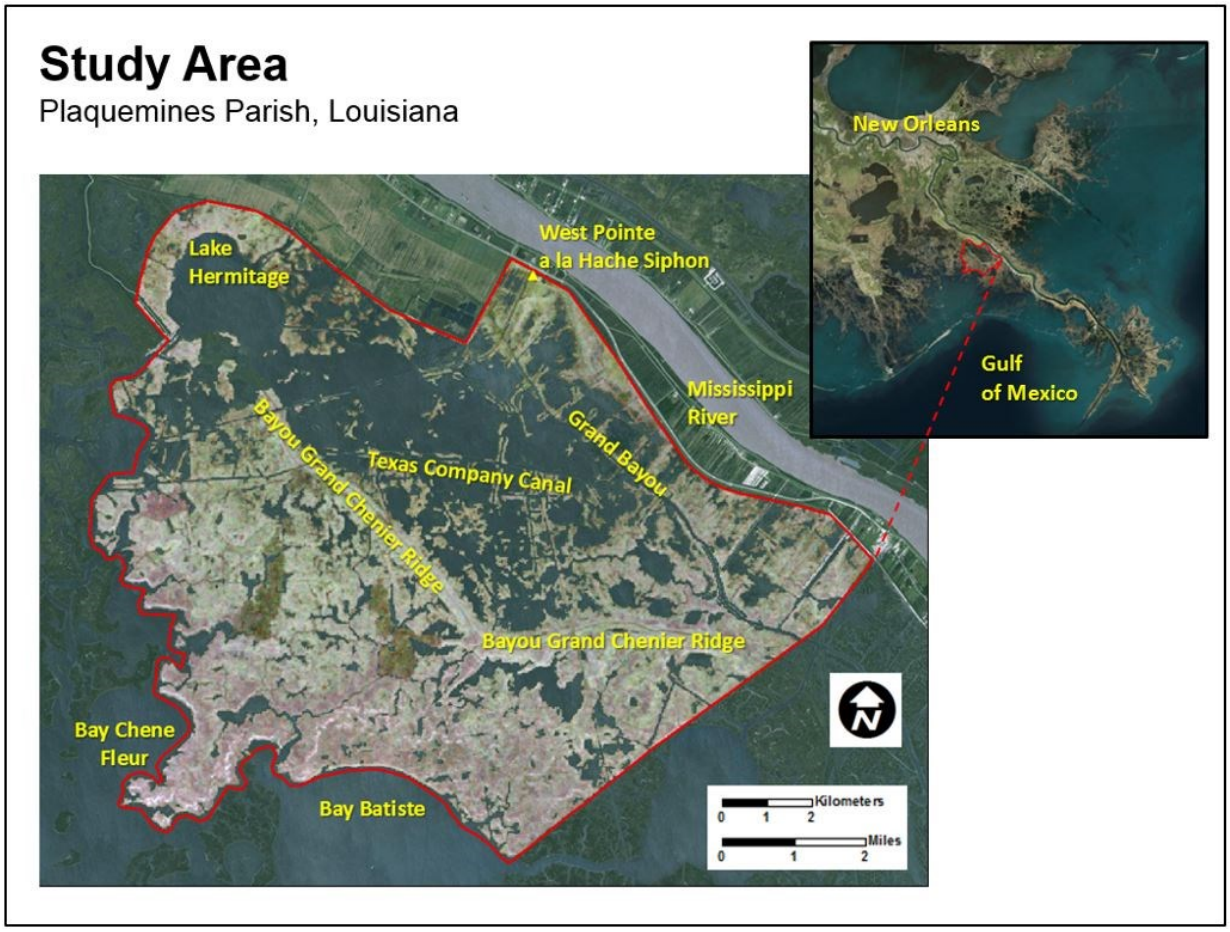

Figure 4.2 Pre-1993 turbidity map adapted from USACE turbidity frequency data.

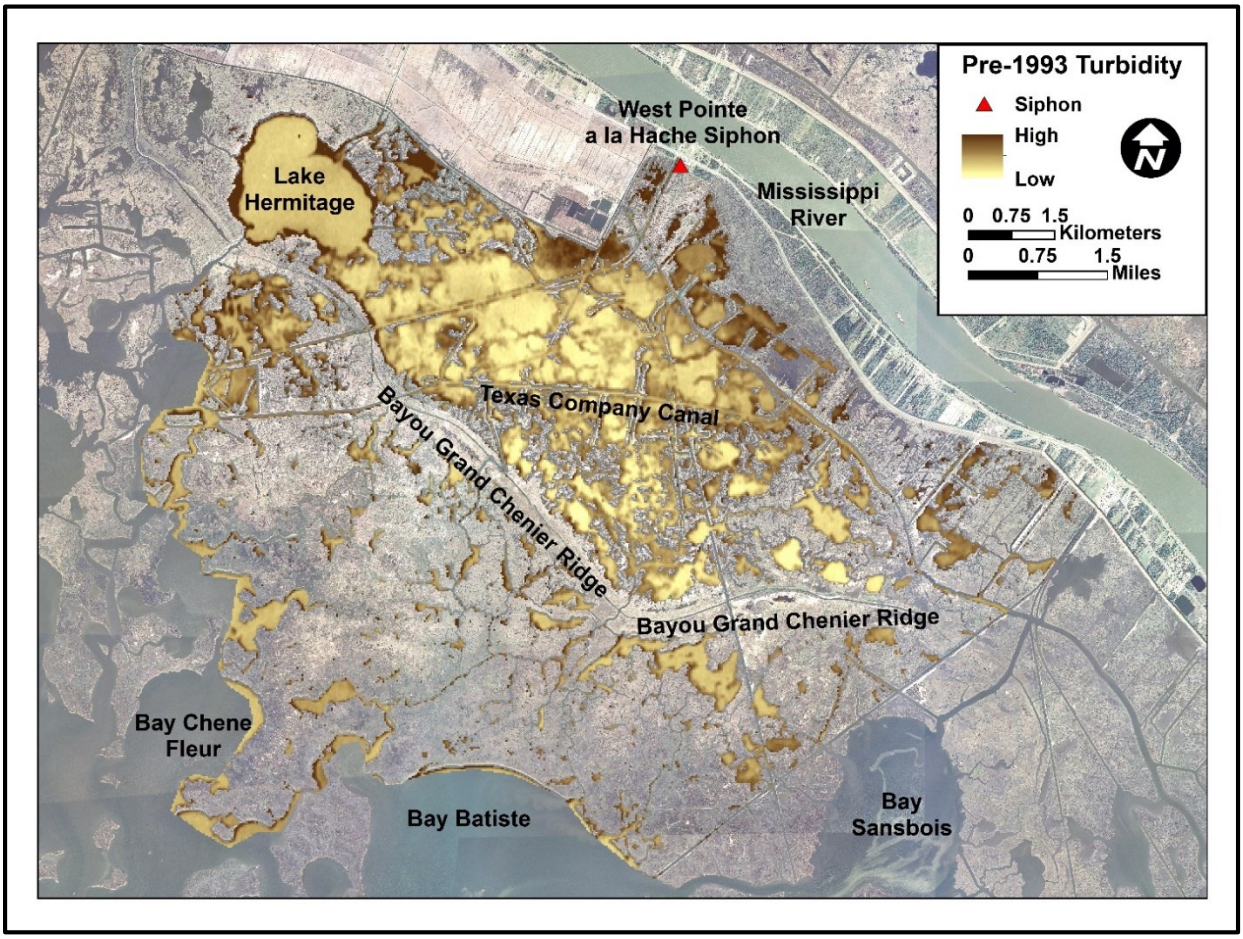

Figure 4.3 Post-1993 turbidity map adapted from USACE turbidity frequency data.

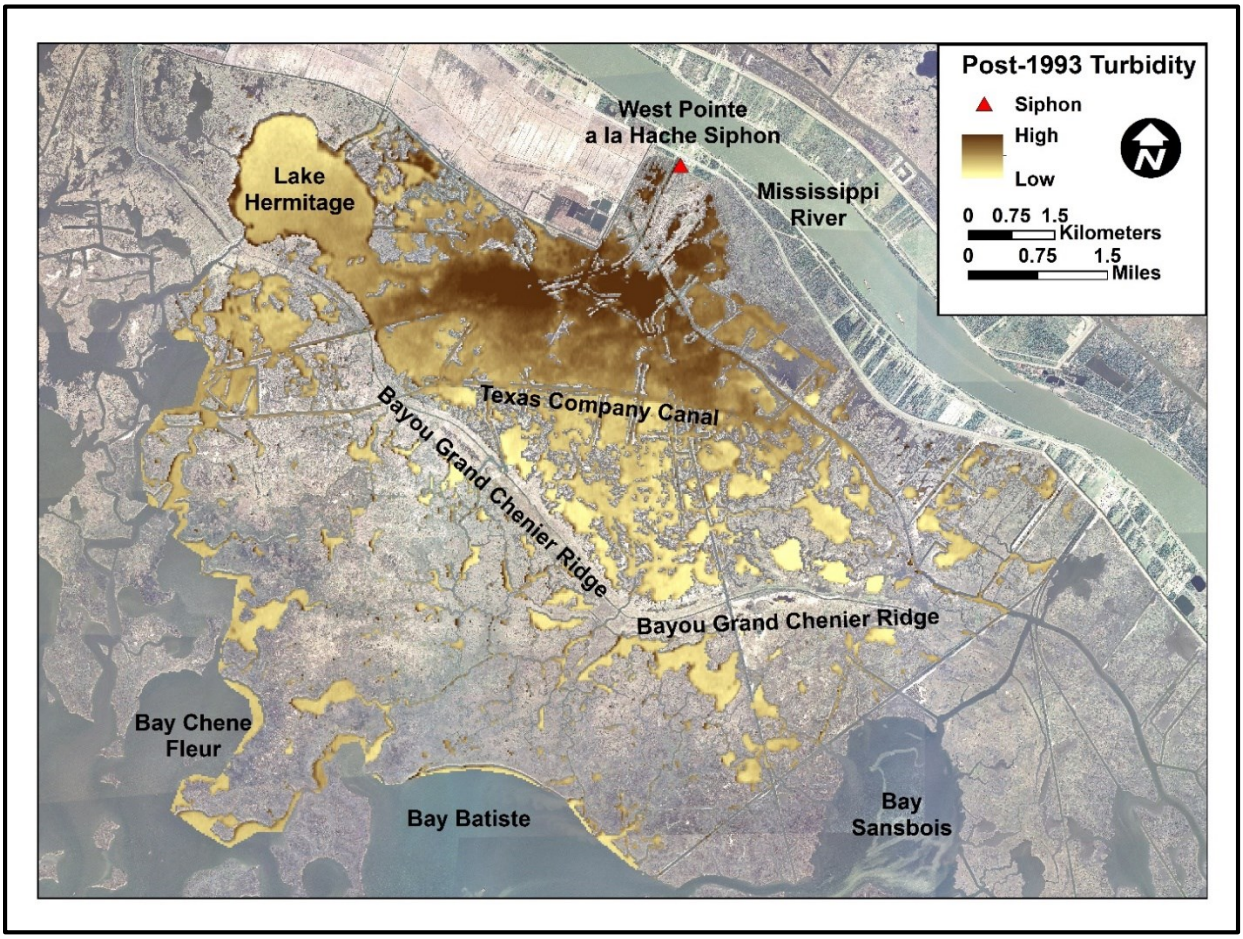

Figure 4.4 Map of study area delineating vegetated marsh areas subject to high and low freshwater impacts.

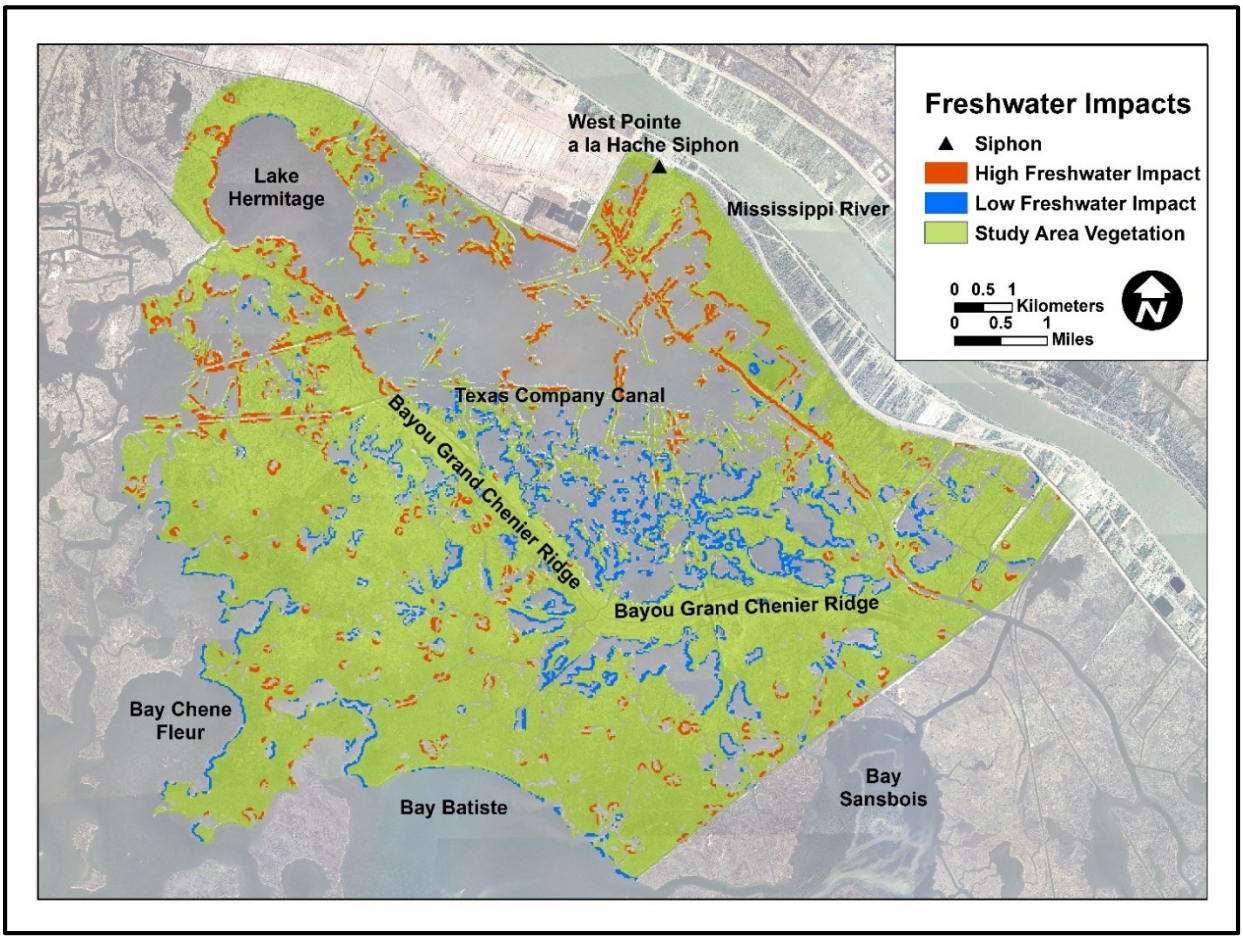

Figure 4.5 Map of study area showing salinity data collection sites in consistently high and low freshwater impact areas.

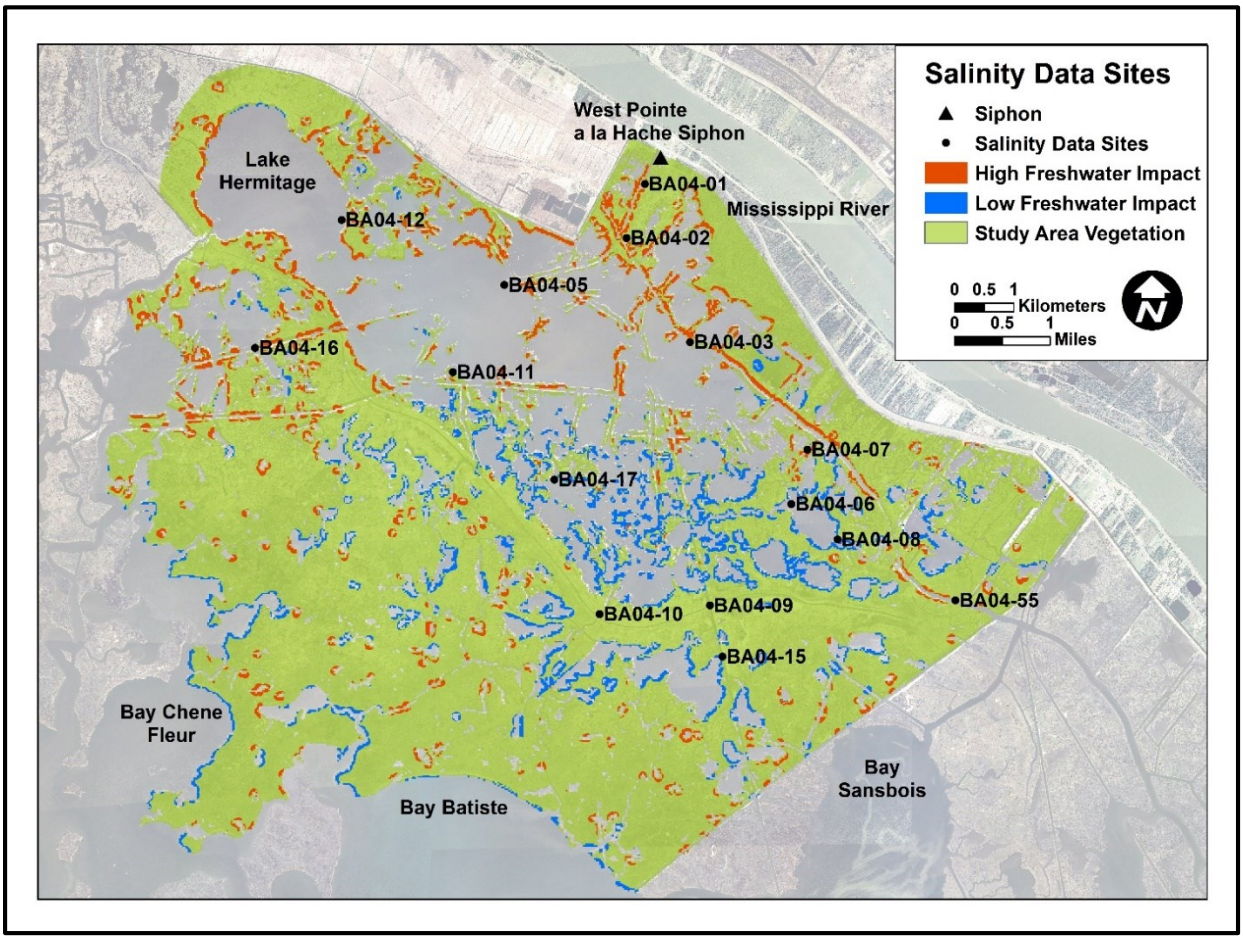

Figure 4.6 Map of study area showing areas of high, medium, and low NDVI values.

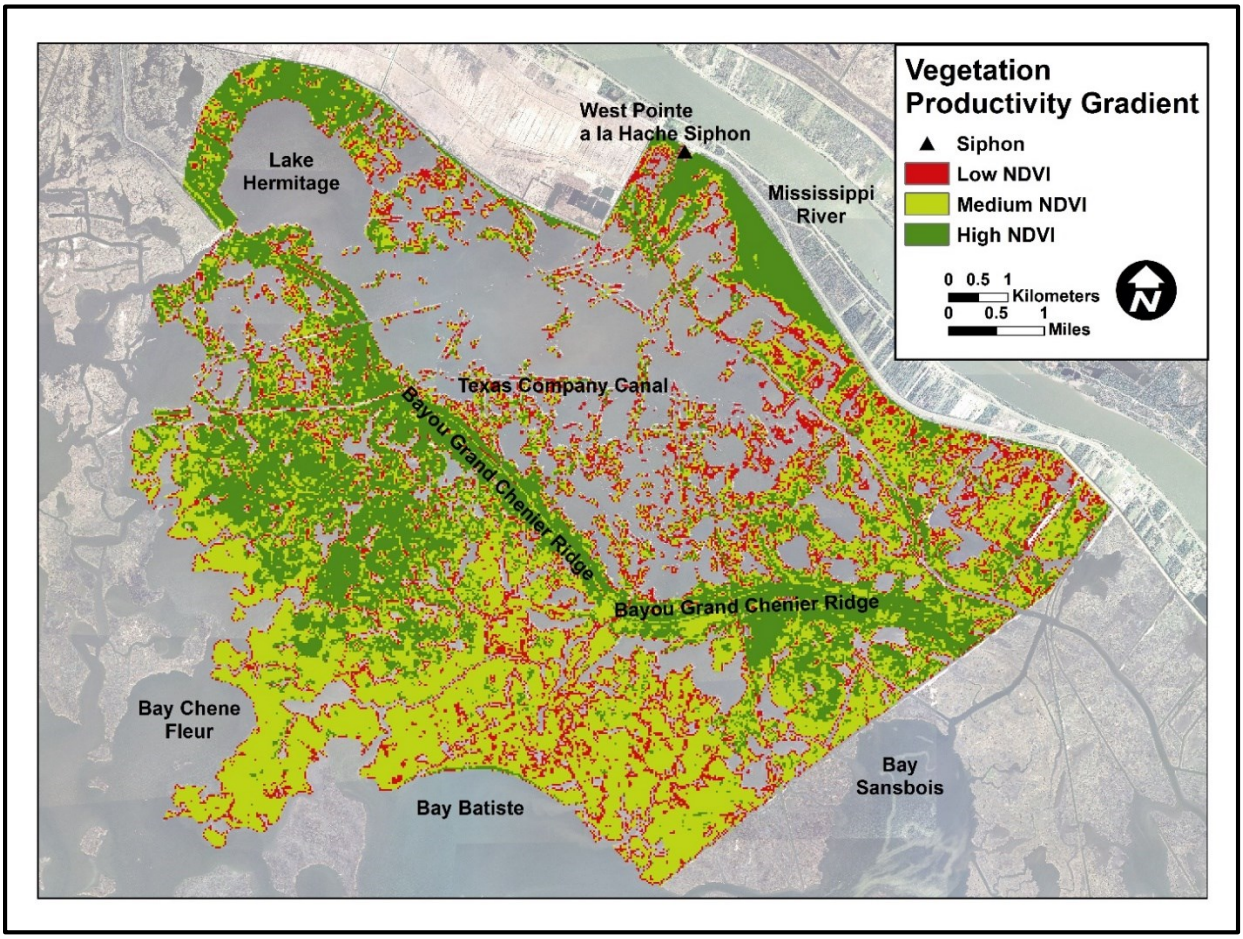

Figure 4.7 Sample sites across vegetation productivity and freshwater impact gradients.

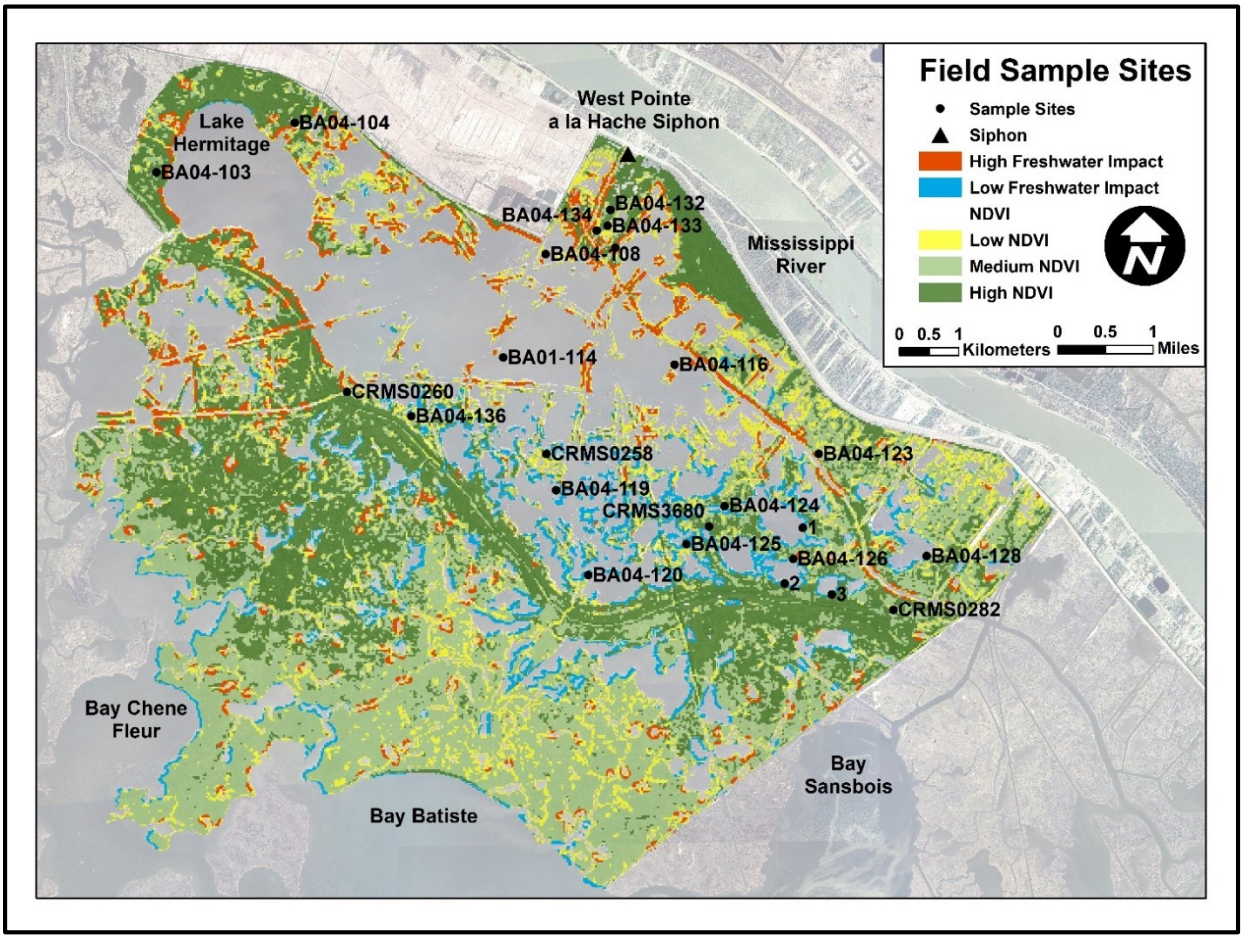

Figure 4.8 (a) Platform and ladder apparatus for data collection from the boat; (b) Computer for spectroradiometer data collection; (c) Improved vantage point for collection of vegetation survey data; (d) Data collection with the Ocean Optics USB4000 spectroradiometer system; (e) Data collection with the LAI-2000 Plant Canopy Analyzer.

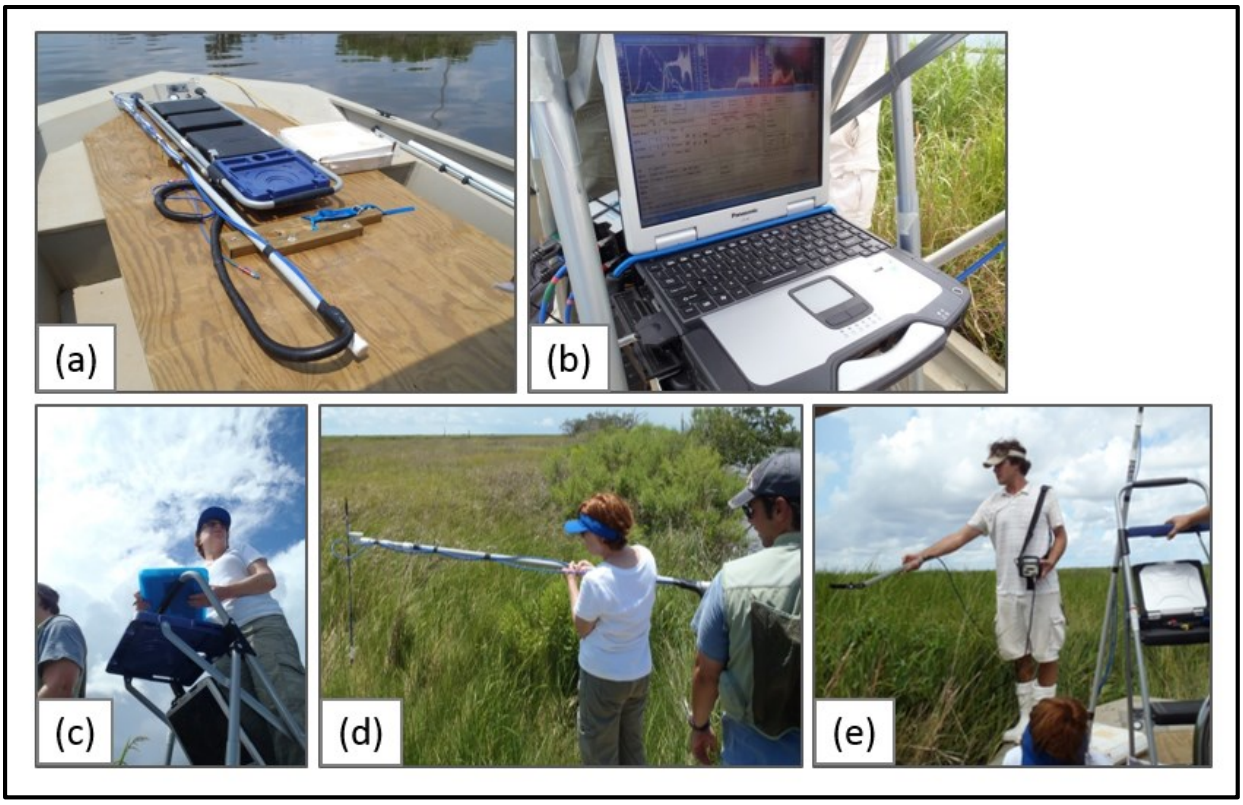

Figure 4.9 Distribution of mean salinity at high and low impact sites during siphon operation and siphon dormancy.

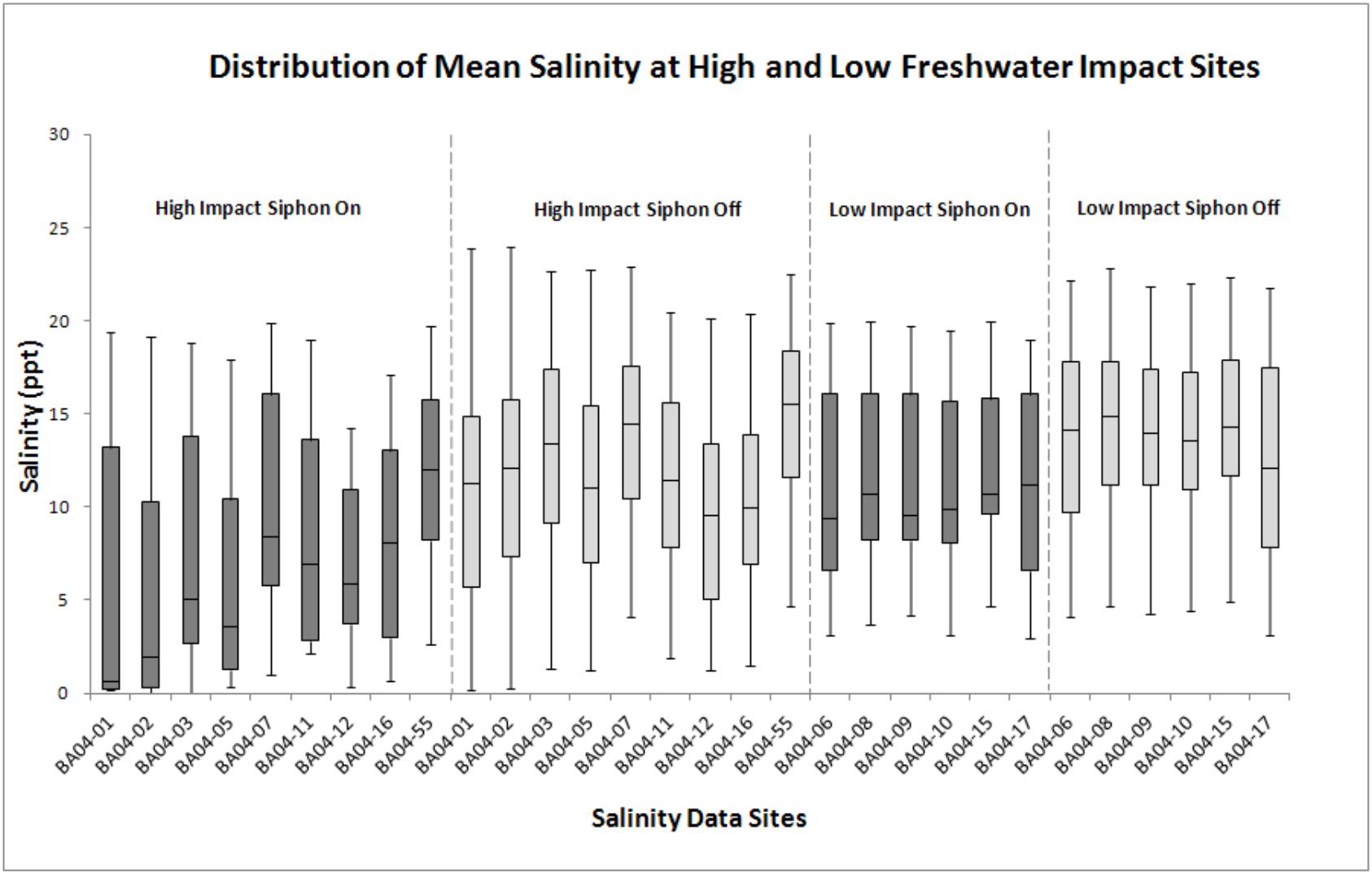

Figure 4.10 Standard deviation of mean salinity at high and low freshwater impact sites during siphon operation and dormancy.

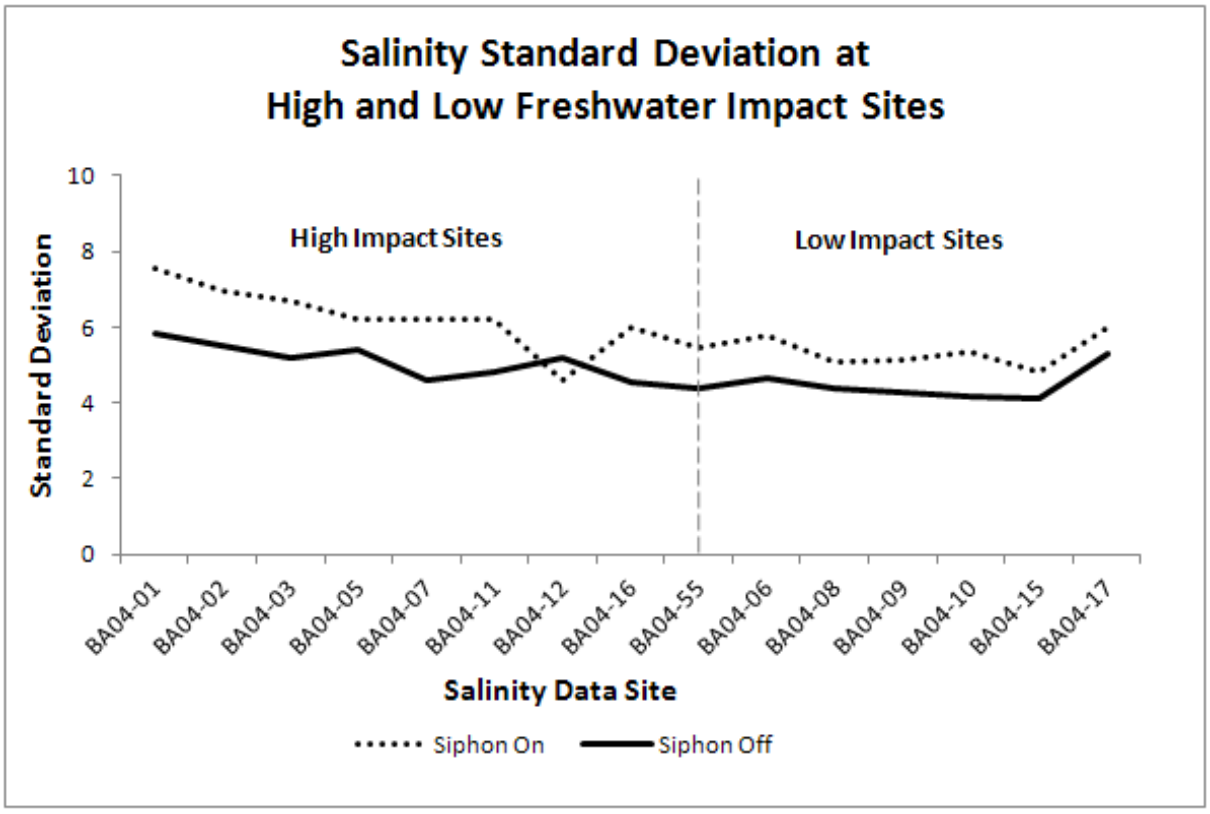

Figure 4.11 Mean salinity at high and low freshwater impact sites during siphon operation and dormancy.

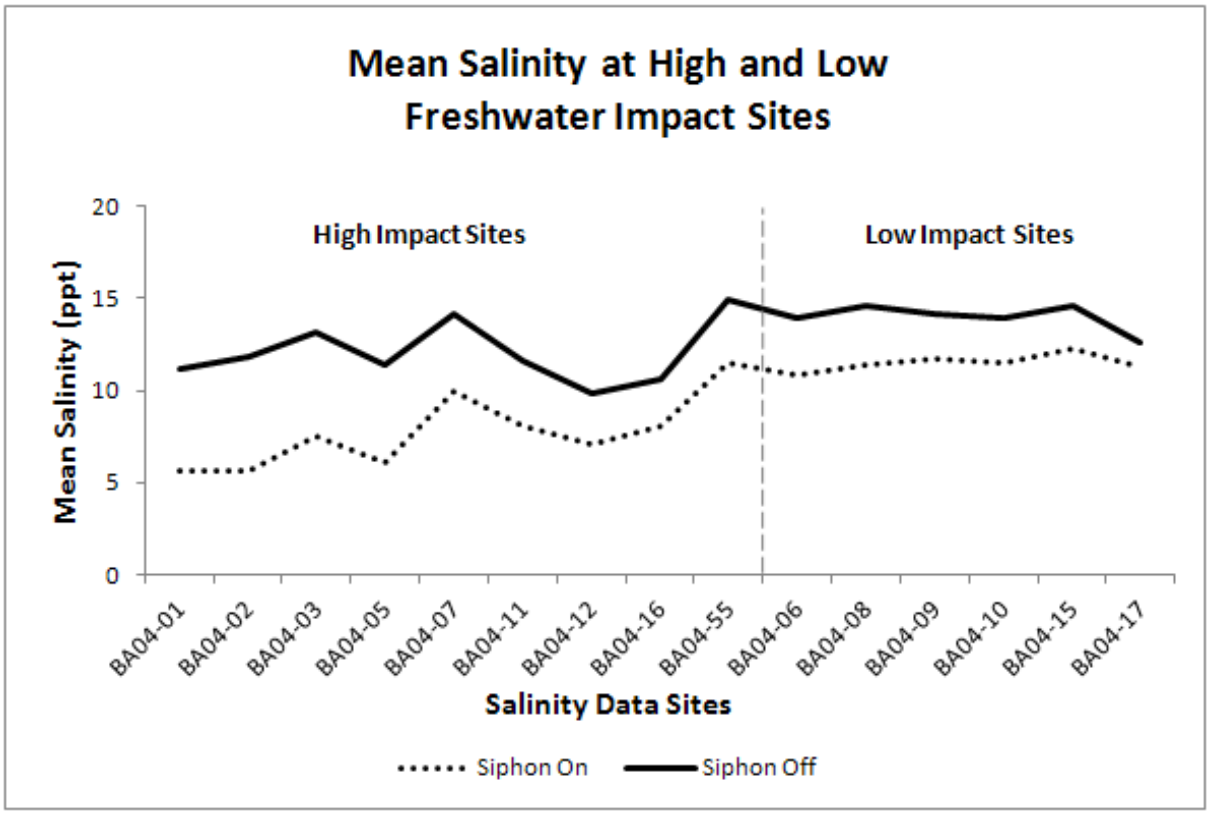

Figure 4.12 Dendrogram results of cluster analysis of vegetation biophysical data.

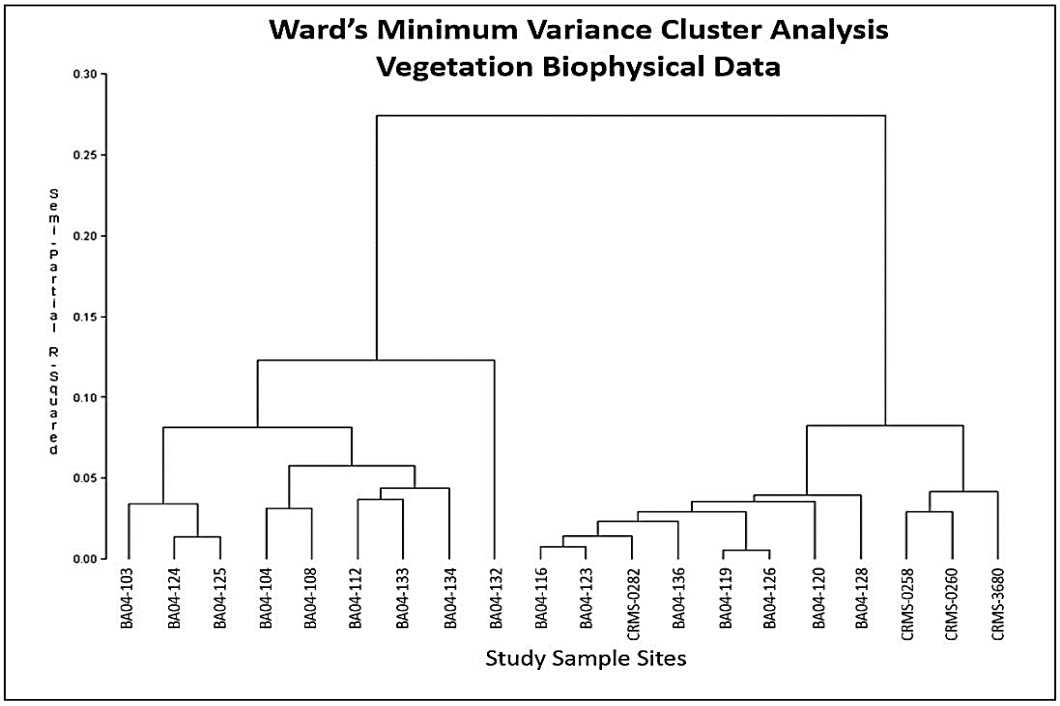

Figure 4.13 Graphs of summary statistics for cluster analysis of vegetation biophysical characteristics.

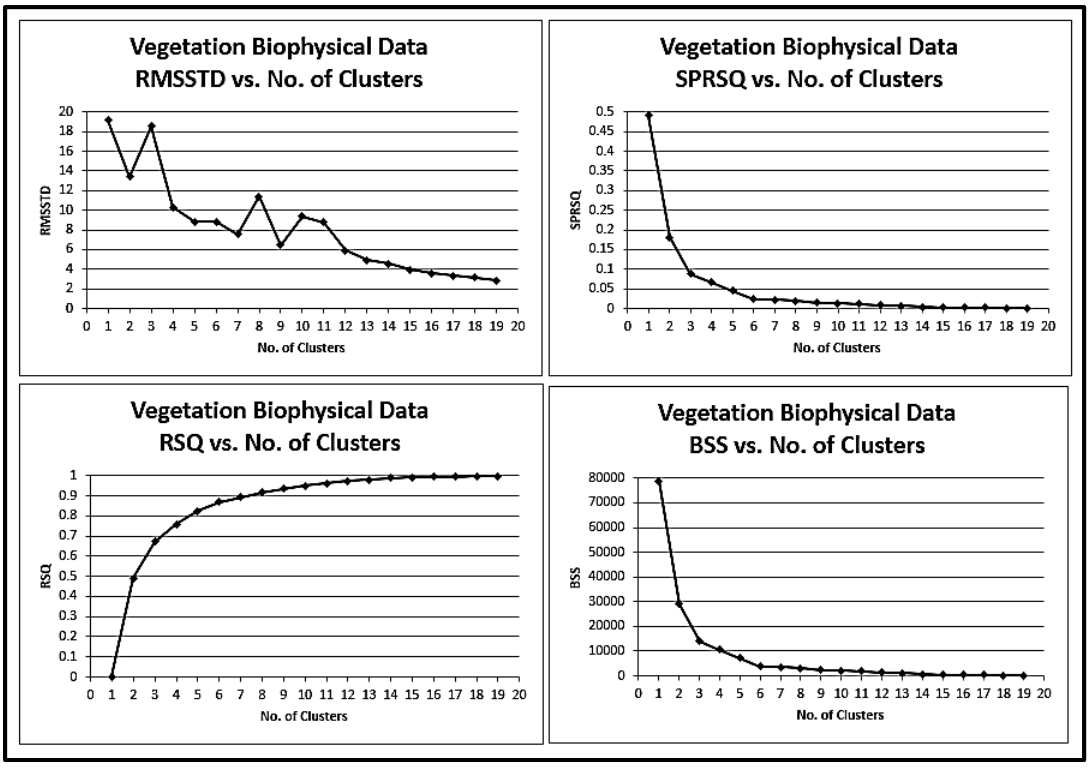

Figure 4.14 Dendrogram results of cluster analysis of DG-WV2 image data.

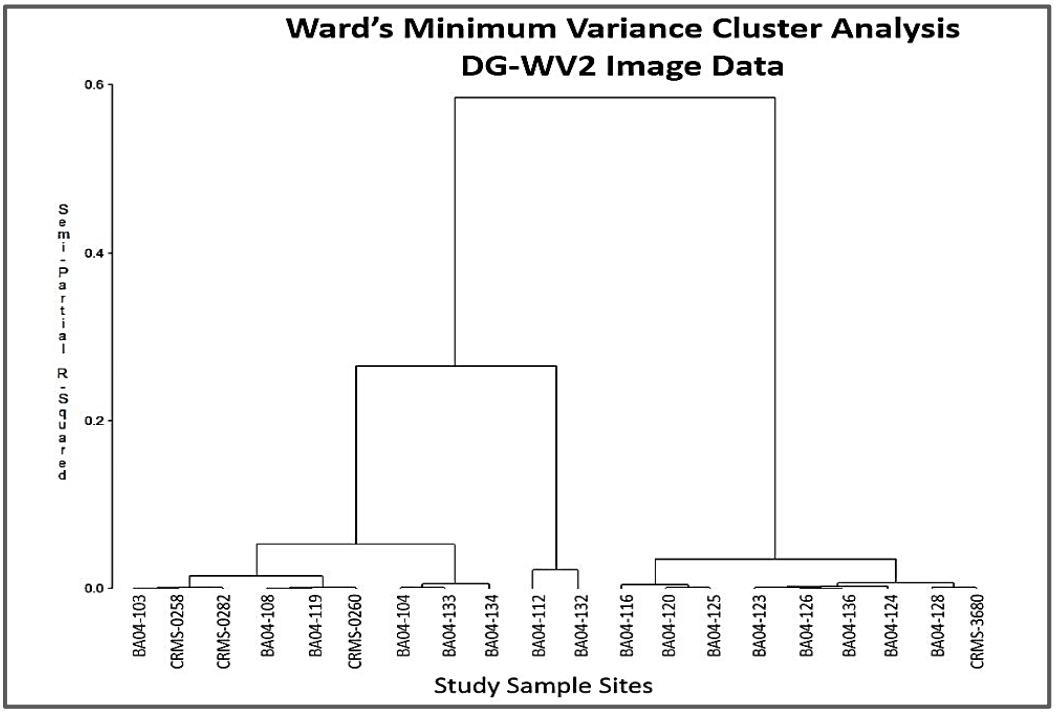

Figure 4.15 Graphs of summary statistics for cluster analysis of DG-WV2 image data.

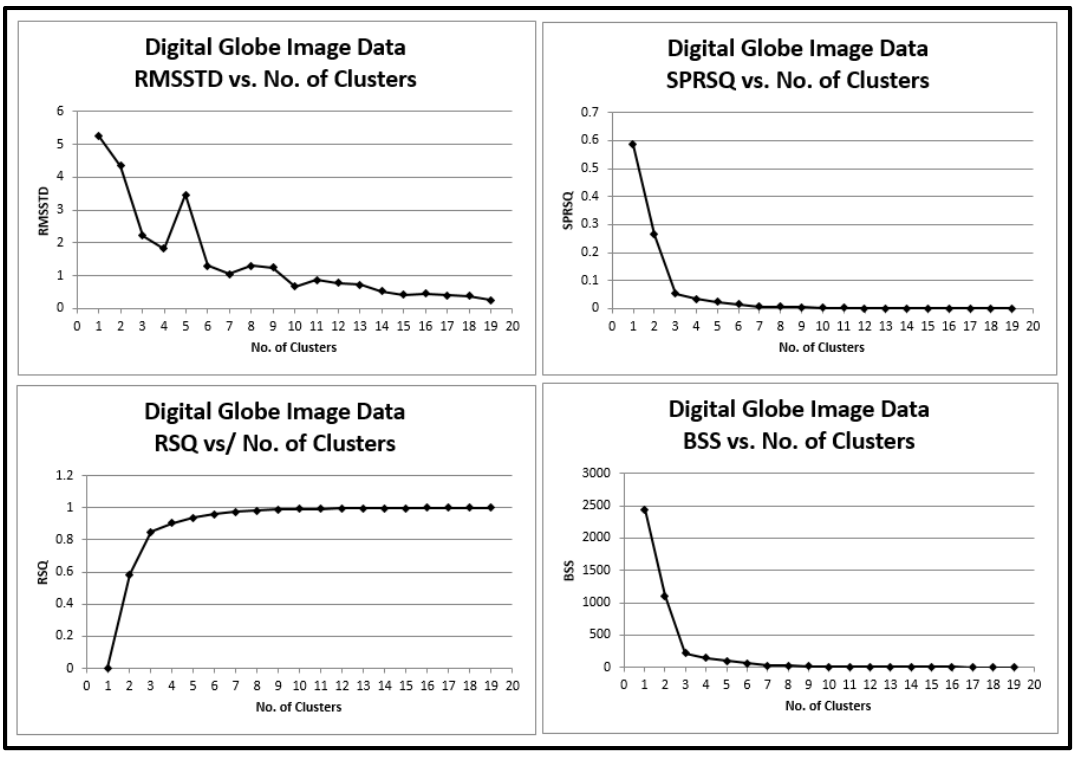

Figure 4.16 Dendrogram results of cluster analysis of vegetation dynamics binary data.

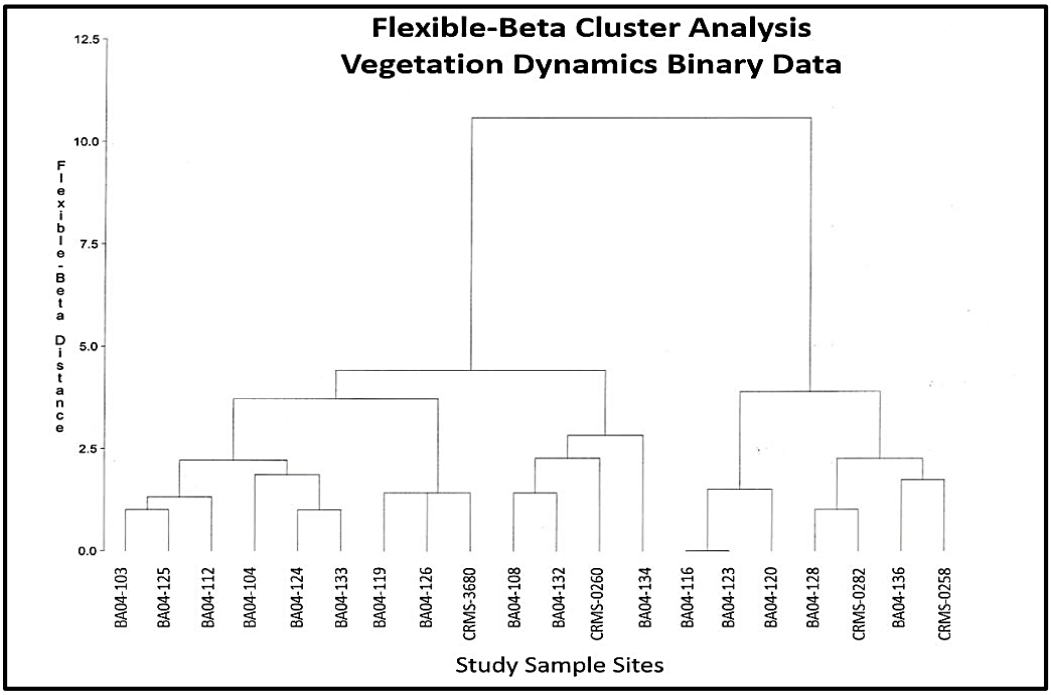

Figure 4.17 Map showing areas of higher and lower vulnerability to eutrophication.

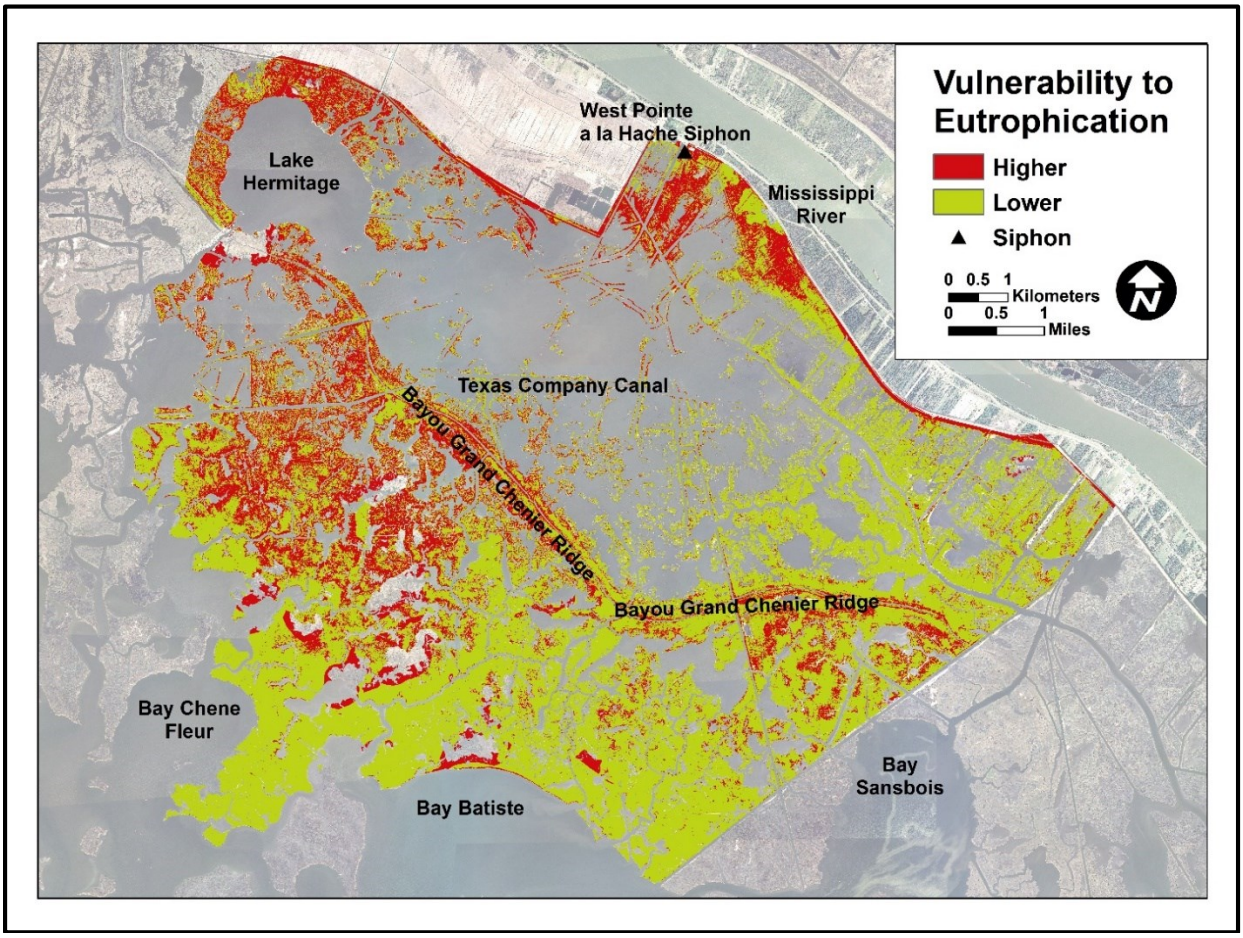

Figure 4.18 Digital elevation model of the study area adapted from a 2010 LiDAR-derived DEM (ArcGIS online; LOSCO, LSU, C4G, 2010).

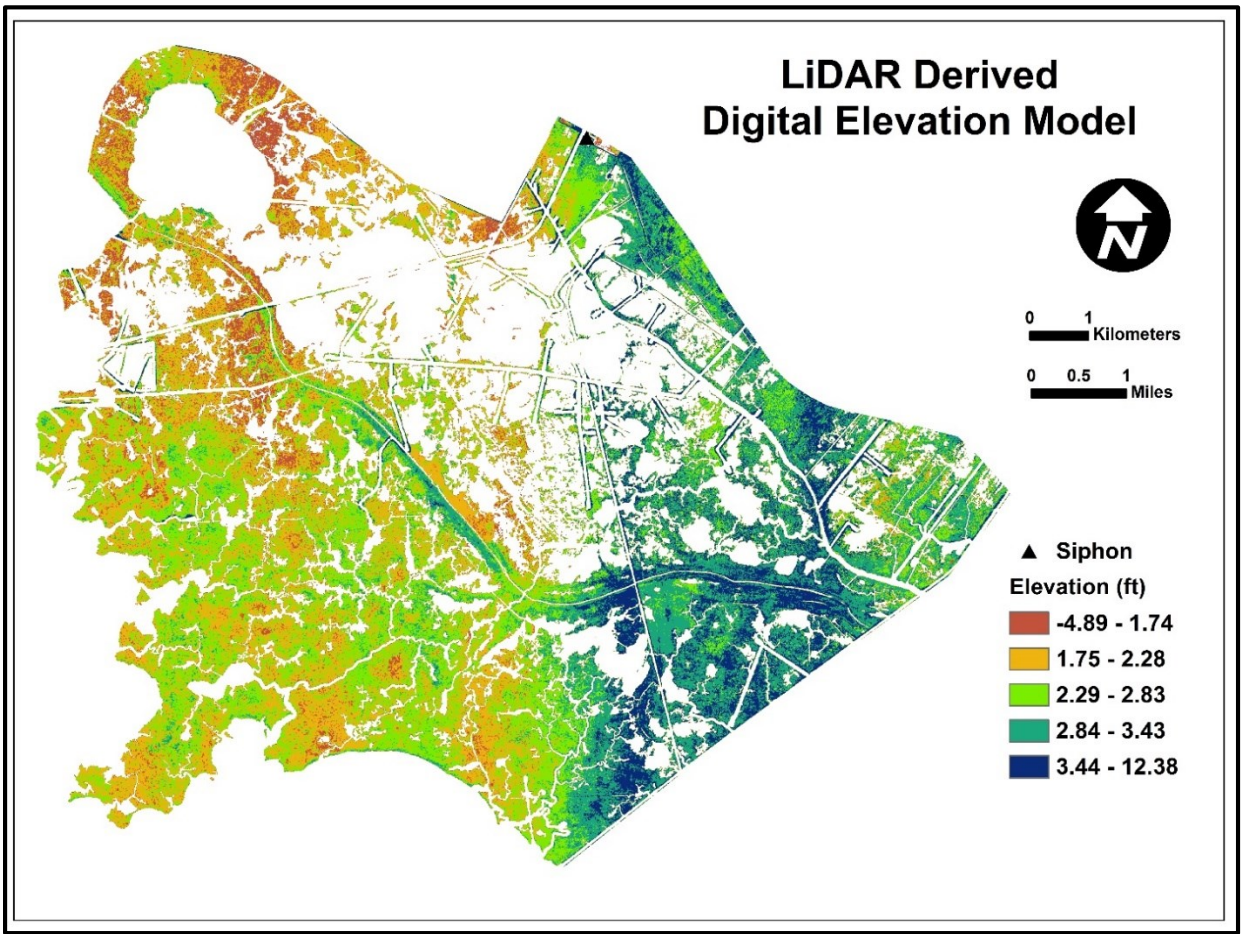

Table 4.1 Satellite image data specifications.

	Band	Wavelength (nm)	Nominal Spectral Location
DigitalGlobe WorldView2	1	400-450	Coastal
Bands 1-8, 2 m	2	450-510	Blue
Panchromatic 0.5 m	3	510-580	Green
	4	585-625	Yellow
	5	630-690	Red
	6	705-745	Red Edge
	7	770-895	NIR1
	8	860-1040	NIR2
	pan	450-800	Panchromatic
Landsat 5 TM	1	450-520	Blue
Bands 1-5 and 7, 30 m	2	520-600	Green
Band 6, 120 m	3	630-690	Red
	4	760-900	NIR
	5	1550-1750	MIR
	6	10400-12500	Thermal
	7	2080-2350	MIR

(Adapted from DigitalGlobe, 2009 and USGS, 2011)

Table 4.2 Pre- and post-siphon operation satellite image dates and associated freshwater flows at WPH siphon diversion project.

Pre-siphon operation (no flow)	Post-siphon operation	
Satellite image dates	Satellite image dates	Freshwater flow (cfs)
04/06/1984	04/02/1994	2023.82
01/19/1985	09/25/1994	118.80
10/08/1987	04/07/1996	1519.67
01/28/1988	02/08/1998	787.01
2/13/1988	02/24/1998	903.08
11/01/1990	01/26/1999	1311.58
11/17/1990	04/18/2000	721.22
03/09/1991	09/17/2000	777.25
02/08/1992	11/20/2000	783.88
10/05/1992	02/27/2002	1327.31
	10/20/2003	1057.15
	02/25/2010	530.66

Table 4.3 Twelve satellite image dates during siphon operation and nearest salinity data dates.

Satellite image dates/ siphon operating	Nearest salinity data dates
04/02/1994	03/29/1994
09/25/1994	09/13/1994
04/07/1996	04/02/1996
02/08/1998	02/17/1998
02/24/1998	02/17/1998
01/26/1999	01/25/1999
04/18/2000	04/18/2000
09/17/2000	09/28/2000
11/20/2000	11/21/2000
02/27/2002	03/07/2002
10/20/2003	10/13/2003
02/25/2010	03/03/2010

Table 4.4 Seventy-one salinity data dates corresponding to no flow periods (siphon not operating for at least 7 days prior to each salinity data date).

No flow dates with available salinity data		
10/11/1994	10/12/1999	01/16/2006
11/09/1994	11/16/1999	02/24/2006
12/07/1994	12/14/1999	03/28/2006
01/04/1995	01/19/2000	04/28/2006
02/15/1995	02/22/2000	05/26/2006
03/14/1995	05/02/2001	06/27/2006
04/10/1995	08/15/2001	07/28/2006
04/26/1995	09/04/2001	08/31/2006
05/23/1995	10/08/2001	09/27/2006
06/06/1995	10/26/2001	10/24/2006
06/07/1995	08/16/2002	08/27/2007
06/22/1995	09/03/2002	10/02/2007
10/17/1995	10/10/2002	11/01/2007
11/02/1995	11/07/2002	11/30/2007
11/14/1995	12/28/2002	12/28/2007
12/12/1995	07/17/2003	08/22/2008
01/17/1996	08/18/2003	09/26/2008
09/16/1997	09/03/2003	10/28/2008
10/21/1997	09/10/2004	12/03/2008
11/17/1997	10/13/2004	01/07/2009
12/16/1997	11/09/2004	02/16/2009
03/16/1999	10/14/2005	10/15/2009
08/25/1999	11/21/2005	10/14/2010
09/16/1999	12/19/2005	

Table 4.5 Mean salinity for high and low freshwater impact sites by siphon flow.

High freshwater impact sites	Low freshwater impact sites	Mean salinity (ppt) (siphon flow)	Mean salinity (ppt) (no siphon flow)
BA04-01	-	5.68	11.13
BA04-02	-	5.59	11.89
BA04-03	-	7.57	13.18
BA04-05	-	6.13	11.38
BA04-07	-	9.90	14.17
BA04-11	-	8.11	11.64
BA04-12		7.07	9.83
BA04-16	-	8.13	10.64
BA04-55	-	11.53	14.91
-	BA04-06	10.85	13.96
-	BA04-08	11.42	14.64
-	BA04-09	11.70	14.16
-	BA04-10	11.49	13.97
-	BA04-15	12.24	14.59
-	BA04-17	11.33	12.59

Table 4.6 Species salinity score assignments based on marsh zones of peak occurrence (i.e. where the species is most commonly found) for application of CPRA Marsh Assignment Algorithm.

Zone of peak occurrence	Salinity score
Fresh	0.25
Fresh to intermediate	1.50
Intermediate	2.75
Intermediate to brackish	7.15
Brackish	11.50
Brackish to saline	17.50
Saline	24.00

(Adapted from Visser and Sasser, 2002.)

Table 4.7 Salinity scores of common marsh vegetation species used in CPRA Marsh Assignment Algorithm to calculate marsh community salinity score and assign marsh community type.

Scientific Name	Common Name	Salinity score
Alternanthera philoxeroides (Mart.) Griseb.	alligatorweed	1.50
Amaranthus australis (A. Gray) Saur	southern amaranth	7.15
Amaranthus cannabinus (L.) Sauer	tidalmarsh amaranth	7.15
Cuscuta indecora Choisy	big seed alfalfa dodder	2.75
Cuscuta L.	dodder	1.50
Cynanchum angustifolium Pers.	gulf coast swallow-wort	17.50
Distichlis spicata (L.) Greene	saltgrass	17.50
Ipomoea sagittata Poir.	saltmarsh morning-glory	1.50
Iva frutescens L.	Jesuit's bark	2.75
Juncus roemerianus Scheele	needlegrass rush	17.50
Schoenoplectus pungens (Vahl) Palla	common threesquare	0.25
Spartina alterniflora Loisel.	smooth cordgrass	24.00
Spartina cynosuroides (L.) Roth	big cordgrass	11.50
Spartina patens (Aiton) Muhl.	saltmeadow cordgrass	7.15
Symphyotrichum subulatum (Michx.) G.L. Nesom	eastern annual saltmarsh aster	2.75
Vigna luteola (Jacq.) Benth.	hairypod cowpea	2.75

(Adapted from the Excel file, "CCscore_Salinities_Update.June.2011," provided by William M. Boshart and Danielle Richardi, Louisiana Department of Natural Resources, for use with Marsh Assignment Algorithm developed by Jenneke M. Visser and Charles E. Sasser).

Table 4.8 Marsh community assignments by community salinity score resulting from CPRA Marsh Assignment Algorithm.

Marsh community assignment	Community salinity score
Fresh	≤ 1.50
Intermediate	>1.50 and ≤ 7.15
Brackish	>7.15 and ≤ 15.00
Saline	>15.00

(Adapted from Visser and, 2002.)

Table 4.9 Example calculation of community salinity score and assignment of community type.

Vegetation Type	Percent cover *(a)*	Species salinity score *(b)*	Percent cover * species salinity score *(ab)*	Community score = *Σ(ab)/ Σ(a)*
Distichlis spicata (L.) Greene	40	17.5	700	
Juncus roemerianus Scheele	10	17.5	175	
Spartina alterniflora Loisel.	50	24	1200	
Totals	100		2075	
Community salinity score				2075/100 = 20.75
Marsh community assignment				Saline marsh community

Table 4.10 Calculated community salinity scores and marsh community types assigned for field data collection period.

Site	Community salinity score	Marsh community type
BA04-103	10.25	Brackish
BA04-104	11.25	Brackish
BA04-108	10.31	Brackish
BA04-112	5.20	Intermediate
BA04-116	20.75	Saline
BA04-119	16.22	Saline
BA04-120	24.00	Saline
BA04-123	20.75	Saline
BA04-124	18.06	Saline
BA04-125	20.75	Saline
BA04-126	20.75	Saline
BA04-128	20.75	Saline
BA04-132	5.82	Intermediate
BA04-133	12.23	Brackish
BA04-134	12.23	Brackish
BA04-136	16.54	Saline
CRMS-0258	20.58	Saline
CRMS-0260	15.71	Saline
CRMS-0282	20.26	Saline
CRMS-3680	20.53	Saline

Table 4.11 Regression equations and resulting r^2 and RMSE values by DigitalGlobe WorldView2 (DG-WV2) image band.

08/01/11 Image			
Band	r^2	Equation	RMSE
1 (Coastal)	.99	Band1 = (0.381859*$n1_080111_radiance(1)) - 32.6621	0.78
2 (Blue)	.99	Band2 = (0.269234723*$n1_080111_radiance(2)) - 21.4367225	0.81
3 (Green)	.99	Band3 = (0.268849236*$n1_080111_radiance(3)) - 13.51864027	0.82
4 (Yellow)	.99	Band4 = (0.316101915*$n1_080111_radiance(4)) - 12.32399846	1.05
5 (Red)	.99	Band5 = (0.298159806*$n1_080111_radiance(5)) - 8.4834054	0.96
6 (Red Edge)	.96	Band6 = (0.371882565*$n1_080111_radiance(6)) - 1.80636633	2.20
7 (NIR1)	.90	Band7 = (-0.0009*($n1_080111_radiance(7)**2) + 0.6552*$n1_080111_radiance(7)) - 7.6661	4.84
8 (NIR2)	.88	Band8 = (-0.002*($n1_080111_radiance(8)**2) + 0.9774*$n1_080111_radiance(8)) - 1.2164	4.40
08/06/11 Image			
Band	r^2	Equation	RMSE
1 (Coastal)	.99	Band1 = (0.330643144*$n1_080611radiance(1)) - 23.19931939	0.73
2 (Blue)	.99	Band2 = (0.234535754*$n1_080611 _radiance(2)) - 14.34778922	0.34
3 (Green)	.99	Band3 = (0.254956446*$n1_080611 _radiance(3)) - 8.98327148	0.68
4 (Yellow)	.99	Band4 = (0.294879488*$n1_080611 _radiance(4)) - 7.432270408	0.95
5 (Red)	.99	Band5 = (0.261416983*$n1_080611 _radiance(5)) - 3.773811245	1.07
6 (Red Edge)	.97	Band6 = (-0.0004*($n1_080611_radiance(6)**2) + 0.4568*$n1_080611_ radiance(6)) - 3.949	3.27
7 (NIR1)	.90	Band7 = (-0.0008*($n1_080611 _radiance(7)**2) + 0.597*$n1_080611_radiance(7)) - 4.775	5.73
8 (NIR2)	.91	Band8 = (-0.0018*($n1_080611_ radiance(8)**2) + 0.8807*$n1_080611_ radiance(8)) + 1.625	6.97

Table 4.12 Regression equations and resulting r^2 values for composite image predicted values.

Band	r^2	Equation
1 (Coastal)	0.05	Band 1 = 2.295 + 0.187 x
2 (Blue)	0.24	Band 2 = 1.393 + 0.477 x
3 (Green)	0.65	Band 3 = 1.086 + 0.762 x
4 (Yellow)	0.70	Band 4 = 0.943 + 0.785 x
5 (Red)	0.72	Band 5 = 0.657 + 0.834 x
6 (Red Edge)	0.89	Band 6 = 6.373 + 0.675 x
7 (NIR1)	0.89	Band 7 = 5.938 + 0.811 x
8 (NIR2)	0.90	Band 8 = 7.663 + 0.799 x

Table 4.13 Vegetation indices and equations.

Vegetation Index	Equation
Normalized Difference Vegetation Index	NDVI = *(NIR-red)/(NIR+red)*
Green NDVI	GNDVI = *(NIR-green)/(NIR+green)*
Wide Dynamic Range Vegetation Index	WDRVI = *(a*NIR-red)/(a*NIR+red)* (where a = a weighting parameter based on vegetation density characteristics*)
Atmospherically Resistant Vegetation Index	ARVI = *[NIR-(2.0*red-blue)]/ [NIR-(2.0*red+blue)]*

* Based on vegetation density characteristics within the study area, a weighting parameter of 0.2 was used to calculate WDRVI, as recommended by Gitelson (2004).

Table 4.14 SONRIS historical vegetation data.

Data collection period	Data collection location (CPRA vegetation station or CRMS transect locations)	Historical data
1997, 2001, 2003, 2006, and 2009	BA04-103, BA04-104, BA04-108, BA04-112, BA04-116, BA04-119, BA04-120, BA04-123, BA04-124, BA04-125, BA04-126, BA04-128, BA04-132, BA04-133, BA04-134, BA04-136	Marsh community type, average height of herbaceous layer in cm, and scientific and common names of vegetation species found at each station
2007, 2008, 2009, and 2010	CRMS0258-V27, CRMS0260-V49, CRMS0282-V28, CRMS3680-V28	Marsh community type, average height of herbaceous layer in cm, and scientific and common names of vegetation species found at each station

Source: SONRIS (2012)

Table 4.15 Marsh community types by sample site and data collection period.

Marsh community type
Fresh = 1; Intermediate = 2; Brackish = 3; Saline = 4

	Data collection period								
Site	1997	2001	2003	2006	2007	2008	2009	2010	*2011
BA04-103	3	2	3	3	-	-	3	-	3
BA04-104	3	3	3	3	-	-	3	-	3
BA04-108	1	2	4	4	-	-	4	-	3
BA04-112	2	3	2	3	-	-	3	-	2
BA04-116	4	4	4	4	-	-	4	-	4
BA04-119	3	4	4	4	-	-	4	-	4
BA04-120	4	4	4	4	-	-	4	-	4
BA04-123	4	4	4	4	-	-	4	-	4
BA04-124	4	4	4	4	-	-	4	-	4
BA04-125	4	4	3	4	-	-	4	-	4
BA04-126	4	4	4	4	-	-	4	-	4
BA04-128	4	4	4	4	-	-	4	-	4
BA04-132	4	1	2	4	-	-	4	-	2
BA04-133	3	1	3	4	-	-	2	-	3
BA04-134	4	1	1	4	-	-	2	-	3
BA04-136	3	4	3	3	-	-	4	-	4
CRMS-0258	-	-	-	-	2	3	4	3	4
CRMS-0260	-	-	-	-	2	3	3	3	4
CRMS-0282	-	-	-	-	4	3	4	4	4
CRMS-3680	-	-	-	-	4	3	2	3	4

- Historical data unavailable
*Field data collection

Table 4.16 Vegetation species found historically and during field data collection by sample site.

Scientific name as originally observed	Common name (*followed by colloquial names)*	*Species site locations, historical data	Species site locations, field data collection
Alternanthera philoxeroides (Mart.) Griseb.	alligatorweed	BA04-104, BA04-134	
Amaranthus L.	pigweed	BA04-112, BA04-132, BA04-133, BA04-134, BA04-136	
Amaranthus australis (A. Gray) Sauer	southern amaranth	BA04-103, BA04-104, BA04-132, BA04-133, BA04-134, CRMS-3680	BA04-103, BA04-133, BA04-134
Amaranthus cannabinus (L.) Sauer	tidalmarsh amaranth	BA04-104, BA04-108, BA04-112, BA04-125, BA04-132, BA04-133, BA04-134	BA04-104, BA04-112, BA04-132
Ammannia coccinea Rottb.	valley redstem	BA04-136	
Ammannia latifolia L.	pink redstem	BA04-133	
Baccharis halimifolia L.	eastern baccharis	BA04-103, BA04-104, BA04-112, BA04-124	
Cephalanthus occidentalis L.	common buttonbush	BA04-132	
Colocasia esculenta (L.) Schott	coco yam	BA04-132	
Cuscuta L.	dodder	BA04-112	BA04-114
Cuscuta indecora Choisy	bigseed alfalfa dodder	BA04-108	
Cynanchum angustifolium Pers.	gulf coast swallow-wart		CRMS-0260

Continued

Table 4.16 Continued

Scientific name as originally observed	Common name (*followed by colloquial names)*	*Species site locations, historical data	Species site locations, field data collection
Cyperus compressus L.	poorland flatsedge	BA04-108	
Cyperus odoratus L.	fragrant flatsedge	BA04-103, BA04-108, BA04-112, BA04-116, BA04-132, BA04-133, BA04-134, BA04-136	
Cyperus polystachyos Rottb.	manyspike flatsedge	BA04-108	
Cyperus virens Michx.	green flatsedge	BA04-108, BA04-123	
Distichlis spicata (L.) Greene	Saltgrass *(seashore saltgrass, spike grass, alkali grass, paille sale)*	BA04-103, BA04-104, BA04-108, BA04-112, BA04-114, BA04-116, BA04-119, BA04-120, BA04-123, BA04-124, BA04-125, BA04-126, BA04-128, BA04-132, BA04-133, BA04-134, BA04-136, CRMS-0258, CRMS-0260, CRMS-0282, CRMS-3680	BA04-103, BA04-104, BA04-108, BA04-112, BA04-114, BA04-116, BA04-119, BA04-123, BA04-124, BA04-125, BA04-126, BA04-128, BA04-133, BA04-134, BA04-136, CRMS-0258, CRMS-0260, CRMS-3680, 1, 2, 3
Echinochloa walteri (Pursh) A. Heller	coast cockspur grass	BA04-104, BA04-108, BA04-116, BA04-132, BA04-133, BA04-134	
Eleocharis cellulosa Torr.	gulf coast spikerush	BA04-104	
Hibiscus moscheutos L.	crimsoneyed rosemallow	BA04-134	
Ipomoea L.	morning glory	BA04-104	

Continued

Table 4.16 Continued

Scientific name as originally observed	Common name (*followed by colloquial names)*	*Species site locations, historical data	Species site locations, field data collection
Ipomoea sagittata Poir.	saltmarsh morning glory	BA04-103, BA04-104, BA04-108, BA04-112	BA04-104, BA04-108
Iva frutescens L.	Jesuit's bark	BA04-108, BA04-112, BA04-114, BA04-119, BA04-132, BA04-133, BA04-134, CRMS-0260	BA04-103, BA04-114, CRMS-0260
Juncus effusus L.	common rush	BA04-103, BA04-124, BA04-125	
Juncus roemerianus Scheele	black rush *(needle rush, needlegrass rush, black needle rush, paille chat tigre)*	BA04-103, BA04-112, BA04- BA04-119, BA04-120, BA04- BA04-124, BA04-125, BA04-126, CRMS-3680	BA04-104, BA04-108, BA04-124, BA04-125, CRMS-0260, CRMS-3680
Kosteletzkya virginica (L.) C. Presl ex A. Gray	Virginia salmarsh mallow	BA04-108, BA04-133	
Leptochloa P. Beauv.	sprangletop	BA04-108	
Ludwigia leptocarpa (Nutt.) H. Hara	anglestem primrose-willow	BA04-133	
Lythrum lineare L.	wand lythrum	BA04-103, BA04-104	
Mikania Willd.	hempvine	BA04-132, BA04-133	
Panicum hemitomon Schult.	maidencane	BA04-132	
Panicum repens L.	torpedo grass	BA04-133, BA04-134	
Phragmites australis (Cav.) Trin. Ex Steud.	roseau cane *(common reed, giant reed, giant reedgrass, roseau, yellow cane, cane)*	BA04-125	

Continued

Table 4.16 Continued

Scientific name as originally observed	Common name (*followed by colloquial names)*	*Species site locations, historical data	Species site locations, field data collection
Phytolacca americana L.	American pokeweed	BA04-104	
Pluchea camphorata (L.) DC.	camphor pluchea	BA04-104, BA04-133	
Polygonum hydropiperoides Michx.	swamp smartgrass	BA04-133, BA04-134	
Polygonum pensylvanicum L.	pennsylvania smartweed	BA04-132, BA04-133, BA04-134	
Polygonum punctatum Elliot	dotted smartweed	BA04-104, BA04-108, BA04-112, BA04-132, BA04-133, BA04-134	
Schoenoplectus americanus (Pers.) Volkart ex Schinz & R. Keller	chairmaker's bulrush	BA04-104	
Schoenoplectus pungens (Vahl) Palla	common three-square	BA04-103, BA04-104	BA04-133, BA04-134
Schoenoplectus robustus (Pursh) M.T. Strong	leafy three-square *(three-square, salt marsh bulrush, coco doux, paille d'oie)*	BA04-104, BA04-114, BA04-126, CRMS-3680	
Sesbania Scop.	riverhemp	BA04-104	
Setaria magna Griseb.	giant bristlegrass	BA04-108	
Solidago sempervirens L.	Seaside goldenrod	BA04-103, BA04-108, BA04-112, BA04-134	

Continued

Continued

Table 4.16 Continued

Scientific name as originally observed	Common name (*followed by colloquial names)*	*Species site locations, historical data	Species site locations, field data collection
Sorghum halepense (L.) Pers.	johnsongrass	BA04-132, BA04-133, BA04-134	
Spartina alterniflora Loisel.	smooth cordgrass *(oystergrass, salt water cordgrass, paille des huitres)*	BA04-104, BA04-108, BA04-112, BA04-114, BA04-116, BA04-119, BA04-120, BA04-123, BA04-124, BA04-125, BA04-126, BA04-128, BA04-132, BA04-133, BA04-134, BA04-136, CRMS-0258, CRMS-0260, CRMS-0282, CRMS-3680	BA04-104, BA04-108, BA04-114, BA04-116, BA04-119, BA04-120, BA04-123, BA04-124, BA04-125, BA04-126, BA04-128, BA04-133, BA04-134, BA04-136, CRMS-0258, CRMS-0260, CRMS-0282, CRMS-3680, 1, 2, 3
Spartina cynosuroides (L.) Roth	big cordgrass	BA04-114, BA04-119	BA04-103, BA04-112, BA04-132
Spartina patens (Aiton) Muhl.	marshhay cordgrass *(wiregrass, salt meadow cordgrass, paille a chat tigre*)	BA04-103, BA04-104, BA04-108, BA04-112, BA04-114, BA04-116, 119, BA04-120, BA04-123, BA04-124, BA04-125, BA04-128, BA04-132, BA04-133, BA04-134, BA04-136, CRMS-0258, CRMS-0260, CRMS-0282, CRMS-3680	BA04-103, BA04-104, BA04-108, BA04-112, BA04-114, BA04-119, BA04-124, 1 BA04-136, CRMS-0260, CRMS-0282
Sphenoclea zeylanica Gaertn.	chickenspike	BA04-133	
Symphyotrichum subulatum (Michx.) G.L. Nesom	eastern annual saltmarsh aster	BA04-103, BA04-119, BA04-120, BA04-125, BA04-126, BA04-133, BA04-136	BA04-104

Continued

Table 4.16 Continued

Scientific name as originally observed	Common name (*followed by colloquial names)*	*Species site locations, historical data	Species site locations, field data collection
Symphyotrichum tenuifolium (L.) G.L. Nesom	perennial saltmarsh aster	BA04-103, BA04-108, BA04-119, BA04-125, BA04-133, BA04-134, CRMS-0260, CRMS-3680	
Triadica sebifera (L.) Small	Chinese tallow	BA04-132	
Typha latifolia L.	broadleaf cattail	BA04-104	
Vigna luteola (Jacq.) Benth.	hairypod cowpea	BA04-103, BA04-104, BA04-108, BA04-112, BA04-114, BA04-116, BA04-124, BA04-125, BA04-132, BA04-133, BA04-134, BA04-136	BA04-104, BA04-108, BA04-112, BA04-114, BA04-132, CRMS-0258, CRMS-0260
Vitis L.	grape	BA04-108	

*Historical species data were not available for sample sites 1, 2, and 3

Table 4.17 Known nutrient and salinity sensitivities of vegetation species found at study sample sites historically and/or during field sampling.

Vegetation species	Sensitivity to nutrient and salinity increases intolerant = 1; somewhat tolerant = 2; moderately tolerant = 3; tolerant = 4; very tolerant = 5	
	Nutrient Sensitivity	Salinity Sensitivity
Baccharis halimifolia L.	2	4
Cephalanthus occidentalis L.	2	1
Distichlis spicata (L.) Greene	2	5
Hibiscus moscheutos L.	2	1
Iva frutescens L.	2	4
Juncus effusus L.	2	3
Juncus roemerianus Scheele	4	*
Phragmites australis (Cav.) Trin. Ex Steud.	5	3
Phytolacca americana L.	3	1
Polygonum hydropiperoides Michx.	2	1
Polygonum pensylvanicum L.	-	1
Polygonum punctatum Elliot	3	3
Solidago sempervirens L.	2	4
Spartina alterniflora Loisel.	2	5
Spartina cynosuroides (L.) Roth	-	5
Spartina patens (Aiton) Muhl.	2	5
Typha latifolia L.	3	1

**Data unavailable*

Table 4.18 Changes in number of species.

Site	Initial number of species	Number of species at field data collection	Change in number of species (final-initial)	Transitions in species number	Fluctuations in species number	Number of possible fluctuations	Fluctuation index (fluctuations/ possible fluctuations) *100
BA04-103	8	5	-3	8-5-4-5-5-5	3	5	0.60
BA04-104	12	9	-3	12-4-7-2-8-9	5	5	1.00
BA04-108	9	7	-2	9-10-7-5-8-7	5	5	1.00
BA04-112	10	8	-2	10-5-5-5-4-7	3	5	0.60
BA04-116	4	2	-2	4-4-2-3-3-2	3	5	0.60
BA04-119	5	3	-2	5-3-3-3-4-3	3	5	0.60
BA04-120	4	1	-3	4-3-2-3-2-1	5	5	1.00
BA04-123	3	2	-1	3-2-2-3-3-2	3	5	0.60
BA04-124	6	4	-2	6-3-3-3-4-4	2	5	0.40
BA04-125	5	3	-2	5-5-2-4-6-3	4	5	0.80
BA04-126	3	2	-1	3-3-3-2-3-2	3	5	0.60
BA04-128	2	2	0	2-3-2-3-3-2	4	5	0.80
BA04-132	9	3	-6	9-5-3-4-3-3	4	5	0.80
BA04-133	13	6	-7	13-5-6-6-6-6	2	5	0.40
BA04-134	5	5	0	5-5-7-6-5-5	3	5	0.60
BA04-136	6	3	-3	6-3-5-3-4-3	5	5	1.00
CMRS-0258	3	3	0	3-3-3-3-3	0	5	0.00
CMRS-0260	5	7	-2	5-6-4-4-7	3	5	0.60
CMRS-0282	2	2	0	2-2-3-3-2	2	4	0.50
CMRS-3680	4	3	-1	4-7-6-6-3	3	4	0.75

Table 4.19 Changes in average herb height.

Site	Initial average herb height (cm)	Final average herb height (cm)	Change in average herb height (cm) (initial-final)	Herb height transitions	Number of fluctuations in average herb height	Number of possible fluctuations	Fluctuation index (fluctuations/ possible fluctuations) * 100
BA04-103	122	61	-61	loss-gain-loss-loss	2	4	0.50
BA04-104	91	56	-35	* -loss-gain-loss	2	4	0.50
BA04-108	46	61	15	loss-gain-loss-gain	3	4	0.75
BA04-112	61	64	3	gain-gain-loss-gain	2	4	0.50
BA04-116	122	74	-48	loss-gain-loss-gain	3	4	0.75
BA04-119	91	76	-15	gain-loss-loss-gain	2	4	0.50
BA04-120	107	122	15	gain-loss-loss-gain	2	4	0.50
BA04-123	91	89	-2	same-gain-loss-gain	3	4	0.75
BA04-124	107	76	-31	same-gain-loss-gain	3	4	0.75
BA04-125	76	71	-5	gain-loss-same-loss	3	4	0.75
BA04-126	91	71	-20	gain-loss-loss-gain	2	4	0.50
BA04-128	107	33	-74	same-loss-loss-loss	1	4	0.25
BA04-132	61	97	36	gain-loss-gain-loss	3	4	0.75
BA04-133	91	66	-25	loss-gain-loss-loss	2	4	0.50
BA04-134	46	46	0	same-gain-loss-loss	2	4	0.50
BA04-136	122	81	-41	loss-gain-loss-loss	2	4	0.50
CMRS-0258	107	74	-33	loss-loss-gain	1	4	0.25
CMRS-0260	107	82	-25	loss-loss-loss		4	0.00
CMRS-0282	107	97	-10	loss-loss-gain	1	3	0.33
CMRS-3680	122	116	-6	loss-gain-gain	1	3	0.33

*Data unavailable

Table 4.20 Changes in sensitivity to nutrient increases.

Sensitivity to nutrient increases: intolerant = 1; somewhat tolerant = 2; moderately tolerant = 3; tolerant = 4; very tolerant = 5

Site	Initial average nutrient tolerance	Average nutrient tolerance at field data collection	Change in nutrient tolerance (final-initial)	Transitions in nutrient tolerance	Number of fluctuations in nutrient tolerance	Number of possible fluctuations	Fluctuation index (fluctuations/ possible fluctuations) *100
BA04-103	3	2	-1	3-2-3-3-3-2	3	5	0.60
BA04-104	2.5	3	0.5	2.5-2-2-2-2-3	2	5	0.40
BA04-108	2.5	3	0.5	2.5-2.5-2-2-2-3	2	5	0.40
BA04-112	3	2	-1	3-2.5-2.5-2-2-2	2	5	0.40
BA04-116	2	2	0	2-2-2-2-2-2	0	5	0.00
BA04-119	3	2	-1	3-2-2-2-2-2	1	5	0.20
BA04-120	2	2	0	2-2-2-2-2-2	0	5	0.00
BA04-123	2	2	0	2-2-2-2-2-2	0	5	0.00
BA04-124	3	3	0	3-2-3-3-3-3	2	5	0.40
BA04-125	3.67	3	-0.67	3.67-2-2-3-3-3	2	5	0.40
BA04-126	3	2	-1	3-2-2-2-2-2	1	5	0.20
BA04-128	2	2	0	2-2-2-2-2-2	0	5	0.00
BA04-132	2.5	*	*	2.5-3-3-2-2-*	2	5	0.40
BA04-133	2	2	0	2-3-2-2-2-2	2	5	0.40
BA04-134	2.5	2	-0.5	2.5-2.5-2-2-2-2	1	5	0.20
BA04-136	2	2	0	2-2-2-2-2-2	0	5	0.00
CMRS-0258	2	2	0	2-2-2-2-2-2	0	5	0.00
CMRS-0260	2	3	1	2-2-2-2-2-3	1	5	0.20
CMRS-0282	2	2	0	2-2-2-2-2-2	0	4	0.00
CMRS-3680	2	3	1	2-3-3-3-3-3	1	4	0.25

*Species sensitivity data unavailable

Table 4.21 Changes in sensitivity to salinity increases.

Sensitivity to salinity increases: intolerant = 1; somewhat tolerant = 2; moderately tolerant = 3; tolerant = 4; very tolerant = 5

Site	Initial average salinity tolerance	Average salinity tolerance at field data collection	Change in salinity tolerance (final-initial)	Transitions in salinity tolerance	Number of fluctuations in salinity tolerance	Number of possible fluctuations	Fluctuation index (fluctuations/ possible fluctuations) *100
BA04-103	4.5	4.5	0	4.5-4-5-5-5-4.5	3	5	0.60
BA04-104	3.25	5	1.75	3.25-5-5-5-5-5	1	5	0.20
BA04-108	4	5	1	4-4-5-4.5-4.5-5	3	5	0.60
BA04-112	4	5	1	4-4-4-4.5-5-5	2	5	0.40
BA04-116	5	5	0	5-5-5-5-5-5	0	5	0.00
BA04-119	5	5	0	5-5-5-5-5-5	0	5	0.00
BA04-120	5	5	0	5-5-5-5-5-5	0	5	0.00
BA04-123	5	5	0	5-5-5-5-5-5	0	5	0.00
BA04-124	4.5	5	0.5	4.5-4-5-5-5-5	2	5	0.40
BA04-125	4	5	1	4-4-5-5-5-5	1	5	0.20
BA04-126	5	5	0	5-5-5-5-5-5	0	5	0.00
BA04-128	5	5	0	5-5-5-5-5-5	0	5	0.00
BA04-132	3	5	2	3-3-3-4.5-5	2	5	0.40
BA04-133	3.33	5	1.67	3.33-3-5-4.5-1-5	5	5	1.00
BA04-134	3.33	5	1.67	3.33-3-4-4.5-3-5	5	5	1.00
BA04-136	5	5	0	5-5-5-5-5-5	0	5	0.00
CMRS-0258	5	5	0	5-5-5-5-5-5	0	5	0.00
CMRS-0260	4.5	4.5	0	4.5-4.5-4.5-4.5-5-4.5	2	5	0.40
CMRS-0282	5	5	0	5-5-5-5-5-5	0	4	0.00
CMRS-3680	5	5	0	5-5-5-5-5-5	0	4	0.00

Table 4.22 Changes in marsh community type.

Marsh community types: Fresh = 1; Intermediate = 2; Brackish = 3; Saline = 4

Site	Initial vegetation community	Vegetation community at field data collection	Change in vegetation community (final-initial)	Transitions in community type	Number of fluctuations in community type	Number of possible fluctuations	Fluctuation index (fluctuations/ possible fluctuations) *100
BA04-103	3	3	0	3-2-3-3-3-3	2	5	0.40
BA04-104	3	3	0	3-3-3-3-3-3	0	5	0.00
BA04-108	1	3	2	1-2-4-4-4-3	3	5	0.60
BA04-112	2	2	0	2-3-2-3-3-2	4	5	0.80
BA04-116	4	4	0	4-4-4-4-4-4	0	5	0.00
BA04-119	3	4	1	3-4-4-4-4-4	1	5	0.20
BA04-120	4	4	0	4-4-4-4-4-4	0	5	0.00
BA04-123	4	4	0	4-4-4-4-4-4	0	5	0.00
BA04-124	4	4	0	4-4-4-4-4-4	0	5	0.00
BA04-125	4	4	0	4-4-3-4-4-4	2	5	0.40
BA04-126	4	4	0	4-4-4-4-4-4	0	5	0.00
BA04-128	4	4	0	4-4-4-4-4-4	0	5	0.00
BA04-132	4	2	-2	4-1-2-4-4-2	4	5	0.80
BA04-133	3	3	0	3-1-3-4-2-3	5	5	1.00
BA04-134	4	3	-1	4-1-1-4-2-3	4	5	0.80
BA04-136	3	4	1	3-4-3-3-4-4	3	5	0.60
CMRS-0258	2	4	2	2-3-4-3-4	4	5	0.80
CMRS-0260	2	4	2	2-3-3-3-4	2	5	0.40
CMRS-0282	4	4	0	4-3-4-4-4	2	4	0.50
CMRS-3680	4	4	0	4-3-2-3-4	4	4	1.00

Table 4.23 Conversion of observations of vegetation dynamics to binary format data.

Questions	Responses by Sample Site (Yes = 1; No = 0)																			
								BA04-									CRMS-			
	103	104	108	112	116	119	120	123	124	125	126	128	132	133	134	136	0258	0260	0282	3680
Did marsh community type change from the initial sample period to the final sample period?	0	0	1	0	0	1	0	0	0	0	0	0	1	0	1	1	1	1	0	0
Did Marsh community type fluctuate between sample periods?	1	0	1	1	0	1	0	0	0	1	0	0	1	1	1	1	1	1	1	1
Was marsh community type fresher at the final sample period than at the initial sample period?	0	0	0	0	0	0	0	0	0	0	0	0	1	0	1	0	0	0	0	0
Did the number of species decline from the initial sample period to the final sample period?	1	1	1	1	1	1	1	1	1	1	1	0	1	1	0	1	0	1	0	1
Did the number of species fluctuate between sample periods?	1	1	1	1	1	1	1	1	1	1	1	1	1	1	1	1	0	1	1	1
Did the average herb height change from the initial sample period to the final sample?	1	1	1	1	1	1	1	1	1	1	1	1	1	1	0	1	1	1	1	1
Did the average herb height fluctuate between sample periods?	1	1	1	1	1	1	1	1	1	1	1	1	1	1	1	1	1	0	1	1

Continued

Table 4.23 Continued

Questions	Responses by Sample Site (Yes = 1; No = 0)																			
								BA04-									CRMS-			
	103	104	108	112	116	119	120	123	124	125	126	128	132	133	134	136	0258	0260	0282	3680
Did the average herb height increase from the initial sample period to the final sample period?	0	0	1	1	0	0	1	0	0	0	0	0	1	0	0	0	0	0	0	0
Did nutrient tolerance change from the initial sample period to the final sample period?	1	1	1	1	0	1	0	0	0	1	1	0	1	0	1	0	0	1	0	1
Did nutrient tolerance fluctuate between sample periods?	1	1	1	1	0	1	0	0	1	1	1	0	1	1	1	0	0	1	0	1
Did nutrient tolerance increase from the initial sample period to the final sample period?	0	1	1	0	0	0	0	0	0	0	0	0	0	0	0	0	0	1	0	1
Did salinity tolerance change from the initial sample period to the final sample period?	0	1	1	1	0	0	0	0	1	1	0	0	1	1	1	0	0	0	0	0
Did salinity tolerance fluctuate between sample periods?	1	1	1	1	0	0	0	0	1	1	0	0	1	1	1	0	0	1	0	0
Total score	8	9	12	10	4	8	5	4	7	9	6	3	12	8	9	6	4	9	4	8

Table 4.24 Study site and nutrient enrichment vulnerability class summary statistics and results of tests for significant difference between vulnerability classes based on cluster analysis variables.

	All sites		Lower eutrophication vulnerability sites		Higher eutrophication vulnerability sites		Mann-Whitney test for significant difference between vulnerability classes	
Vegetation biophysical data	Mean	Standard deviation	Mean	Standard deviation	Mean	Standard deviation	Z value	P value ($\alpha = 0.05$)
Initial marsh community	3.30	0.92	3.80	0.45	2.86	1.07	-1.54	0.062
Final marsh community	3.55	0.69	4.00	0.00	2.71	0.49	-2.76	0.003
Change in marsh community	0.25	0.97	0.20	0.45	-0.14	1.21	-0.65	0.258
Fluctuation in marsh community	0.42	0.37	0.12	0.27	0.63	0.34	2.03	0.021
Initial number of species	5.90	3.23	3.80	1.48	9.43	2.64	2.6	0.005
Final number of species	4.00	2.29	2.00	0.71	6.14	2.04	2.68	0.004
Change in number of species	-2.10	1.83	-1.80	1.30	-3.29	2.43	-0.89	0.187
Fluctuation in number of species	0.66	0.25	0.80	0.20	0.71	0.23	-0.57	0.284
Initial average herb height	93.75	24.39	109.80	12.91	74.00	28.25	-1.95	0.026
Final average herb height	75.65	21.43	79.80	31.98	64.43	15.80	-1.14	0.127
Change in average herb height	-18.10	26.85	-30.00	36.02	-9.57	32.81	1.06	0.145
Fluctuation in average herb height	0.51	0.21	0.55	0.21	0.57	0.12	0	0.500
Initial nutrient tolerance	2.43	0.51	2.00	0.00	2.57	0.35	2.35	0.009
Final nutrient tolerance	2.30	0.47	2.00	0.00	2.29	0.49	0.73	0.233
Change in nutrient tolerance	-0.13	0.61	0.00	0.00	-0.29	0.64	-0.73	0.232
Fluctuation in nutrient tolerance	0.23	0.20	0.00	0.00	0.41	0.12	2.76	0.003
Initial salinity tolerance	4.42	0.71	5.00	0.00	3.63	0.54	-2.76	0.003
Final salinity tolerance	4.80	0.68	5.00	0.00	4.50	1.12	-0.73	0.233
Change in salinity tolerance	0.38	0.73	0.00	0.00	0.87	1.03	1.54	0.062
Fluctuation in salinity tolerance	0.27	0.34	0.00	0.00	0.63	0.29	2.76	0.003
Leaf area index	4.27	1.29	3.79	1.66	4.99	1.21	1.14	0.127

Continued

Table 4.24 Continued

	All sites		Low nutrient enrichment vulnerability sites		High nutrient enrichment vulnerability sites		Mann-Whitney test for significant difference between vulnerability classes	
	Mean	Standard deviation	Mean	Standard deviation	Mean	Standard deviation	Z value	P value ($\alpha = 0.05$)
Chlorophyll concentration	245.40	79.41	220.60	81.94	292.86	98.48	0.65	0.258
Stem height	175.00	18.63	181.40	15.85	179.29	25.63	-0.65	0.258
DG-WV2 image data								
Coastal Band 1 (400-450 nm)	3.37	0.71	3.20	0.71	3.97	0.64	1.54	0.062
Blue Band 2 (450-510 nm)	3.40	0.57	3.22	0.85	3.68	0.47	0.97	0.166
Green Band 3 (510-580 nm)	6.48	0.83	5.83	0.80	7.20	0.61	2.76	0.003
Yellow Band 4 (585-625 nm)	5.91	0.74	5.68	1.40	6.02	0.23	0.49	0.312
Red Band 5 (630-690 nm)	5.27	0.92	5.43	1.48	4.80	0.67	-0.65	0.258
Red Edge Band 6 (705-745 nm)	21.43	4.14	17.73	1.47	25.40	4.04	2.76	0.003
NIR Band 7 (770-895 nm)	38.26	10.71	28.34	3.12	49.12	9.51	2.76	0.003
NIR Band 8 (860-1040 nm)	41.11	9.20	32.65	3.45	50.22	7.94	2.76	0.003
NDVI (NIR Band 7)	0.74	0.08	0.68	0.08	0.81	0.05	2.76	0.003
NDVI (NIR Band 8)	0.76	0.07	0.71	0.07	0.82	0.04	2.76	0.003
GNDVI (NIR Band 7)	0.70	0.05	0.66	0.04	0.74	0.03	2.60	0.005
GNDVI (NIR Band 8)	0.72	0.04	0.70	0.04	0.75	0.02	1.95	0.026
WDRVI (NIR Band 7)	0.74	0.08	0.68	0.08	0.81	0.05	2.76	0.003
WDRVI (NIR Band 8)	0.76	0.07	0.71	0.07	0.82	0.04	2.76	0.003
ARVI (NIR Band 7)	0.66	0.11	0.58	0.10	0.78	0.08	2.76	0.003
ARVI (NIR Band 8)	0.69	0.10	0.62	0.09	0.78	0.07	2.60	0.005
Vegetation dynamics binary data scores	8.05	2.87	4.40	1.14	9.71	1.70	2.76	0.003

Table 4.25 Cluster analyses results.

	DG-WV2 image data		Vegetation parameters		Vegetation dynamics binary data	
Site	Cluster 1	Cluster 2	Cluster 1	Cluster 2	Cluster 1	Cluster 2
BA04-103	1		1		1	
BA04-104	1		1		1	
BA04-108	1		1		1	
BA04-112	1		1		1	
BA04-116		2		2		2
BA04-119	1			2	1	
BA04-120		2		2		2
BA04-123		2		2		2
BA04-124		2	1		1	
BA04-125		2	1		1	
BA04-126		2		2	1	
BA04-128		2		2		2
BA04-132	1		1		1	
BA04-133	1		1		1	
BA04-134	1		1		1	
BA04-136		2		2		2
CRMS 0258	1			2		2
CRMS 0260	1			2	1	
CRMS 0282	1			2		2
CRMS 3680		2		2	1	

Table 4.26 Summary statistics for cluster analysis of vegetation biophysical data.

No. of Clusters	RMSSTD	SPRSQ	RSQ	BSS
19	2.84	0.0012	1.00	184.98
18	3.17	0.0014	1.00	231.74
17	3.35	0.0016	1.00	257.67
16	3.58	0.0018	0.99	294.42
15	3.93	0.0022	0.99	356.12
14	4.55	0.0037	0.99	594.42
13	4.92	0.0068	0.98	1094.20
12	5.88	0.0081	0.97	1295.00
11	8.77	0.011	0.96	1769.90
10	9.39	0.0126	0.95	2029.70
9	6.45	0.0148	0.94	2384.40
8	11.40	0.0186	0.92	2988.70
7	7.53	0.0222	0.89	3569.50
6	8.81	0.0234	0.87	3765.10
5	8.84	0.0452	0.83	7251.80
4	10.26	0.066	0.76	10593.00
3	18.51	0.0871	0.67	13991.00
2	13.39	0.1812	0.49	29096.00
1	19.17	0.491	0.00	78866.00

Table 4.27 Summary statistics for cluster analysis of DG-WV2 image data.

No. of Clusters	RMSSTD	SPRSQ	RSQ	BSS
19	0.26	0.0001	1.00	0.52
18	0.37	0.0003	1.00	1.11
17	0.41	0.0003	1.00	1.32
16	0.45	0.0005	1.00	2.16
15	0.41	0.0005	1.00	2.21
14	0.53	0.0008	1.00	3.19
13	0.73	0.001	1.00	4.24
12	0.78	0.0012	1.00	4.89
11	0.86	0.0014	0.99	5.95
10	0.66	0.0017	0.99	7.19
9	1.24	0.0045	0.99	18.67
8	1.31	0.0055	0.98	23.11
7	1.04	0.0067	0.98	27.92
6	1.30	0.0145	0.96	60.68
5	3.47	0.0231	0.94	96.25
4	1.83	0.035	0.90	145.96
3	2.22	0.0527	0.85	219.87
2	4.35	0.2651	0.59	1105.70
1	5.24	0.5850	0.00	2440.30

Chapter 5 - **Conclusions**

This study was undertaken to investigate the feasibility of modeling eutrophication vulnerability of a coastal Louisiana marsh receiving turbid Mississippi River water. The major objective was to integrate remotely sensed data with field measurements of vegetation biophysical characteristics and historical ecosystem survey data to delineate landscape patterns suggestive of vulnerability to eutrophication. The initial step in accomplishing this goal was to use turbidity frequency data to model high and low freshwater impacts associated with the operation of the West Pointe a la Hache siphon diversion. Turbidity reflectance levels were effectively used as a proxy for freshwater impacts to identify wetland areas most frequently and least frequently exposed to turbid Mississippi River water due to siphon operation. The resulting freshwater impacts model accurately identified high and low impact areas based on corresponding time series salinity data. A general reduction in freshwater impacts with increasing distance from the siphon diversion was observed, as was greater freshening of high impact areas compared to low impact areas during siphon operation. A high degree of fluctuation in mean salinity related to siphon operation was also observed throughout the study area, especially in high freshwater impact areas, suggesting the possibility that ecosystem regime changes may be occurring based on a freshwater introduction threshold.

The second step in completing this research was the development of a eutrophication vulnerability model using spectral data that were highly correlated with vegetation characteristics suggestive of nutrient enrichment. High correlation between ARVI using DG-WV2 NIR band 8 (860-1040 nm) and field measured chlorophyll content allowed accurate prediction of estimated chlorophyll concentration across the study area. Since functional indicators of eutrophication, such as increased biomass production, are closely associated with high chlorophyll content, the

observed spatial patterns suggest that vulnerability to eutrophication, like chlorophyll concentration, decreases with increasing distance from the siphon. Additionally, areas most consistently impacted by freshwater introduction are associated with the highest vulnerability, while least impacted areas are associated with the lowest vulnerability. This methodology allows clear identification of optimal sample sites for future studies related to identification and monitoring of eutrophication risks associated with the WPH siphon diversion.

The final step in accomplishing the major research objective was the development of a methodology that integrates remotely sensed image data, field measurements of vegetation biophysical characteristics, and historical ecosystem survey data to model eutrophication vulnerability. Higher and lower eutrophication vulnerability classes were identified based on agglomerative hierarchical clustering of the data, after which statistical analyses confirmed the separability of the classes in a majority of parameters. Results indicated significant differences between the vulnerability classes in key spectral bands and vegetation indices known to be highly correlated with functional indicators of eutrophication, such as increased biomass production. An accurate eutrophication vulnerability model was derived from classification of satellite image data based on cluster analyses results. Resulting spatial patterns suggest that eutrophication vulnerability tends to be higher near the source of introduced freshwater, as well as west and southwest of the siphon. Additionally, visual comparison of the eutrophication vulnerability map and a LiDAR-derived DEM revealed relatively consistent spatial patterns, suggesting that regions of higher vulnerability tend to coincide with lower elevation areas within the study area. Analysis of the data used in this eutrophication model also revealed that sites classified as having higher eutrophication vulnerability exhibited a greater degree of fluctuation in marsh community type and in nutrient and salinity tolerance. These results once again suggest

that ecosystem regime changes based on a freshwater introduction threshold may be occurring within the study area. This supports the evidence that intermittent siphon operation may be causing alternative stable states that can further disrupt and undermine the fragile stability of the ecosystem, adversely affecting flora and fauna within the study area. This finding underscores the need for well informed and consistent siphon operation management practices for existing and future river diversions.

The results of this study suggest that potentially eutrophic and relatively unenriched wetland areas can be successfully delineated using the remote sensing-based methodologies described in this dissertation. The methods described here can form the basis of sound sample collection protocols, aiding in future research and facilitating effective assessment and monitoring of eutrophication risks. Furthermore, this research has the potential to inform the current debate surrounding existing and future restoration projects, while contributing to the understanding of the impacts of river diversions on Louisiana's coastal wetlands.

Appendix A - Turbidity Frequency Datasets

The water turbidity frequency datasets were produced for this study by the U.S. Army Corps of Engineers (USACE) based on a method developed by Allen *et al*., 2008. Allen *et al*.'s method includes subsetting the time-series images to the study area boundary and radiometrically adjusting each image to minimize atmospheric effects. A land-water classification is then created for each image based on the Kauth-Thomas Tasselled Cap Transformation (TCAP). The TCAP technique transforms the image data to 3 bands representing brightness, greenness, and wetness (Kauth and Thomas, 1976). Discrimination between land and water is based on a threshold value chosen at a clear inflection point in the histogram of the wetness band. A turbidity classification is performed on the water extent of each image based on turbid water's relatively higher reflectance in the red wavelengths compared to clear water. The turbidity classification of each pixel is then compared across all image dates and the frequency of classification as turbid water is evaluated and mapped, providing an indication of areas that are consistently turbid (Allen *et al*., 2008).

References

Allen, Y.C.; Constant, G.C., and Couvillion, B.R., 2008. Preliminary classification of water areas within the Atchafalaya Basin Floodway System by using Landsat imagery: U.S. Geological Survey Open-File Report 2008-1320, 14p. URL: http://pubs.usgs.gov/of/2008/1320/

Kauth, R.J., and Thomas, G.S., 1976. The tasselled cap-a graphic description of the spectral-temporal development of agricultural crops as seen by Landsat. LARS Symposia, Paper 159.

Appendix B - Hybrid Classification Methodology

The hybrid classification method described by Bethel *et al*. (2011) incorporates Maximum Likelihood supervised classification and Iterative Self-Organizing Data Analysis Technique (ISODATA) unsupervised classification. First, a supervised classification is applied to the image data using a minimum of 10 areas of interest (AOIs) representing each class as training clusters. A low spectral Euclidean distance is maintained during AOI selection, with the goal of obtaining training clusters that include at least 25 pixels and that have a low standard deviation of ~3. Results of the supervised classification include a distance file and threshold image representing classified and unclassified pixels.

Second, an ISODATA unsupervised classification, specifying between 25 and 75 classes, is applied to the image data. The resulting classified image is linked geographically to the threshold image created during supervised classification, then the unsupervised image is used to guide classification of any remaining unclassified pixels in the threshold image. Once all pixels in the threshold image have been assigned to classes, the image is recoded and a smoothing technique based on neighborhood analysis is applied to reduce classification error related to noise inherent in the data.

References

Bethel, M.B.; Brien, L.F.; Danielson, E.J.; Laska, S.B.; Troutman, J.P.; Boshart, W.M.; Giordino, M.J., and Maurice A. Phillips, 2011. Blending Geospatial Technology and Traditional Ecological Knowledge to Enhance Coastal Restoration Decision-Support Processes in Coastal Louisiana. Journal of Coastal Research, 27(3), 555-571.